DEVELOPMENTS IN CAPILLARY ELECTROPHORETIC INSTRUMENTATION AND FT-IR SPECTROMETRIC DETECTION, AND SEMI-AUTOMATED FT-IR SPECTROMETRIC SAMPLE DEPOSITION

by

JESSICA LEA JARMAN

(Under the direction of JAMES A de HASETH)

ABSTRACT

Capillary electrophoresis (CE) and Fourier transform infrared (FT-IR) spectrometry are powerful analytical techniques currently utilized in a wide variety of problem-solving methodologies. CE is renowned for high resolution, rapid, flexible separation capabilities while FT-IR spectrometry is used for compound identification due to its characteristic functional group fingerprinting ability. Both techniques are commercially available in a wide variety of types and configurations. In this work, one branch of CE, micellar CE with and without the use of cyclodextrin chiral selectors, is used to investigate enantioselective degradation patterns in chiral pesticides. It was determined that one of three compounds investigated in three soils from various geographical regions exhibited enantioselective microbial degradation while the other two compounds showed evidence of hydrolytic degradation. Further, CE has been interfaced to an FT-IR spectrometer in an effort to expand the versatility and applicability of both techniques. The interface was characterized for electrical contact and stability, deposition characteristics, separation efficiency, and robust nature. Interface deposits were characterized for size, shape, splatter patterns, and recoverability. It was determined that separations were performed quickly and efficiently and that analytes were easily deposited, recoverable, and available for multiple analysis methods. High quality spectral identification was the primary method of analyte identification. Finally, many areas of spectral analysis require the manipulation of minute sample quantities. These samples, either in solvated or liquid form, can be easily deposited on transmission analysis windows or on a single-bounce internal reflection element. Deposits from the novel semi-automatic depositor have been characterized for size, shape, precision of placement, and success of solvent elimination. The depositor apparatus has been analyzed for stability and ease of analysis. In addition, a study was completed to determine depth of penetration coverage.

INDEX WORDS: Capillary electrophoresis, Fourier transform infrared spectrometry, CE/FT-IR, Interface, Nebulizer, Semi-automated sample depositor, Attenuated total reflection, ATR, Chiral pesticide degradation

DEVELOPMENTS IN CAPILLARY ELECTROPHORETIC INSTRUMENTATION AND FT-IR SPECTROMETRIC DETECTION, AND SEMI-AUTOMATED FT-IR SPECTROMETRIC SAMPLE DEPOSITION

by

JESSICA LEA JARMAN

B.A., Wesleyan College, 1999

A Dissertation Submitted to the Graduate Faculty
of The University of Georgia in Partial Fulfillment
of the
Requirements for the Degree

DOCTOR OF PHILOSOPHY

ATHENS, GEORGIA
2003

DEVELOPMENTS IN CAPILLARY ELECTROPHORETIC INSTRUMENTATION AND FT-IR SPECTROMETRIC DETECTION, AND SEMI-AUTOMATED FT-IR SPECTROMETRIC SAMPLE DEPOSITION

by

JESSICA LEA JARMAN

Approved:

Major Professor: James A de Haseth

Committee: James L. Anderson
Lionel Carreira
Ron Orlando
Robert S. Phillips

Electronic Version Approved:

Maureen Grasso
Dean of the Graduate School
The University of Georgia
May 2003

DEDICATION

This dissertation is dedicated to my parents, Dr. Robert O. and Leasa A. Jarman, without whom I would never have believed it was possible, and to my grandmother, Joyce E. Thompson Shaw, who is never afraid to give an honest opinion.

Thank you.

For M.

ACKNOWLEDGMENTS

When I think about all the people who played a part in my education, both in school and in life, I am overwhelmed. One of the most influential people in this circus was my major advisor, Dr. James A. de Haseth. Between putting up with my antics in the lab and encouraging my scientific progress, I believe he has helped me to realize my potential as a chemist and as a person. I also owe a large part of my success to Dr. Glenda K. Ferguson from Wesleyan College. It was she who encouraged me to apply to graduate school and recommended I speak with Dr. de Haseth. She is an inspiration to all aspiring chemists, and especially to women who are pursuing success in a male-dominated profession. To my committee members, Jim Anderson, Robbie Phillips, Butch Carreira, and Ron Orlando, thank you for your guidance and for being willing to sit through all those presentations.

In the de Haseth group, I met several talented scientists who would become my support system both in and out of the lab. I would like to thank Andrew Thomas, Dr. Andy Todebush, Tracey (Cash) Ward, Dr. Brian Melkowits, and Ushiri Kulatunga, as well as the undergraduate researchers who shared their college years with us: Shelly Seerley, Jennifer Gurley, Asher Newsome, Myles Sedgwick, and Scott Pannell. Thanks for all the entertainment and encouragement over the years. Additionally, I am heavily indebted to many others including Dr. Lindell Ward, Elizabeth (Mengelt) Walters, Melinda (Craven) Thomas, and Jeremi Johnson for softball, shooting pool, shooting other things, and surviving this thing called life.

The list would be far from complete, however, without my family. Mom and Dad, I know you are secretly terrified I'll spend the rest of my life in school. You are my inspiration; thanks for being there through all the ups and downs. Jo and Jason McCabe, you are instrumental in keeping a healthy degree of insanity and a large amount of love in my life. I wish you the best of luck out there on the west coast, and I plan to be visiting. John, I am positive you have a fabulous future ahead of you. Thank you for always being there to give a hug. Big Mama, thank you for the much needed support and wisdom you've shared with me. I wish you and Albert all the best.

There are many others who, over the years, kept me going and helped me stay relatively focused. While I could probably write an entire dissertation about all the influences in my life, it is not possible to fully express my love and gratitude. I hope to be able to repay the kindnesses someday.

"If you're not to be forgotten, when you're dead and rotten; write something worth reading, or do something worth the writing."

- Benjamin Franklin

TABLE OF CONTENTS

LIST OF FIGURES

CHAPTER 1

CHAPTER 2

CHAPTER 3

CHAPTER 4

CHAPTER 5

CHAPTER 1

INTRODUCTION AND LITERATURE REVIEW

Analytical chemistry may best be described as the art of problem solving. As with any set of questions, there are many possible tools available to answer those in the chemical field. The problems encountered in this dissertation are best addressed by infrared (IR) spectrometry and capillary electrophoresis (CE). In many cases, these two techniques complement each other such that considerable insight to even the most complex problems may be gained. In an effort to support this hypothesis and to appraise both advantages and disadvantages of these analytical methods, several research projects have been completed and analyzed. Before discussing these projects, however, a thorough examination of both methods is necessary.

Fourier Transform Infrared Spectrometry

Fourier transform infrared (FT-IR) spectrometry is a widely used spectrometric technique that is functional-group specific, and, therefore, can reveal a large amount of structural information. Mid-infrared radiation, that is, radiation in the region of 400 cm^{-1} to 4000 cm^{-1}, excites molecules at vibrational energy levels and is detected as absorbances at specific wavenumbers. These absorbance patterns are directly associated with the functional group that was excited, are highly reproducible, and are dependable as identification tools for chemical compounds.

FT-IR spectrometry has been applied to compounds of nearly every type, and it is often used to analyze samples through a variety of characteristics. Because of the high structural dependence of infrared spectra, FT-IR spectrometry has been used to determine molecular orientation,[1] analyte concentrations,[2] chemical component distributions,[3]and compositional and structural modifications.[4-6] Due in part to the non-destructive nature

of this technique, it is often regarded as an invaluable tool for pharmaceutical, industrial, and forensic analyses, and for biological determinations. For example, FT-IR spectrometry is used as a mapping technique, such as in the determination of areas of differing analyte concentrations in larger sample areas,[7,8] or to distinguish healthy cells from unhealthy cells that have undergone pathological changes.[9-12] FT-IR spectrometry is also easily enhanced with the application of computational techniques, which allows researchers to obtain spectral correlations that cannot be distinguished by the human eye.

The governing principle behind FT-IR spectrometric analysis is known as the Bouguer-Lambert-Beer Law, which states that at a given wavelength:

$$A = abC \tag{1.1}$$

where A is the measured absorbance of the sample and is directly proportional to the molar absorptivity (a) of the analyte, the radiation pathlength (b) through the analyte, and the analyte concentration (C). For transmission analyses, the pathlength is simply the sample thickness. For traditional reflection methods, however, the beam penetrates the analyte matter entirely and is reflected back from the substrate, which causes the pathlength to double the sample thickness. This property of reflection analyses is particularly attractive for optically thin sample material, from which high-quality transmission spectra are difficult to obtain. In other available methods of reflection analysis, such as attenuated total reflection (ATR), pathlength is governed by a variety of experimental parameters. The method-specific phenomenon associated with ATR analyses is discussed in detail below, as ATR analyses are involved in research presented herein.

Some of the distinct advantages of FT-IR spectrometry, other than the structural specificity of the spectra, include versatility, high sensitivity, and rapid analysis capabilities. Infrared analyses can be performed on any sample that is active in the IR region. While this may not seem to be a distinctive advantage, there are numerous compounds that do not fluoresce nor are active in the ultraviolet to visible (UV-vis) radiation range. Because of the low energy absorption required for infrared excitation, however, a large number of compounds absorb extremely well in the IR range. Sample material can be in gas, liquid, or solid form and are often recoverable. A high- quality infrared spectrum is characterized by a large signal-to-noise ratio (SNR), which indicates that the characteristic bands of the analyte can be easily distinguished from noise in the spectrum. Other than measuring the approximate signal and noise levels in the spectrum, the SNR can be calculated by:

$$SNR = U_v(T)\frac{\Theta \Delta\tilde{\upsilon}\xi\sqrt{t}}{\sqrt{A_D}} \quad \text{where} \quad \Theta = \Omega A_L \tag{1.2}$$

where $U_v(T)$ is the spectral energy density, Θ is the throughput, Ω is the solid angle, A_L is the limiting aperture, $\Delta\tilde{\upsilon}$ is the resolution, t is the measurement time, ξ is the spectrometer efficiency, and A_D is the area of the detector.

High-quality IR spectra have been obtained from very small sample quantities, especially in microspectrometry. While the actual detection limits vary slightly with the sampling method, FT-IR microspectrometry has been used to analyze samples in the picogram range.[13-16] FT-IR spectrometry is often employed in the analysis of minute sample quantities in biochemistry, forensics, and other areas of science.

The best signal-to-noise ratio in an IR spectrum is achieved when multiple spectra are co-added and random noise cancels out; however, systematic noise due to time-

dependent instrumental factors tends to increase if analysis time is increased. Therefore, it is important that spectra are collected rapidly in order to achieve high quality spectra in a timely manner. For a typical FT-IR spectrometer or microspectrometer, 100 scans at a resolution of 8 cm^{-1} can be collected and averaged in about ninety seconds. With current software packages, spectral manipulations such as corrections for pathlength differences and spectral subtraction can be performed almost instantly, which enhances the ease of analysis.

In addition, the versatility of FT-IR spectrometry adds flexibility to the methods available for sample analyses. There are two main options when considering the appropriate analysis method: transmission and reflection. While there are many possible techniques for both transmission and reflection experiments, the two used in the work presented here are transmission microspectrometry and single-bounce attenuated total reflection spectrometry. Both of these techniques have characteristic advantages and disadvantages, and were chosen to best fit the samples of interest.

Fourier Transform Infrared Microspectrometry

Fourier transform infrared microspectrometry is simply the combination of FT-IR spectrometry and a microscope. It has quickly become a popular method of analysis for small quantities of material or small, specific areas of much larger samples. Spectral quality of microspectrometric techniques has been shown to be a vast improvement over bulk methods.[6] FT-IR microspectrometry is also widely used in food science,[3,17,18] textiles,[19,20] polymers,[2,21,22] and in forensics.[23-26]

A FT-IR microscope may have a digital camera for viewing the sample and a computer-controlled (x,y)-translational stage, which can be used to map a large area of a sample or be used to find a region of a sample for spectral analysis. In addition, there are two available beam paths: one for visual observation of the sample and one for IR analysis. For added adaptability, FT-IR microspectrometric analyses can be performed in transmission or reflection mode. A schematic of the FT-IR microspectrometer, shown in Figure 1.1, depicts the analysis mode configuration in which the cassegrain optics are arranged to direct transmitted radiation toward the detector while visible radiation is eliminated from the beam path. During normal viewing mode, the beam path changes as shown in Figure 1.2, such that only visible radiation reaches the sample. For the purposes of the work presented here, transmission microspectrometric analyses were performed on a variety of samples. Additional sample characterization was also performed with the visualization and mapping features of the microspectroscope.

The instrument has an effective analysis range of 700-4000 cm^{-1} due to the operative region of the liquid-nitrogen cooled mercury cadmium telluride (MCT) detector. The radiation passes through a variable aperture that allows the user to define a sampling area between 10-μm and 100-μm diameter or square, depending upon whether the aperture is defined as round or square. Control of this aperture allows selection of appropriate areas of the sample for spectral analysis. Samples are placed on IR-transparent windows, typically zinc selenide (ZnSe) or calcium fluoride (CaF_2), which are then fixed to the translation stage and moved beneath the microscope optics. This method of sampling can be quite time-consuming, and a new background spectrum must be collected between each sample due to significant variations in the transmission

Figure 1.1. A typical FT-IR microspectrometer beam path while in analysis mode. Three cassegrain optics direct radiation from the interferometer through the sample and into the detector. The visible objective is not in use while the microspectrometer is in this mode.

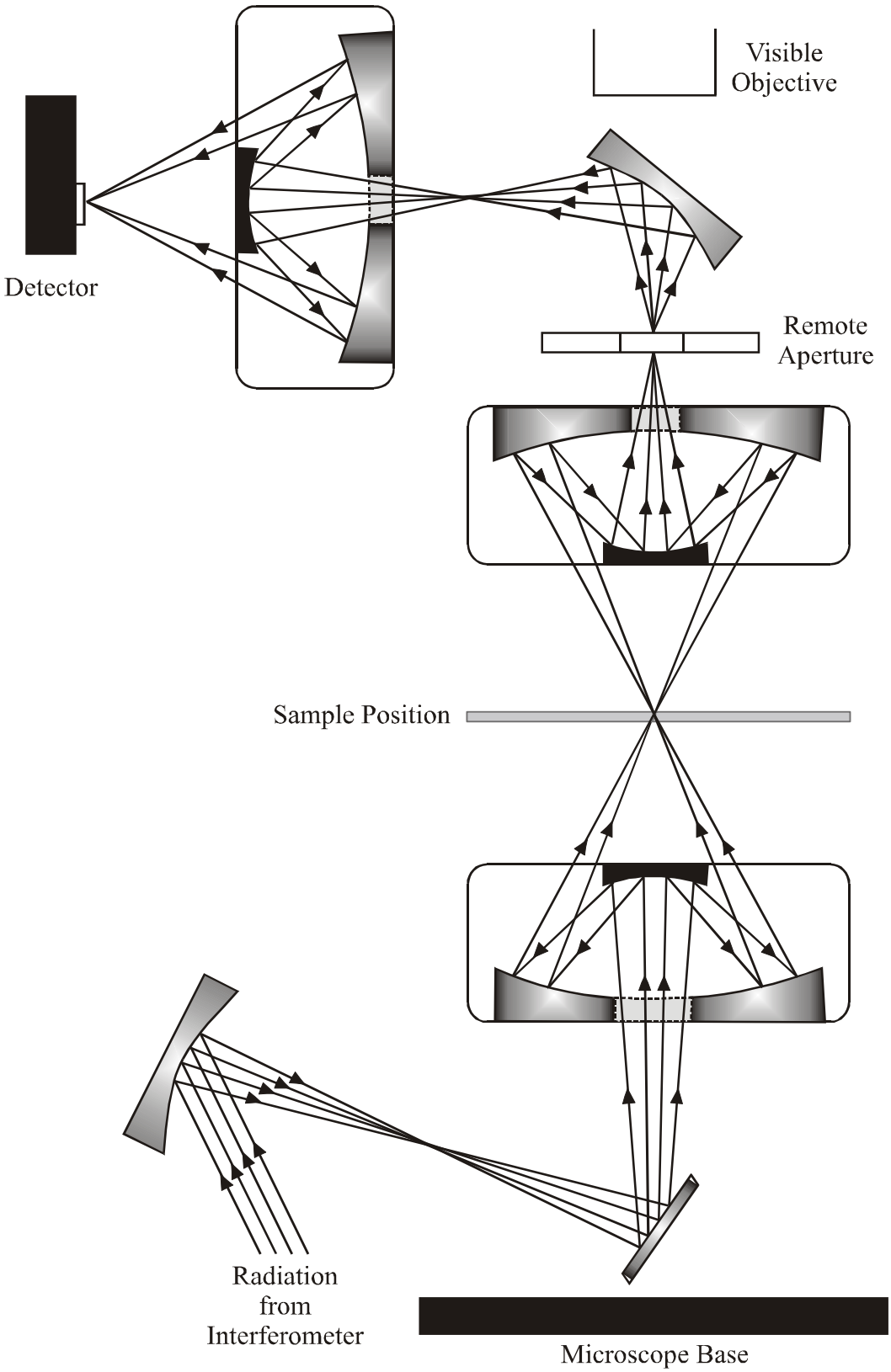
Visible
Objective
Detector
Remote
Aperture
Sample Position
Radiation
from
Interferometer
Microscope Base

Figure 1.2. A typical FT-IR microspectroscope while in visualization mode. Two of the three cassegrain optics direct light from the illuminator at the base of the microscope through the sample and into the viewing objective. Infrared radiation is isolated from the entire microscope area while the microspectrometer is in this mode.

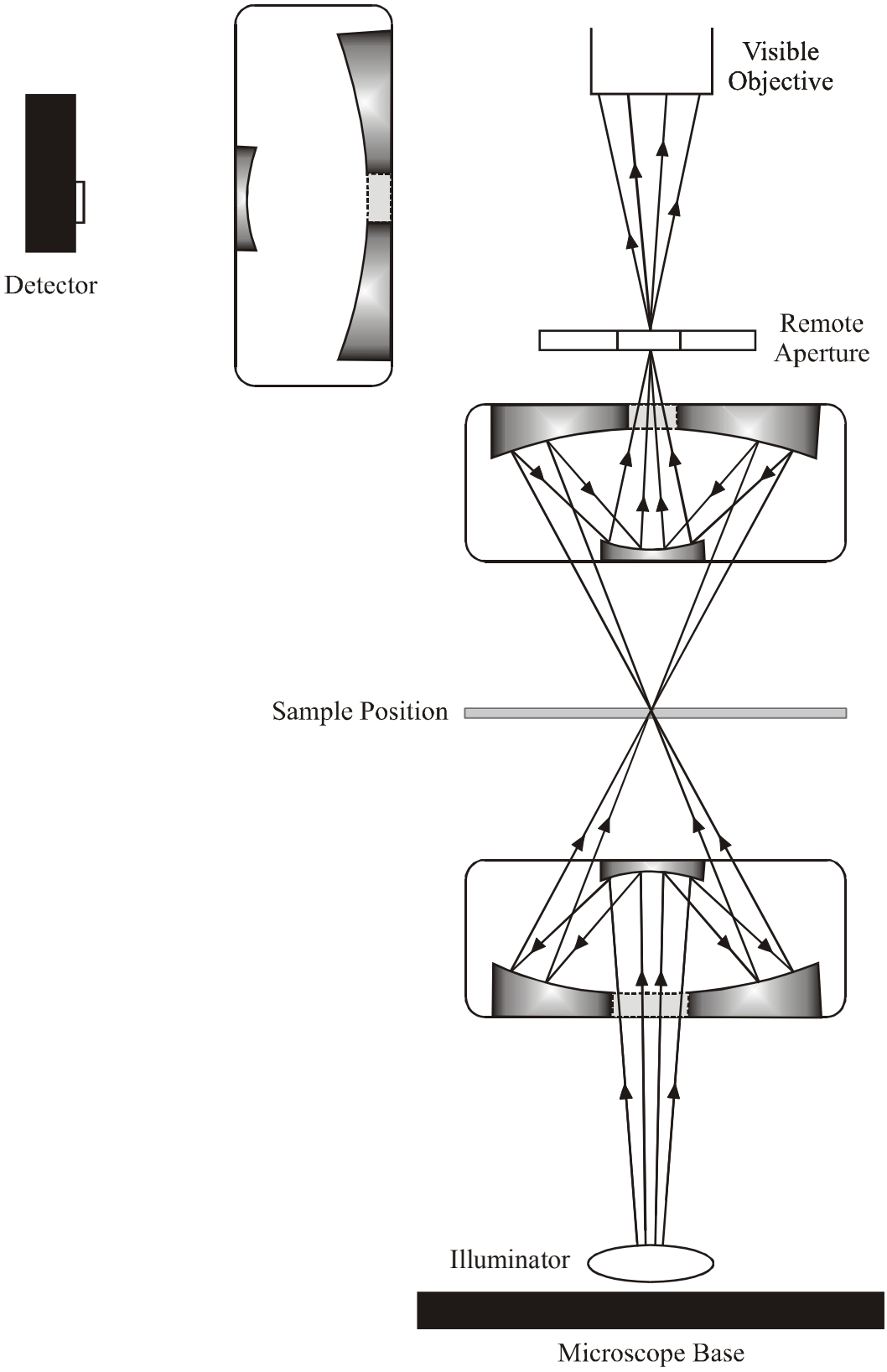
Detector
Visible
Objective
Remote
Aperture
Sample Position
Illuminator
Microscope Base

windows. A considerable amount of operator error is possible due to variations in focusing and sample area selection.

Samples suitable for FT-IR microspectrometric analyses meet several criteria. The material can be in either the liquid or solid phase, but most importantly, the sample must be optically thin. In order to properly prepare samples for microspectrometric analysis, there are several methods used. Among these are microtoming,[3,27] stretching,[2] and compression.[20,28] While some of these methods may cause changes in sample morphology,[1,29] all are documented preparation methods suitable for a variety of samples.

In order to obtain a high signal-to-noise ratio, the analyte must have relatively strong absorbance in the IR region. Further, the concentration and pathlength of the sample should be such that the characteristic bands of the analyte are easily identified. This requirement, especially for quantitative analyses, can be quite challenging and differs dramatically among samples. This may require spectral normalization prior to concentration determinations. Samples that are too thick, however, may prevent sufficient transmission and produce absorbance values that are not compatible with the linearity between A and C shown in Equation 1.1. Common samples that are unsuitable for transmission analyses may contain a large number of crystals or amorphous imperfections, which can also cause scattering of the infrared radiation. Scattered radiation can significantly distort the sample spectra, rendering spectral analysis futile. Therefore, manual inspection of each sample should be completed as a safeguard prior to spectral analysis.

Attenuated Total Reflection Spectrometry

Attenuated total reflection (ATR) analyses are quickly and easily accomplished on a variety of sample types. When two materials with different refractive indices are placed adjacent to one another, and a beam of radiation is passed through the high refractive index material toward the low refractive index material, one of two possibilities occurs. The radiation be completely transmitted, or it may be reflected back into the first material. The angle of incidence of the incoming radiation governs which of the two scenarios occurs.

As shown in Figure 1.3A, a critical angle (θ_c) with respect to the surface normal exists such that radiation entering the denser medium travels exactly along the interface with the less dense medium. This critical angle, θ_c, can be calculated from:

$$\theta_c = sin^{-1}\left(\frac{\eta_2}{\eta_1}\right) \tag{1.3}$$

where η_1 and η_2 are the refractive indices of the denser and less dense materials, respectively. In ATR analyses, the denser medium is the ATR element itself, which is commonly made of silicon, germanium, diamond, calcium fluoride or zinc selenide and often referred to as the internal reflection element (IRE). If the incident radiation enters the denser medium at an angle smaller than θ_c, the beam obeys Snell's Law and travels completely through the less dense material as well. Snell's law states that the angle ratio of incident and transmitted radiation is inversely proportional to the ratio of the refractive indices of the materials:

$$\frac{\eta_1}{\eta_2} = \frac{\sin\theta_2}{\sin\theta_1} \tag{1.4}$$

where η_1 and η_2 are the refractive indices of the denser and less dense materials, respectively and θ_1 and θ_2 refer to the angles shown in Figure 1.3B.

If, however, the incident radiation enters at an angle larger than θ_c, the radiation is internally reflected. This reflection creates an evanescent wave on the surface of the denser material, which exponentially decreases in strength with increased distance from the surface as shown in Figure 1.4. When the beam is reflected, this wave excites the sample material in a non-destructive manner. This wave of energy penetrates the second material, usually the sample material, to a specific distance, called the depth of penetration (d_p), given by:

$$d_p = \frac{\lambda}{2\pi\eta_1\sqrt{\sin^2\theta - \eta_{21}^2}} \tag{1.5}$$

where λ is the wavelength, η_1 is the refractive index of the internal reflection element, θ is the angle of incidence radiation, and η_{21} is the ratio of the refractive indices of the sample and the element, respectively. Because d_p is directly dependent upon the refractive index of the IRE, it governs several properties about the analyses performed with that element. Elements with lower refractive indices allow for larger depths of penetration and may therefore yield higher signal-to-noise spectra, but require slightly more sample. In addition, these same elements require a larger overall sampling area, known as the active site of the element. Identical elements of two different materials may have very different active areas due to the difference in refractive indices.

There are several different IRE shapes, such as truncated triangular prism, parallel-piped, and hemispherical, that can be used in ATR analyses. Multiple reflection elements are extensively covered by Harrick[30-32] and will not be covered here. For single

Figure 1.3. A. A depiction of the effect the angle of incidence has on the path traveled by radiation directed into a denser material and toward a less dense material. Radiation entering at an angle larger than that of the critical angle is internally reflected while the same radiation introduced at a smaller angle passes through both materials. In the event that radiation enters exactly at the critical angle, the beam travels along the upper surface of the heavier material. **B.** A pictorial description of Snell's Law in which the angles of incidence and refraction are mathematically related to the refractive indices of the two materials.

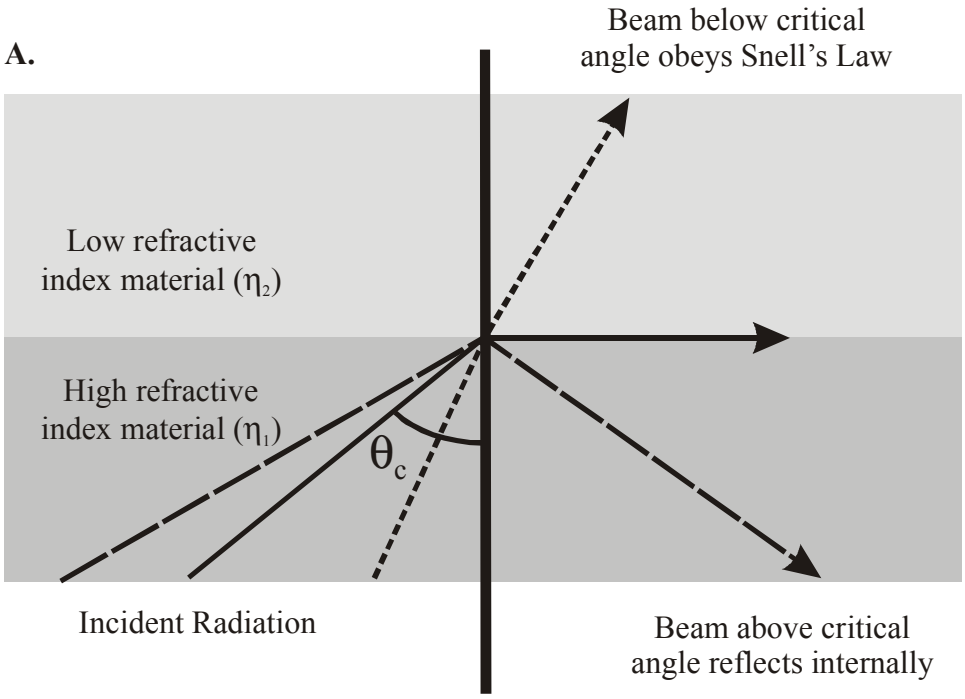
A.
Beam below critical angle obeys Snell's Law
Low refractive index material (η_2)
High refractive index material (η_1)
θ_c
Incident Radiation
Beam above critical angle reflects internally

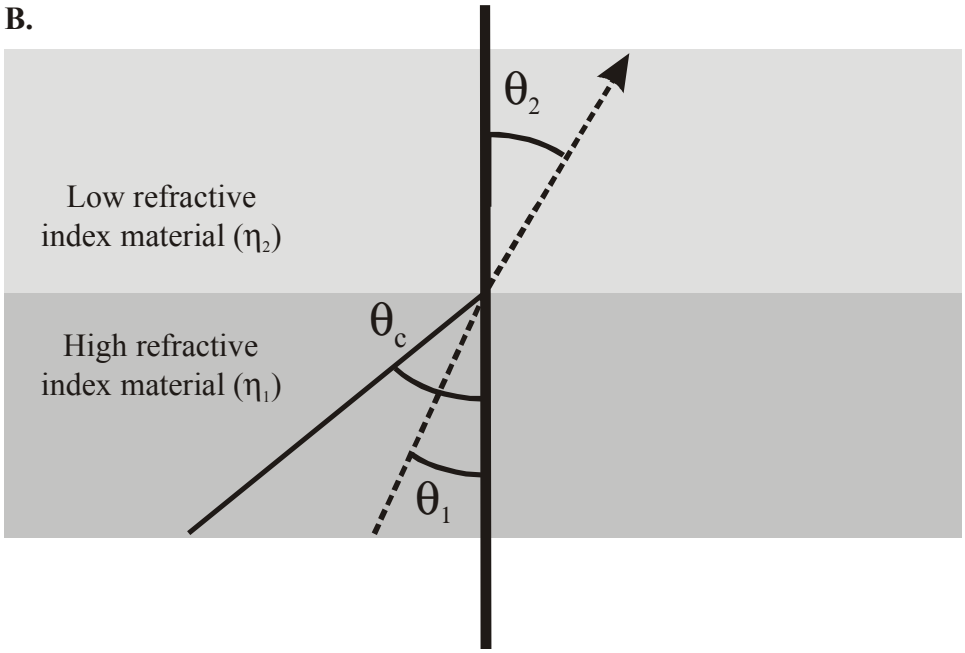
B.
θ_2
Low refractive index material (η_2)
θ_c
High refractive index material (η_1)
θ_1

Figure 1.4. The evanescent wave created by internally reflected radiation. The energy of this wave decreases exponentially as distance from the surface of the ATR element increases, represented here by black (the high energy region) fading into white.

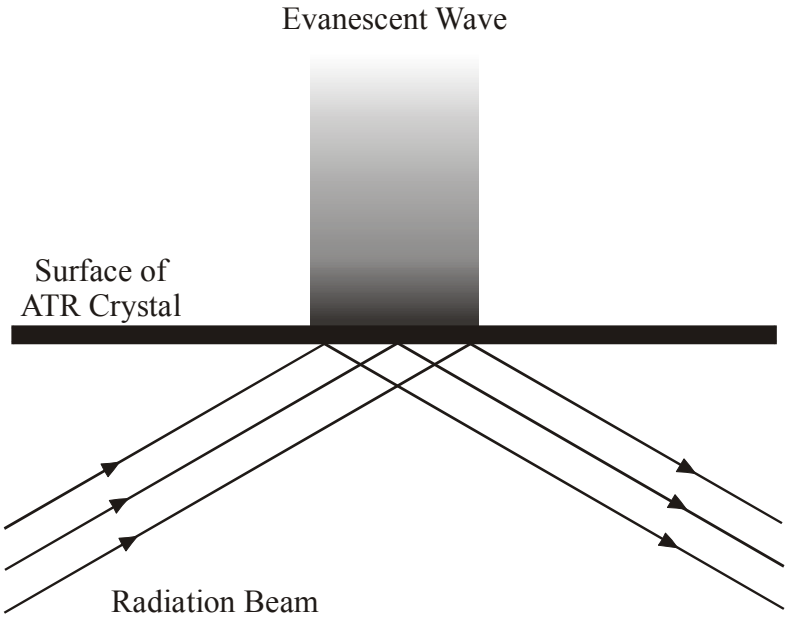
Evanescent Wave
Surface of
ATR Crystal
Radiation Beam

reflection elements, such as the Harrick SplitPea™ used in the studies herein, the elements are much smaller and, as a result, require significantly less sample.

Each single reflection IRE geometry has performance characteristics associated with it. Fixed-angle elements are typically prisms such as the one shown in Figure 1.5A. Because the radiation beam entering a prism is not condensed, the width of the incident beam determines the active site dimensions for the element. For samples of moderate to large quantities that have good inherent contact with the surface of the IRE, this type of element is quite useful. A variable-angle hemispherical element, however, is much better suited for smaller sample quantities. As shown in Figure 1.5B, the properties of the hemisphere cause the beam to converge and focus to a much smaller width than that of the incident radiation. The convergence and focus of the radiation result in much higher sensitivity for the analysis of small samples.

Instead of requiring both a microscope and a spectrometer, FT-IR/ATR analyses are performed with an ATR accessory mounted in the sample compartment of a typical spectrometer. The deuterated triglycine sulfate (DTGS) detector is effective between 400 cm^{-1} and 4000 cm^{-1}. The accessory is fitted for the sample compartment, which aids in maintaining appropriate purge characteristics. The beam path through the accessory is relatively simple; incoming radiation is directed up into the IRE, and reflected radiation is collected and sent to the detector. A schematic of this process is shown from two viewpoints in Figure 1.6.

ATR samples also have specific requirements, although there is a higher degree of flexibility associated with the technique due to the ability to measure opaque or optically thick samples without losing spectral quality. Because the radiation is reflected, samples

Figure 1.5. A comparison of single reflection ATR element shapes, a prism (**A**) and a hemisphere (**B**). The focusing induced by a hemispherical shape helps to increase sensitivity and reduce the sampling area.

A.

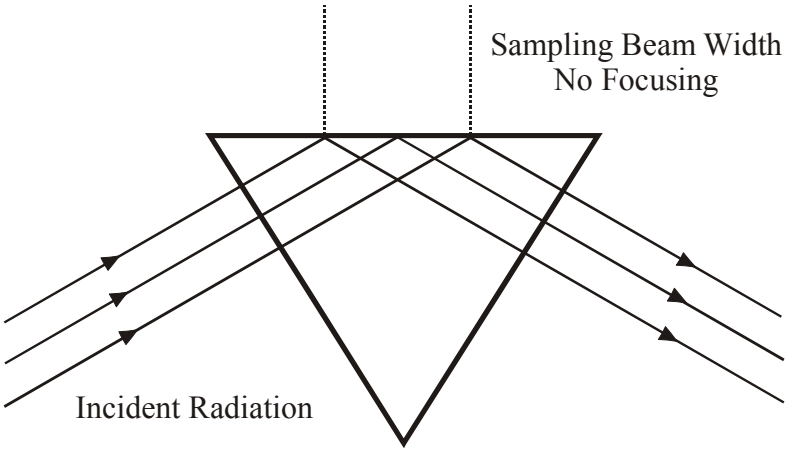
Sampling Beam Width
No Focusing
Incident Radiation

B.

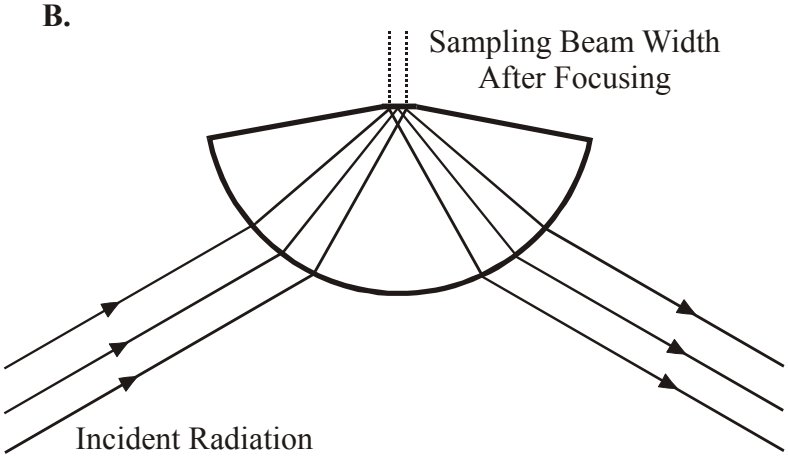
Sampling Beam Width
After Focusing
Incident Radiation

Figure 1.6. The infrared radiation beam path through the Harrick SpitPea™ single bounce ATR accessory shown from both the side view (**A**) and the top view (**B**).

A.

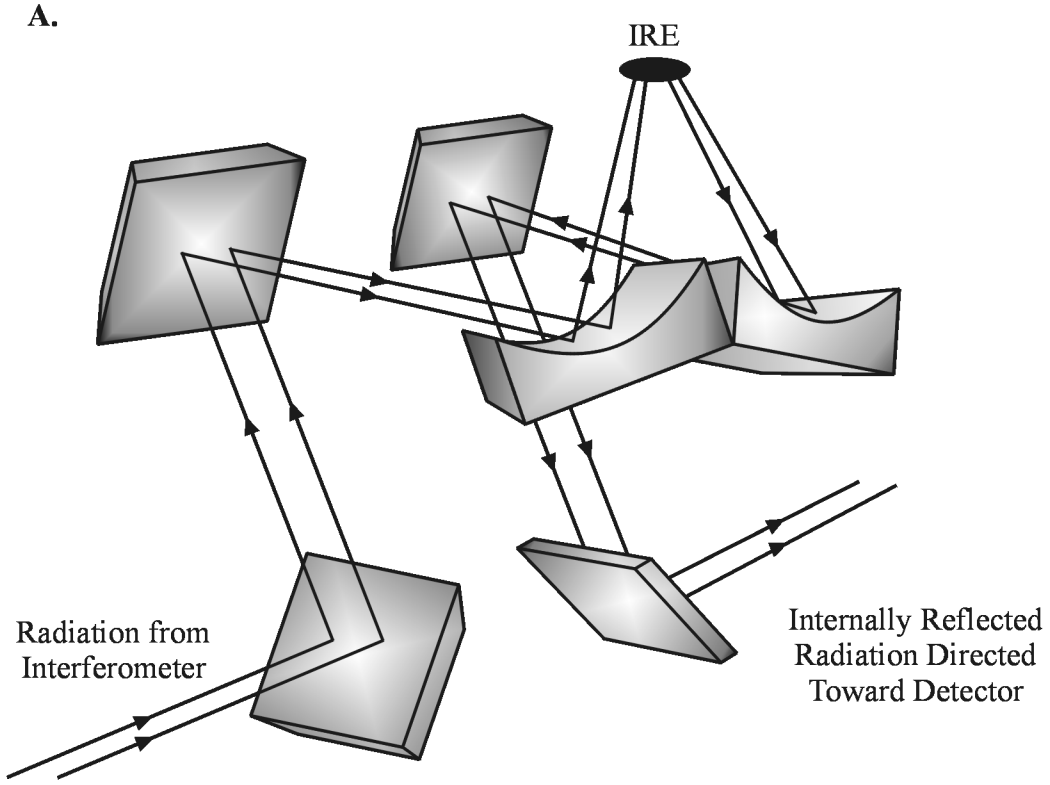

Side View

B.

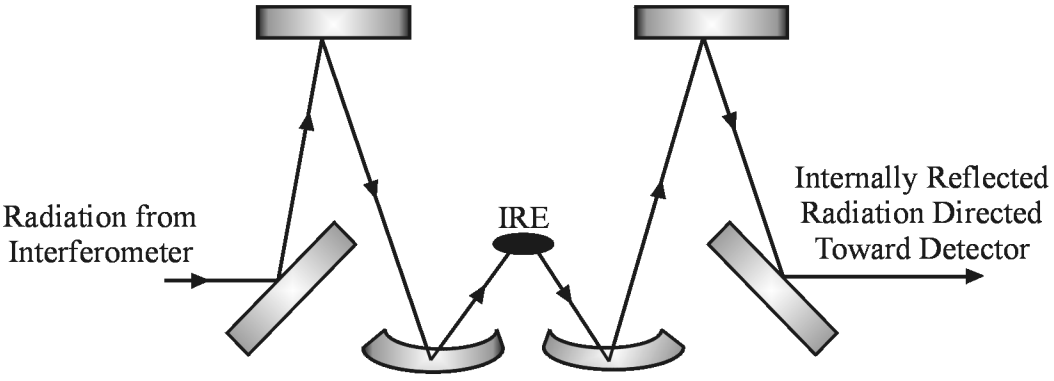

Top View

can be liquid or solid, and do not need to be optically thin or transparent. As a result, sample preparation is minimal. The main requirement is that the sample maintains good contact with the surface of the IRE. Pressure is easily applied to enhance contact for some samples that do not maintain good surface contact. Ideally, the sample is thick enough to fully cover d_p which produces adequate absorbance. However, high-quality qualitative analysis is still easily accomplished on samples that do not cover d_p.

While the studies described here exploit the versatility of FT-IR spectrometry, the increase of the number of analysis methods available is dependent upon the development of new techniques, such as the CE/FT-IR interface described in Chapters 3 and 4. Because of the inherent sensitivity, small sample requirement, and structural identification capability, the prospect for new application of FT-IR spectrometry is considerable, and its potential is far from being fully realized.

.

Capillary Electrophoresis

Although the concept of using an electrical current to manipulate chemical species was first attempted in the 1930s,[33,34] the first (CE) system was developed between 1958 and 1965,[35,36] and the first commercial instruments were not available until around 1990.

CE is a separations technique similar to traditional liquid chromatographic systems, but utilizes an electrical current to separate analyte molecules. CE was first popularized by a series of papers from Jorgenson and Lukacs.[37-39] In these papers, the typical CE instrument (Figure 1.7) was described as having a fused silica capillary, electrode reservoirs, a high voltage power supply, and a detector. Early CE detectors

Figure 1.7. A schematic of a typical capillary electrophoresis instrument showing two buffer (electrolyte) reservoirs, a sample reservoir, immersed electrodes, a high voltage power source, and the fused silica capillary. Traditional detection occurs on-column through the detection window.

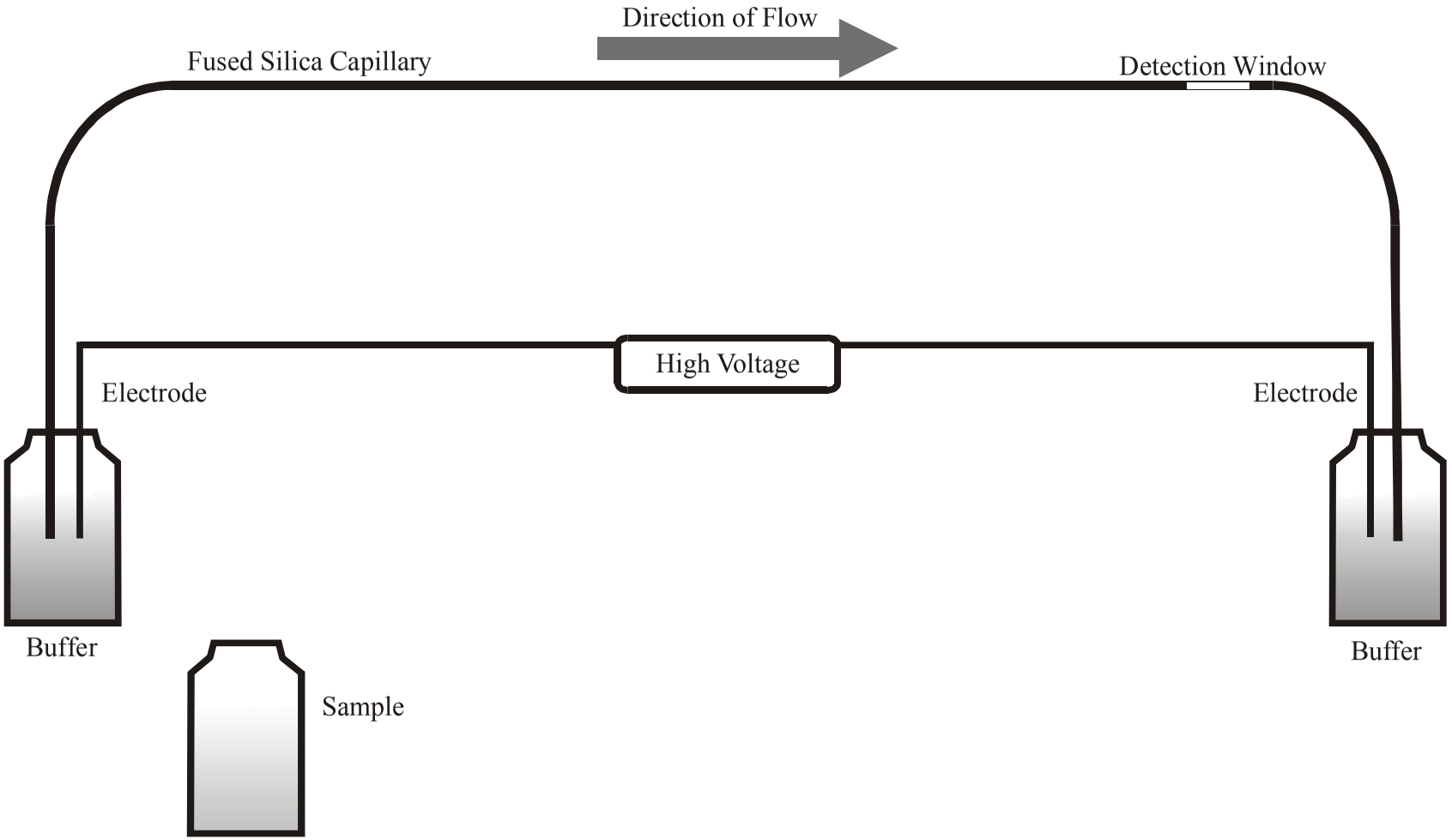
Direction of Flow
Fused Silica Capillary
Detection Window
High Voltage
Electrode
Electrode
Buffer
Buffer
Sample

were usually modified optical high-performance liquid chromatography (HPLC) detectors. Current instrumentation, however, includes a wide range of possibilities such as UV-vis photodiode arrays (PDA), pulsed amperometric detectors (PAD), and laser-induced fluorescence (LIF) detectors. The silica capillaries are externally coated with a protective coating that also introduces a great deal of flexibility. Therefore, they are easily wound into small cartridges and are relatively hardy with regard to fractures.

Typically, a small portion of the protective polyimide outer coating is burned off the column in order to create a detection window. A voltage is applied across the column, with high voltage applied to one end of the capillary and the other end held at electrical ground. The conductive properties of the electrolyte solution create an electrical current throughout the interior of the capillary. In order to maintain electrical contact and constantly replenish electrolyte molecules inside the column, the electrode and column are both immersed in a vial containing the electrolyte solution, known as the running buffer.

CE has several distinct characteristics. Perhaps the most obvious is that using a capillary as the separation column drastically reduces the sample and buffer volume requirements, needing only nanoliters of sample material. Additionally, CE systems are known for high resolution and mass sensitivity of analyte compounds, and analyses are carried out relatively quickly, and with little expense. Although traditional CE does not resolve neutral molecules, buffer modifications and additives that achieve neutral separations are readily available in order to develop highly efficient methods of separation. Experimental parameters such as temperature and pH are easily varied, and

the separations are carried out near ambient pressure, which preserves the high-resolution capabilities as discussed below.

There are several variations of capillary electrophoresis including capillary zone electrophoresis (CZE), capillary gel electrophoresis (CGE), micellar electrokinetic chromatography (MEKC), and capillary electrokinetic chromatography (CEC). CZE is also known as traditional CE, and refers to a system in which there are no buffer additives or packing materials inside the column. CGE is performed with gel-filled capillaries, MEKC involves the use of surfactant modifiers with CZE columns, and CEC uses columns filled with material similar to liquid chromatographic column packing. The principles discussed in this section refer mainly to open tubular systems such as CZE and MEKC, which is discussed in greater detail in Chapter 2. Other techniques retain several of the CZE principles and characteristics but have other properties that impact the capabilities and performance of these techniques.

In an effort to elucidate the separation mechanism in CE systems, the phenomena occurring inside a CE column should be further examined. Voltage application across a CE column creates two forces, electrophoretic and electroosmotic, within the system. Each of these forces results in ion movement within the column, although the stronger of the two forces creates a net movement of solution through the capillary. This solution movement is referred to as the electroosmotic flow (EOF) while the secondary force creates an electrophoretic flow (EPF) that is directly dependent upon the ionic properties of the molecule. Analyte separation is achieved when molecules travel at different rates in the column due to their inherent electrophoretic properties. Therefore, when the EPF

of an analyte is zero, separation cannot occur. A schematic diagram of the ion movement associated with pure EPF and with the added effects of an EOF is shown in Figure 1.8.

EPF is defined as the movement of individual chemical species within the system due to charge. It is determined by the electrophoretic mobility of each species, and the direction may match or oppose the electroosmotic flow, depending on the charge of the molecule. The electrophoretic flow of a molecule is highly dependent upon the conditions of the CE system. All charged molecules have an electrophoretic mobility with an associated velocity determined by the charge and mass of the particle. Electrophoretic mobility (μ_{ep}) is given by:

$$\mu_{ep} = \frac{q}{6\pi\eta r} \tag{1.6}$$

where q is the charge on the particle, η is the viscosity of the buffer, and r is the Stokes' radius of the particle. The direction of flow is solely determined by the attraction of the particle to the electrode at one end of the capillary. Negative particles flow toward the more positive end of the capillary while positive particles are attracted to the opposite end. Neutral particles do not possess an electrophoretic mobility, as q = 0.

EOF refers specifically to the flow of solvent in an applied potential field, and results from the highly charged walls of the bare silica capillary. The EOF of a CE system is the driving force that moves analyte molecules past the detector window. The EOF inside the capillary originates from ionic interactions at the highly charged silica walls. Three main layers of ionic interactions are formed along the walls of the capillary. The layer closest to the wall of the capillary is a stagnant layer of cations immobilized by the strong interactions with the negatively charged silica. A second, compact layer is formed, also primarily of cations, in an attempt to stabilize the highly negative

environment of the silica surface. The third layer is referred to as the diffuse layer and consists of mobile cations with an increasing number of anions.

Because each layer is predominantly composed of cations, typically Na^+, the cations travel along the length of the column toward the cathode at the column outlet. Since the molecules are solvated, the cation movement results in net solution migration through the column, with electrolyte molecules (and solution) from the inlet buffer vial maintaining each layer. The potential across each of these layers is defined as the zeta potential (ζ). The zeta potential is given by:

$$\zeta = \frac{4\pi\delta e}{\varepsilon} \tag{1.7}$$

where δ is the double layer thickness, e is the charge per unit surface area, and ε is the dielectric constant of the solution. The thickness of the double layer can be approximated by:

$$\delta = \frac{1}{(\text{Electrolyte Concentration})} \tag{1.8}$$

A schematic diagram of these layers is shown in Figure 1.9. The diffuse layer moves toward the outlet end of the capillary, or the cathode, and causes the solvent molecules to migrate in the same direction. The velocity (v) of the EOF is dependent upon the applied voltage and corresponding current. More specifically, the velocity is given by:[35,36]

$$v = \frac{\varepsilon}{4\pi\eta L} V\zeta \tag{1.9}$$

where V is the magnitude of the applied voltage and L is the length of the column. Therefore, particles have electroosmotic mobility (μ_{eo}) as well, that can be defined as:

$$\mu_{eo} = \frac{\varepsilon\zeta}{4\pi\eta} \tag{1.10}$$

While pressure driven systems exhibit flow profiles that are laminar in shape, the origination of the EOF from the capillary walls creates a plug flow profile inside the CE column (Figure 1.10). The plug flow can be expected for capillaries with inner diameters at least seven times greater than the thickness of the double layer.[40] Because of the plug flow profile, EOF should not contribute to the broadening of solute zones within the capillary.

In some applications, such as isoelectric focusing and CGE, the generation of an EOF is detrimental to resolution. In CZE and MEKC, however, the EOF is an integral part of the separation mechanism and allows the systems to operate without applying external pressure.[40] The absence of pressure in the system preserves the plug flow found in electrokinetic systems and the high resolution achieved in these separations. However, because the migration time is directly dependent upon the EOF, both the efficiency and resolution are affected indirectly by changes in the EOF.

If both electrophoresis and electroosmosis are present in the system, the migration time (t) and the migration velocity (v) can be determined by:

$$t = \frac{L^2}{(\mu_{eo} + \mu_{ep})V} \tag{1.11}$$

and

$$v = \frac{(\mu_{eo} + \mu_{ep})V}{L} \tag{1.12}$$

From Eq. (1.11), neutral particles are carried along at the same flow rate as the overall EOF, which indicates that they will not undergo separation and will migrate with the solvent front. Particles with a positive μ_{ep} will migrate faster than the EOF while those with a negative μ_{ep} will migrate slower than the EOF, thereby facilitating analyte

Figure 1.8. A schematic diagram of ion movement due to strictly electrophoretic forces (**A**), and with the influence of electroosmotic forces (**B**) that typically occur within a CE column when using a cationic running buffer. Arrows indicate the direction and magnitude of ion movement, assuming each ion has the same net charge but a variable mass.

A.

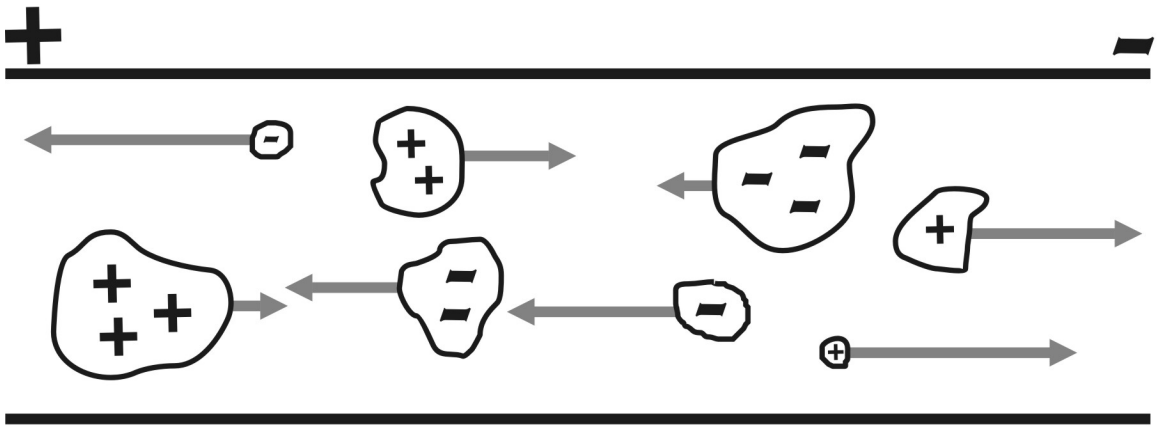

B.

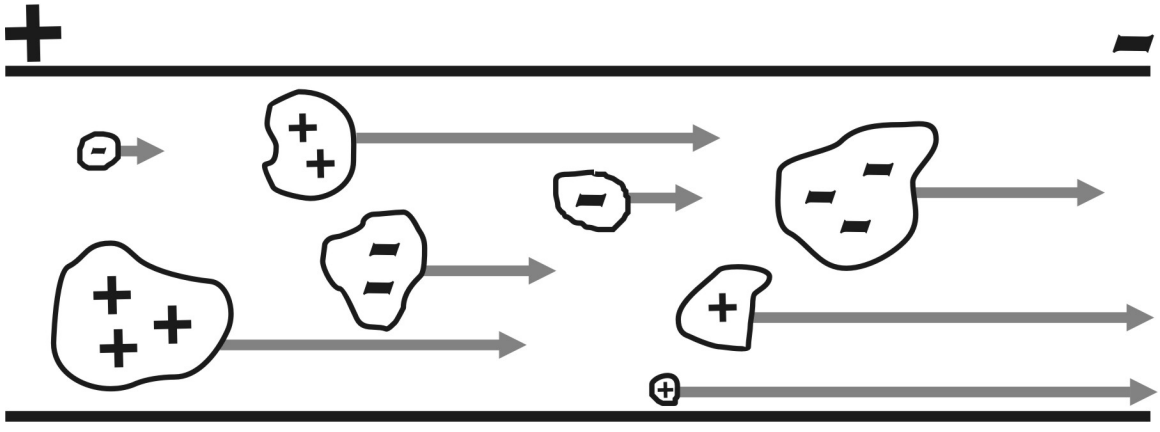

Figure 1.9. A schematic of the charges present that create the electroosmotic flow integral in CE analyses.

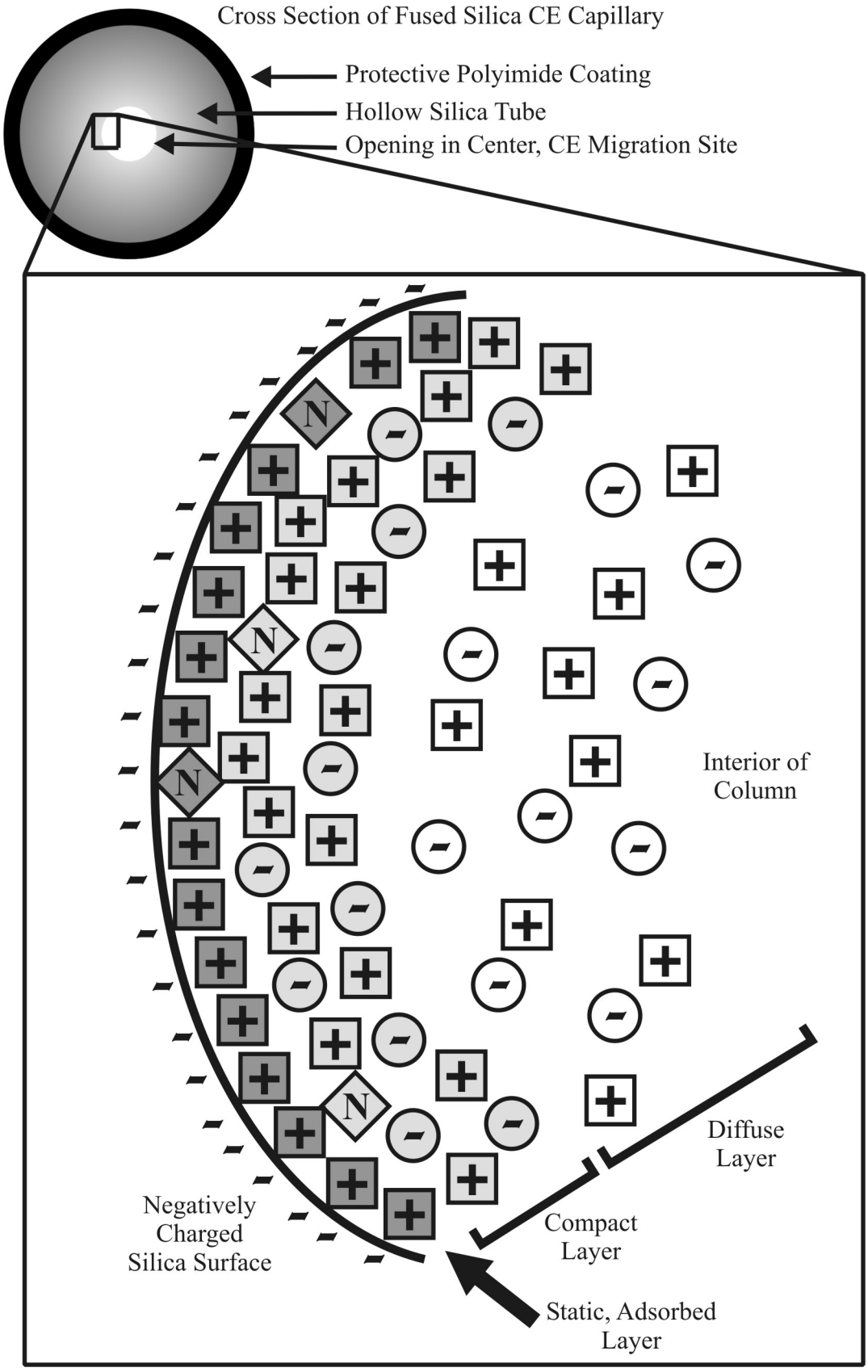
Cross Section of Fused Silica CE Capillary
Protective Polyimide Coating
Hollow Silica Tube
Opening in Center, CE Migration Site
N
N
N
Interior of Column
Diffuse Layer
Compact Layer
Static, Adsorbed Layer
Negatively Charged Silica Surface

Figure 1.10. A comparison of flow profiles found in pressure-driven systems, such as HPLC, and in electrophoretically-driven systems such as CE. Laminar flows can lead to peak broadening and decreased analyte resolution.

HPLC Column

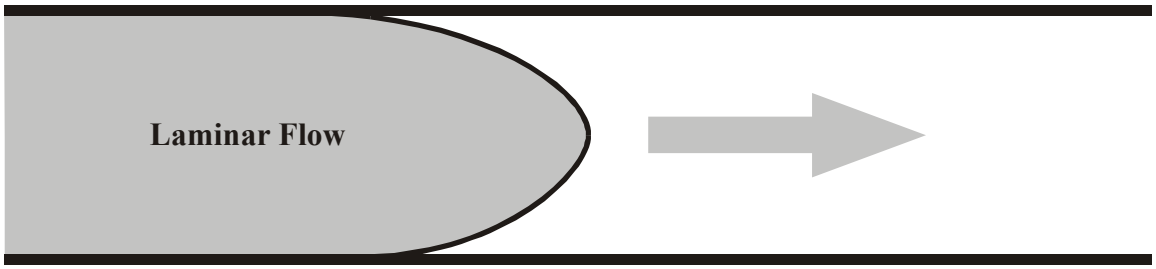

CE Column

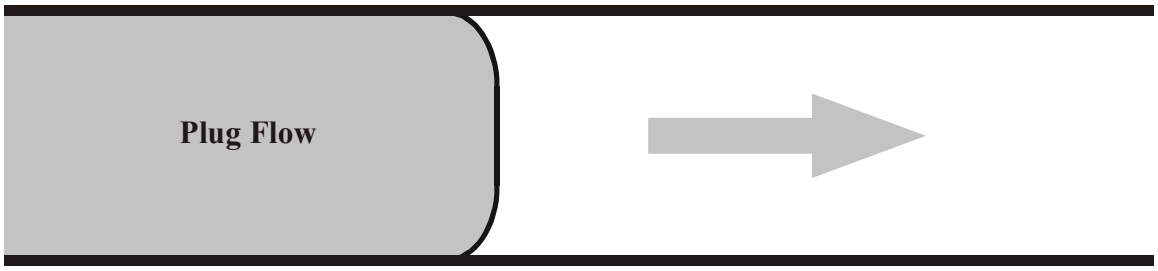

separation. Further, when the magnitude of the EOF exceeds the μ_{ep} of anionic particles, and the flow is in the opposite direction, all ions will migrate in the same direction and, therefore, are detectable.

Particles migrate specifically according to the charge-to-mass ratio as shown in Figure 1.11. Efficiency of the system can be measured in zone variance, or variance in peak width (σ^2), and by the number of theoretical plates (N). Ideal systems have very low peak width variance and large numbers of theoretical plates. Because the CE system is a diffusion-limited system, molecular diffusion (D) is the primary cause of peak broadening and other contributions such as mass transfer limitations and frictional forces at the capillary walls can be eliminated. Therefore, σ^2 is determined by:

$$\sigma^2 = 2Dt \tag{1.13}$$

and N is determined by:

$$N = \frac{L^2}{\sigma^2} \tag{1.14}$$

Further examination of Equations (1.13) and (1.14) leads directly to three important characteristics of CE:

1. Application of a high voltage increases the plate number by decreasing analysis time and, therefore, reducing time for diffusion to occur.
2. Highly mobile solutes increase the number of plates in the same manner.
3. Solutes with low diffusion coefficients yield high efficiencies.

Further, the resolution of two peaks, or zones, is given by:

$$R = \frac{\sqrt{N}}{4}\left[\frac{\mu_{ep2} - \mu_{ep1}}{\mu_{ep} + \mu_{eo}}\right] \tag{1.15}$$

where μ_{ep_1} and μ_{ep_2} are the electrophoretic mobilities for the two solutes and $\bar{\mu}_{ep}$ is the average electrophoretic mobility. According to Eq. (1.15), the highest resolution is achieved when $\mu_{eo} = -\bar{\mu}_{ep}$, but to achieve that, experiment times approach infinity. It can also be noted that when the cathode is at the outlet end of the column, better resolution is achieved for anions due to the increased attraction to the anode.

Even with the absence of packing materials and pressure-induced turbulence, there are several factors that affect peak resolution in open-tubular CE systems. Essentially, there are those factors that are operator-dependent and those that are operator-independent. Operator-dependent parameters include factors such as column size, buffer concentration and pH, applied voltage, and temperature. Independent factors are those that are inherently associated with electrophoretic processes, and will be discussed in further detail below.

Capillary size and type can be carefully selected in order to produce high quality analyses. There are several advantages in using capillaries, especially in the range of 20-200 μm i.d. as are common in CZE. Due to the small size and high surface area-to-volume ratio, heat dissipation is easily accomplished and allows much higher voltages to be used. The small diameter increases detector mass-sensitivity in minimizing dilution. Columns are manufactured in coated and uncoated forms with respect to the inner surface of the silica, and are quite inexpensive. There are many types of coatings available and used in analyses that benefit from additional interactions between analyte molecules and various functional groups. In analyses using uncoated silica, the same column can be used repeatedly for any number of buffer systems and compounds, attesting to the robust nature and chemical flexibility of the silica. As with

Figure 1.11. Order of particle migration in a cationic buffer system. Particles migrate according to charge-to-mass ratio, with the smallest, most positive particles migrating through the column at a faster rate than other particles.

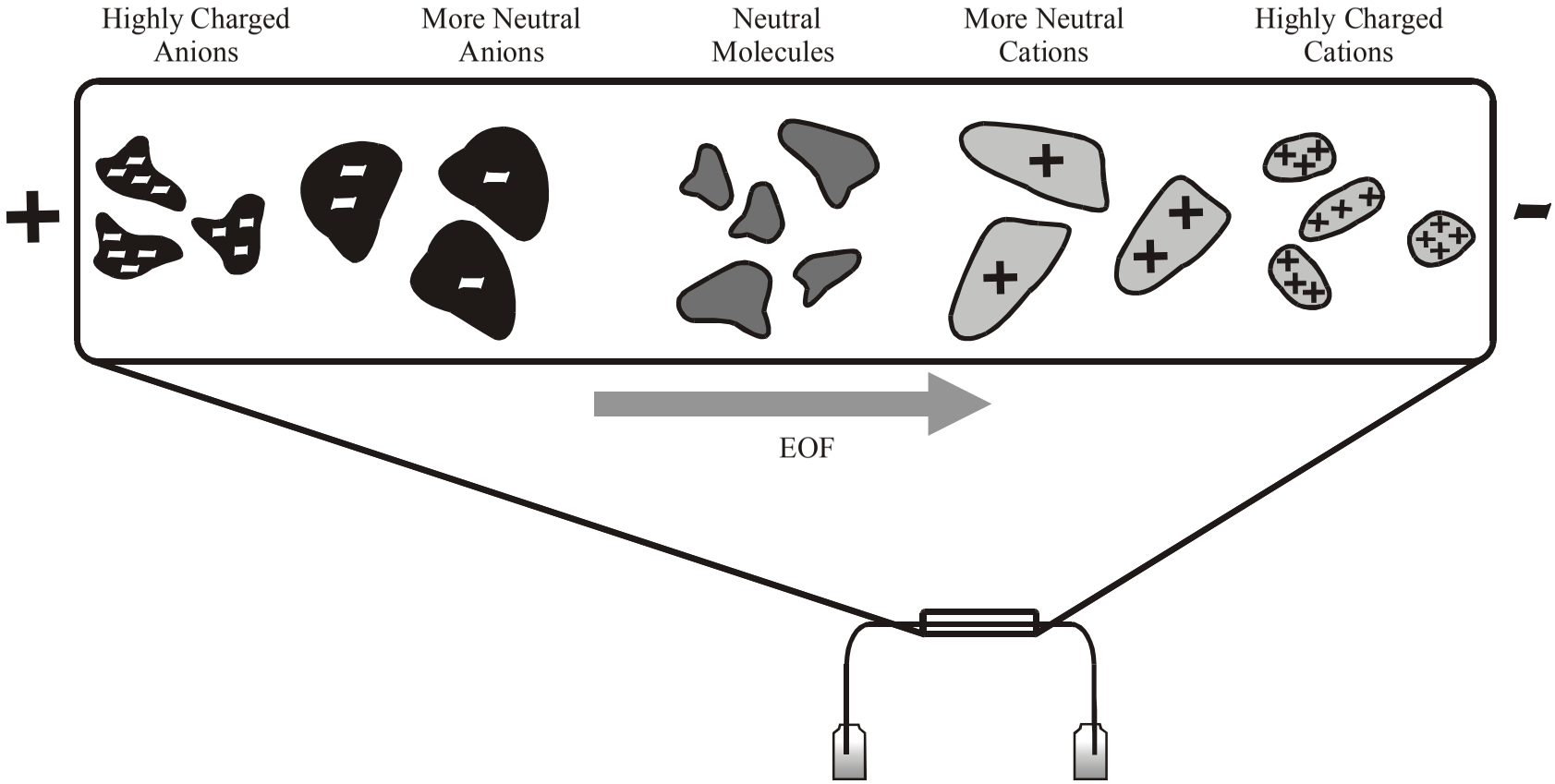
Highly Charged Anions
More Neutral Anions
Neutral Molecules
More Neutral Cations
Highly Charged Cations
+
-
EOF

traditional chromatographic systems, longer columns result in longer analysis time as well as peak broadening. However, longer columns are sometimes needed in order to increase the number of theoretical plates and, therefore, peak resolution.

Running buffer selection is possibly the most important aspect of successful CE analyses. Generally, a suitable buffer has the following characteristics:[41]

1. High buffer capacity in the selected pH range
2. Low detector response
3. Low mobility in order to minimize current generation
4. Availability in high purity grade quantities
5. Low temperature coefficient

There are many guidelines currently established for finding suitable buffers, including information on which buffer systems are most effective with specific classes of analyte compounds.[42] Buffer concentration, theoretically, should be as strong as possible in order to carry the maximum current. However, dilution is often necessary to prevent excess heat generation. Fused silica is relatively stable in the 2-12 pH range,[43] which allows a great deal of experimental optimization for buffer pH. At times, the pH stability of analyte molecules may dictate a definite pH, but generally the pH value is selected such that the analyte molecules are completely ionized. At pH greater than 2-3, the silanol groups along the inner surface of the capillary are completely ionized, although the strongest negative charge is accomplished at a pH less than 9-10. At pH less than 2-3, silanol ionization diminishes to such an extent that the EOF approaches zero.[41,44]

For analyses requiring specialized buffers such as neutral or chiral separations, complexing agents such as borate buffers can be used. In this manner, neutral molecules

complex with buffer molecules in slightly different ways, yielding different electrophoretic mobilities and migration times. Chiral separations often require buffer additives that are discussed in more detail in Chapter 2.

Applied voltage strength affects analysis time and peak resolution in that it is directly related to the current in the system; CE current is a measurement of the EOF rate. Combination of Equations (1.11), (1.13), and (1.14) gives:

$$N = \frac{(\mu_{eo} + \mu_{ep})V}{2D} \tag{1.16}$$

such that the resolution given in Equation (1.15) becomes:

$$R = \frac{1}{4}\sqrt{\frac{(\mu_{eo} - \mu_{ep})V}{2D}} \bullet \left(\frac{\mu_{ep2} - \mu_{ep1}}{\overline{\mu}_{ep} + \mu_{eo}} \right) \tag{1.17}$$

Examination of Equation (1.17) indicates that resolution is directly proportional to the square root of the applied voltage. That is, to increase the resolution by a factor of two, the applied voltage should be quadrupled. However, because of the limitations of CE instrumentation, this can be difficult in that typical CE instruments only apply voltages up to 30 kV. One way to optimize applied voltage is to complete an Ohm's Law plot where current is plotted against the ionic strength of the buffer. This type of plot can also be used to optimize the concentration of electrolyte in the buffer system. Ohm's Law plots are usually linear in some middle region, and confining experimental parameters to this region yields the best results.

Temperature of the column is an important consideration due to its ability to affect the buffer viscosity and to aid in heat dissipation. Generally, instrumentation thresholds and the effectiveness of the cooling system govern the limits of analysis temperature. Without adequate temperature control, sample stability, injection

reproducibility, band broadening, and quantification problems can arise.[41] A highly efficient cooling system can be used to increase heat dissipation and thus allows for higher voltages and buffer concentrations. In addition, higher temperatures decrease analysis time and can improve peak shape while lower temperatures may aid in column stability with buffers that approach the extremes of pH stability. For example, buffers at pH 12 degrade the column at a much faster rate than buffers with pH 10 or 11, but that degradation can be slowed if the analyses are carried out under slightly lower temperatures.

The final operator-dependent factor for peak resolution is the method and time of analyte injection. There are two main methods of analyte injection, electrokinetic and hydrodynamic. An electrokinetic injection is accomplished by replacing the buffer vial at the inlet of the capillary with the sample vial such that both the electrode and the inlet of the capillary are immersed in the sample solution. An injection voltage, governed by instrument limitations, is then briefly applied, and the sample migrates into the column toward the cathode as a result of both electrophoresis and the EOF. This type of injection has advantages in that the sample plug retains the same plug profile from the electroosmotic flow, and the total space occupied by the sample plug inside the column may be smaller that the plug size from a pressure injection, which leaves more column available for the actual separation. However, there are disadvantages as well. The application of voltage creates a preferential injection in which those particles with the highest mobility and attraction to the cathode are injected in larger quantities than those with lower mobilities. In addition, if there is a large difference between the conductivities of the buffer and the sample solutions, the EOF rates and electrophoretic

mobilities of the solutions are different, and it is more difficult to determine the total amount of sample injected.

A hydrodynamic injection is typically performed in the same manner but uses an applied external pressure, usually up to 50 mbar, in place of the applied voltage. The main advantage of this method is that all species are injected at the same relative quantities without preference to more mobile molecules. Because of this property, the injection volume is much more reproducible for solutions of varying concentrations. In contrast, these same solutions injected electrokinetically would exhibit decreased peak areas with increased solution resistance. Fortunately, the main sources of operator influence over injection volume are the magnitude and time of the applied pressure or voltage. Because CE systems are now readily available and automated, a large portion of operator variability is removed.

Experimental parameters can often be used to minimize or eliminate those factors that are operator-independent such as electrodispersion, Joule heating, and interactions between the solution and the capillary wall. Electrodispersion is a result of conductivity (mobility) differences between the running buffer and the analyte. As shown in Figure 1.12, separation is best achieved when the buffer and sample solutions have closely matched conductivities. Solutes with higher mobilities, as in Figure 1.12a, have diffuse leading edges in which sample molecules diffuse from the injected plug into the surrounding buffer, and sharp trailing edges where there is a high concentration of analyte ions at the edge of the sample plug. This ion distribution causes uneven analyte concentrations within the sample plug and is revealed as a heavily tailed peak in the electropherogram. When the solutions are carefully matched (Figure 1.12b), heavy peak

Figure 1.12. Three possible scenarios of buffer and sample conductivities and the resulting peak shapes.

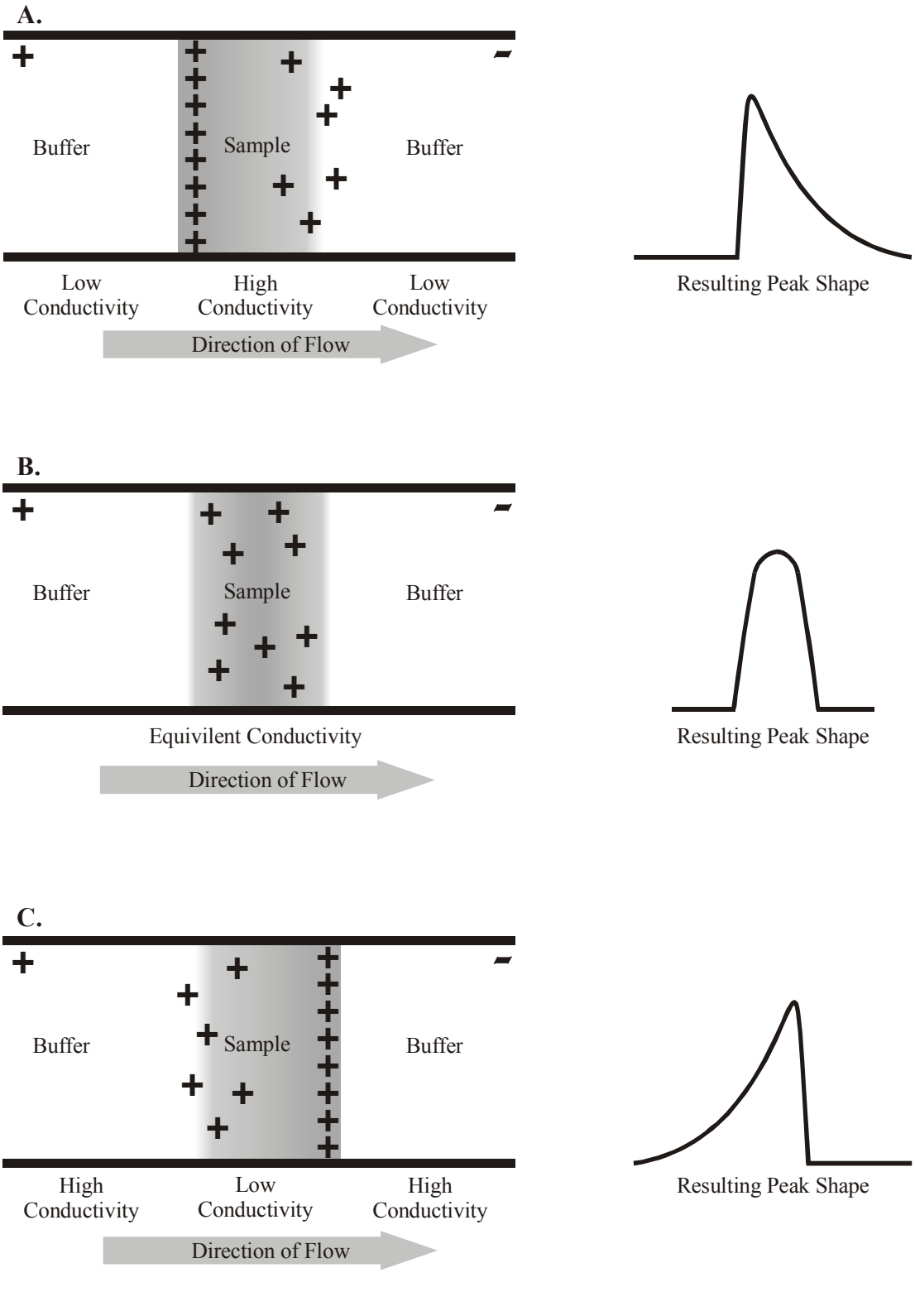
A.
+
-
Buffer
Sample
Buffer
Low Conductivity
High Conductivity
Low Conductivity
Direction of Flow
Resulting Peak Shape
B.
+
-
Buffer
Sample
Buffer
Equivilent Conductivity
Direction of Flow
Resulting Peak Shape
C.
+
-
Buffer
Sample
Buffer
High Conductivity
Low Conductivity
High Conductivity
Direction of Flow
Resulting Peak Shape

trailing due to electrodispersion does not occur and the ion concentration inside the analyte plug remains relatively constant without overly sharp or highly diffuse edges. In contrast, if the buffer has a higher mobility than the sample plug, as shown in Figure 1.12c, the leading edge of the sample plug is sharp and highly concentrated while the trailing edge is much more diffuse, and some analyte molecules trail behind the plug in the buffer. This situation also produces a heavily tailed peak as in the previously described scenario, but in the opposite direction. The diffuse and sharp edges are a result of voltage drops encountered by ions diffusing across the sample-buffer interface and accelerating either toward or away from the interface determined by the charge and direction of the voltage drop.

Perhaps the most common resolution-depleting factor is known as Joule heating. Joule heating refers to excess heat produced when an electrical current is passed through an electrolyte solution. Because voltages can be quite high in CE, this phenomenon can be very significant. As long as a CE system is efficiently dissipating this produced heat through cooling systems or modifications of experimental parameters, Joule heating is controlled. If these measures are not effective, however, the temperature of the column and the solution inside rises gradually. As the temperature increases, several consequences, such as bubble formation and reduction in conductivity can occur in addition to those effects discussed above. Although high buffer concentration and relatively large applied voltages are favored for high resolution, a great deal of heat generation is also associated with both. Higher temperatures lower the viscosity and increase the mobility of the buffer and analyte solutions. As a result, the plug-flow profile normally seen in CE changes into a more parabolic shape, which drastically

reduces separation efficiency. While narrow capillaries seem to dissipate heat more efficiently, they are plagued with other problems such as inaccurate sample loading, capillary clogging, and decreased optical sensitivity due to decreased path length. Many factors can be altered in order to preserve separation efficiency, eliminate Joule heating, and retain high resolution, but there is usually a balance achieved in which some parameters are ideal while others are not.

Finally, solute interactions with the capillary walls can decrease analyte separation success. Because CE columns are highly charged in the interior surface, any buffer or sample components with an opposite charge is attracted to the wall which slows its mobility in the column and decreases peak resolution. Solute-capillary interactions have been addressed and well documented in the literature. Among the proposed solutions are altered buffer concentrations and pH, wall coatings on the silica, and solute-wall charge matching.[45-52] Unfortunately, most manipulations increase the probability of other detrimental factors, such as Joule heating. As a result, solute-capillary wall interactions should be dealt with on an experiment-by-experiment basis.

One of the goals of the research presented here is to increase the awareness and use of CE in basic separations as well as in the development of new techniques. As has been shown, CE requires many considerations in order to perform successful analyses. With these considerations properly addressed, however, CE also has a great deal of untapped potential as a powerful separations technique.

Capillary Electrophoretic Interfaces

The combination of CE with various secondary detection systems has several advantages. Because traditional CE detection is often performed on-column even in an interfaced system, a reference detection method is automatically built into the interface. By far, the most common CE interfaces are with mass spectrometry (MS), specifically electrospray ionization MS. While there are several ways this is accomplished, the basic features include the nebulization of the CE eluent directly into the sample chamber of the MS instrument. Because molecules are charged within the CE system, additional ionization steps are rarely necessary, and solvent elimination is accomplished in the nebulization process. Perhaps the most common difficulty encountered in early CE-MS attempts is the introduction of sodium or potassium ions into the MS system from commonly used CE buffers, although many researchers have successfully overcome this obstacle.[53-56]

Recently, two successful interfaces between CE and FT-IR spectrometry have been developed.[7,57,58] This type of interface is highly advantageous in that FT-IR spectrometry is known for its high sensitivity, structural specificity, and non-destructive nature. There are two types of CE/FT-IR interfaces, on-column and off-column. An on-column interface works in much the same way as traditional UV-vis detection in that it detects buffer-analyte complexes as they move past the detection window.[58] For those interested in neat analyte spectra, this method is not appropriate. An off-column FT-IR detector is capable of spectrally analyzing deposits that are composed only of sample molecules.[7,57] In this manner, more direct spectral comparisons are possible with less required spectral processing, such as buffer subtraction.

There are three general requirements for CE interfaces in which the second instrument is used as an off-column detector.[59] First and foremost, electrical contact must be maintained. Breaking electrical contact disrupts the current in the system and interrupts the EOF, leading to band broadening, loss of solvent flow, and possible analyte mixing. In order to prevent these consequences, a wide variety of schemes has been developed including sheath liquids,[55,59-61] coupled columns,[59,62-65] cracked or pierced columns,[66] wires that surround or are inserted into the columns,[64,65,67] and metal coatings.[7,64,68,69] Sheath liquids, however, can significantly dilute eluent volume, while coupled column and cracked or pierced column interfaces tend to be quite difficult to prepare and fragile when in use. Wires have been shown to block the column or to promote bubble formation, and can be difficult to properly position so as to minimize disturbance of the narrow solute bands.[70] Metal coating interfaces have been shown to be highly robust and can vary significantly in nature, including metal flakes glued to the column surface and conductive paint applied directly to the column. Electrical contact is monitored in CE systems by recording the current trace. Significant dips or spikes in the trace indicate weak or unstable electrical contact.

The second general interface requirement is that the low flow rate of the CE system be adapted to the required flow for the interfaced instrument. Typical CE flow rates are approximately 100 nL/min, and there are no commercially available nebulizers designed to operate at very low flow rates. The most common adaptation for this particular characteristic is the use of make-up buffers,[54,55,59,60] which have the same disadvantage as sheath liquids in dilution of CE eluent. A more advantageous and increasingly popular approach is to design a nebulizer to operate at these flow

rates.[7,57,63,65,67] Nebulizer designs include pulled or etched CE capillary tips and custom-designed microconcentric glass nebulizers. Other researchers simply choose to accept this loss of resolution rather than develop a volume equalizing system.[53]

When the CE and interface volumes are not equalized, the third concern becomes quite significant. The pulling of liquid by the nebulizer creates a laminar flow inside the capillary column. As a result, narrow solute bands are degraded and migration times can undergo dramatic shifts. Furthermore, the number of theoretical plates is somewhat decreased, which leads directly to a drastic loss of resolution. Theoretical and experimental investigation of this resolution reduction is well documented.[60,71] Methods used to prevent laminar flow introduction include nebulization of a separate liquid that never enters the chromatographic system,[59] minimization of nebulizer gas flows,[66,72] and the application of a negative pressure on the inlet vial to counteract any positive pressure exerted by the nebulization system.[73]

Interfacing CE and FT-IR spectrometry has an additional requirement that must be met. The electrolyte solutions used as running buffers are generally highly absorbant in the IR region and can mask any characteristic analyte bands. Therefore, complete solvent elimination should occur during the nebulization process and prior to spectral interrogation. This is best accomplished with highly volatile buffers such as ammonium acetate or ammonium formate. Unfortunately, a loss of electrical conductivity is also expected with the use of these solutions.

Once these requirements are satisfied, there are two considerations for CE/FT-IR interfaces: spectral sensitivity and method of deposition. The combination of any

separation method with FT-IR spectrometry is best accomplished when the sensitivity is maximized. Sensitivity for a fixed mass of analyte is defined as:

$$Sensitivity = SNR \times \frac{Sample\ Quantity \times Absorptivity \times Pathlength}{Area\ of\ the\ Sample} \qquad (1.18)$$

As seen from Equation (1.2) and Equation (1.18), the sensitivity of the system is maximized when the area of the sample closely matches the area of the limiting aperture. It is also important to match the sample size to that of the detector area. If the sample size is smaller than the detector area, the amount of noise in the system is increased with respect to the signal, the SNR decreases, and sensitivity suffers. If the sample area greatly exceeds that of the limiting aperture or detector, however, it is not possible to achieve the theoretical SNR due to loss of signal when transmitted or reflected radiation does not reach the detector.

Finally, sample deposition methods are significantly different from those in CE-MS interfaces. In a MS interface, the sample is sprayed into an evacuated chamber, and ions are accelerated toward the mass spectrometer. CE/FT-IR interfaces, however, are operated at ambient pressure, and the outlet of the nebulizer is left open to the atmosphere. While ambient pressure is easier to accommodate in an experimental setting, the sample spray must be contained to as small of an area as possible. Additionally, the deposit should be a single droplet instead of a mist of smaller droplets in order to maximize analyte concentration possible within a small area. Without splatter patterns, the highest possible concentration of analyte in the deposit is accomplished, which yields the optimum quality IR spectrum.

Carbohydrate Analysis

The term "carbohydrate" refers to compounds composed of one or more monosaccharides, which are found in virtually every living organism as well as some inert organisms. They are frequently associated with cancerous cells, debilitating diseases, and, of course, eating habits. Because of the multitude of responsibilities carbohydrates have, there are millions of possible structures and combinations of these molecules. Of particular interest in biochemical communities and cancer research are complex carbohydrates known as oligosaccharides. These compounds are typically found attached to other cell parts such as proteins and lipid molecules. A protein with attached oligosaccharides is called a glycoprotein, and is often responsible for cell-cell interactions, virus recognition, and other life-sustaining processes. These attached oligosaccharides are said to govern any number of biological processes, with the possibilities increasing daily. For example, oligosaccharides have been shown to affect glycoprotein folding and subunit structure,[74] and hormone and enzyme activity.[75,76] Furthermore, many of these glycoproteins are found along the outer portion of cell membranes and, therefore, are responsible for cellular recognition and potential immunological responses.[77-82] Carbohydrates have also been shown to be reliable disease markers.[12,79,83-85]

While there are many kinds of oligosaccharides, there are two groups in mammalian glycoproteins: N-linked and O-linked. Mammalian N-linked compounds are connected to the parent protein or lipid through the amide group of an asparagine side chain in an Asn-X-Ser(Thr) molecule while O-linkages are through the hydroxyl group of Ser or Thr residues. In addition, mammalian oligosaccharides differ slightly from plant

oligosaccharides such that the subgroup of N-linked mammalian oligosaccharides is a somewhat smaller portion of all possible molecules. These compounds are all composed of various combinations of six monosaccharide units, L-fucose (Fuc), *N*-acetyl-D-glucosamine (GlcNAc), *N*-acetyl-D-galactosamine (GalNAc), *N*-acetyl-D-neuraminic acid (NANA), D-galactose (Gal), and D-mannose (Man). The core structure of all mammalian N-linked oligosaccharides, shown in Figure 1.13, always consists of two GlcNAc residues and three Man residues, and can sometimes include a Fuc molecule. From the core structure, there are nearly an infinite number of possibilities in the overall structure, including multiple branching, various numbers of NANA on the terminus of each branch, and varying composition. However, of these possibilities, researchers estimate that only about two thousand structures actually exist, and approximately two hundred of these are known and characterized.

Unfortunately, separation and identification of known oligosaccharides is tedious, destructive, and somewhat variable in reliability. Determination of unknown structures is at least as difficult, and often nearly impossible. Current methods of analysis include liquid chromatography-mass spectrometry (LC-MS) systems in which compounds are separated not into individual components, but into groups of similar components at best.

To increase the scientific knowledge and more effectively fight carbohydrate-related diseases, an additional analysis method is needed. Therefore, the application of CE and FT-IR spectrometry has been attempted. Because of the small sample requirements of both techniques, the necessary amounts of costly and rare oligosaccharide samples are minimized, and due to the non-destructive nature of the interface, the compounds may be recovered for future analyses with traditional methods.

Figure 1.13. N-linked mammalian oligosaccharide core structure, without (**A**) and with (**B**) the possible Fucose molecule.

A.

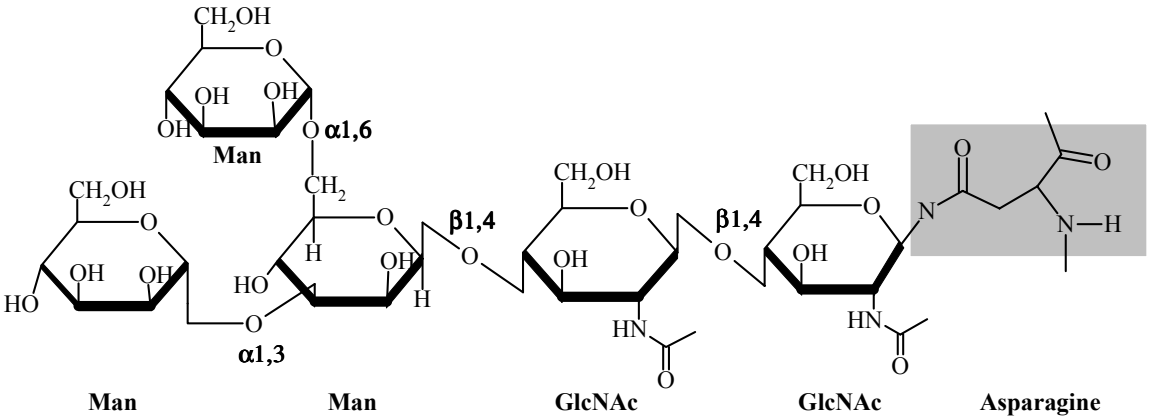
α1,6
Man
α1,3
β1,4
β1,4
Man
Man
GlcNAc
GlcNAc
Asparagine

B.

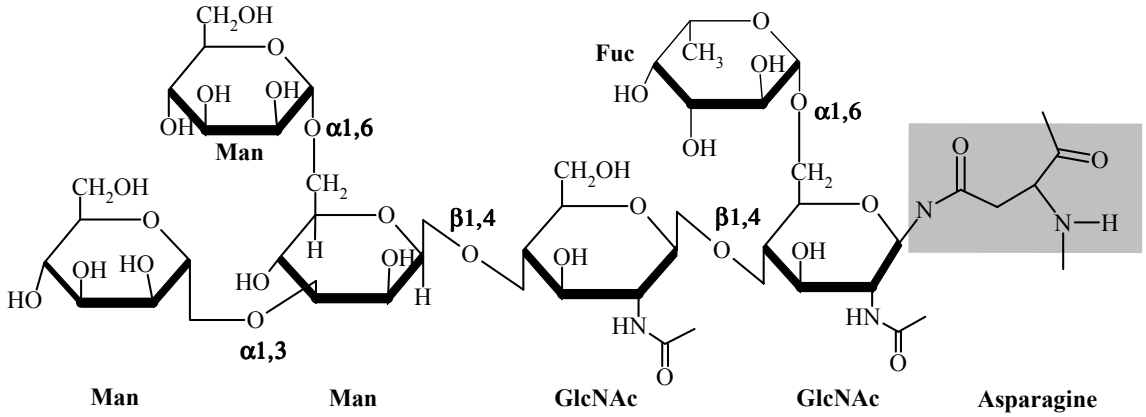
Fuc
α1,6
Man
α1,3
β1,4
β1,4
Man
Man
GlcNAc
GlcNAc
Asparagine

FT-IR spectrometry has long been used to investigate monosaccharides and polysaccharides in the paper and food industries,[86]but has not been utilized often for carbohydrate analysis in biochemical areas due to difficulty in distinguishing characteristic bands. Recently, however, chemometric methods were successfully applied to address this problem.[87-90] CE is often used to characterize derivatized oligosaccharides,[91-94] but is currently limited in the ability to separate and detect oligosaccharides in the pure native form.

FT-IR spectrometry and CE are both powerful techniques with high sensitivity and small sample requirements. A combination of the two techniques, especially applied to complex carbohydrates, dramatically increases the available information and methodology available for high quality analytical analyses.

References

1. Wilson, R.; Smith, A.; Kacurakova, M.; Saunders, P.; Wellner, N.; Waldron, K. *Plant Physiology* **2000**, *124* (1), 405.
2. Sohn, I.; Park, C. *Industrial & Engineering Chemistry Research* **2002**, *41* (10), 2424.
3. Himmelsbach, D.; Khalili, S.; Akin, D. *Journal of the Science of Food and Agriculture* **2002**, *82* (7), 696.
4. Iglesias, M.; de la Puente, G.; Fuente, E.; Pis, J. *Vib. Spectrosc.* **1998**, *17* (1), 52.
5. Lin, S.; Li, M.; Liang, R.; Lee, S. *Spectrochimica Acta Part A-Molecular and Biomolecular Spectroscopy* **1998**, *54* (10), 1517.
6. Ruau, O.; Landais, P.; Gardette, J. *Fuel* **1997**, *76* (7), 653.
7. Jarman, J.; Todebush, R.; de Haseth, J. *J. Chromatogr. A* **2002**, *976* (1-2), 26.
8. Jarman, J. L.; Seerley, S. I.; Todebush, R. A.; de Haseth, J. A. *Submitted for publication in Applied Spectroscopy.* **2003**.
9. Lester, D. S.; Kidder, L. H.; Levin, I. W.; Lewis, E. N. *Cellular and Molecular Biology* **1998**, *44* (1), 29-38.
10. Kidder, L. H.; Colarusso, P.; Stewart, S. A.; Levin, I. W.; Appel, N. M.; Lester, D. S.; Pentchev, P. G.; Lewis, E. N. *Journal of Biomedical Optics* **1999**, *4* (1), 7-13.
11. Kneipp, J.; Lasch, P.; Baldauf, E.; Beekes, M.; Naumann, D. *Biochimica Et Biophysica Acta-Molecular Basis of Disease* **2000**, *1501* (2-3), 199.
12. Yano, K.; Ohoshima, S.; Gotou, Y.; Kumaido, K.; Moriguchi, T.; Katayama, H. *Anal. Biochem.* **2000**, *287* (2), 218-225.

13. Filippelli, M. *Appl. Organomet. Chem.* **1994**, *8* (7-8), 687-691.

14. Smith, B. C. *Fundamentals of Fourier Transform Infrared Spectroscopy*; CRC Press: Boca Raton, FL, 1996.

15. Meyer, A.; Budzinski, H.; Powell, J. R.; Garrigues, P. *Polycyclic Aromatic Compounds* **1999**, *13* (3), 329-339.

16. Spectra-Tech. "Contaminant Analysis by FT-IR Microsocpy," 2 (1); Spec-Tech Inc.; 2 (1): Stamford, CT.

17. Fu, W. R.; Lien, W. R. *Journal of Food Science* **1998**, *63* (1), 80-83.

18. Rampon, V.; Robert, R.; Nicolas, N.; Dufour, E. *Journal of Food Science* **1999**, *64* (2), 313-316.

19. Cho, L. L.; Reffner, J. A.; Gatewood, B. M.; Wetzel, D. L. *Journal of Forensic Sciences* **1999**, *44* (2), 275-282.

20. Chen, R.; Jakes, K. *Appl. Spectrosc.* **2002**, *56* (5), 650.

21. Hoshino, A.; Tsuji, M.; Fukuda, K.; Nonagase, M.; Sawada, H.; Kimura, M. *Soil Science and Plant Nutrition* **2002**, *48* (4), 473.

22. Abbott, T.; Felker, F.; Kleiman, R. *Appl. Spectrosc.* **1993**, *47* (2), 189.

23. Bartick, E. G.; Tungol, M. W.; Reffner, J. A. *Anal. Chim. Acta* **1994**, *288* (1-2), 35-42.

24. ZiebaPalus, J. *Mikrochim. Acta* **1997**, 359.

25. Gal, T.; Veress, T.; Ambrus, I. *Mikrochim. Acta* **1997**, 379.

26. Ferrer, N. *Mikrochim. Acta* **1997**, *Suppl. 14*, 329-332.

27. Aparicio, S.; Doty, S.; Camacho, N.; Paschalis, E.; Spevak, L.; Mendelsohn, R.; Boskey, A. *Calcified Tissue International* **2002**, *70* (5), 429.

28. Lin, S.; Niu, D.; Tu, C.; Lin, H.; Li, M.; Cheng, Y. *Ultrastructural Pathology* **2001**, *25* (5), 360.

29. Dukor, R.; Liebman, M.; Johnson, B. *Cellular and Molecular Biology* **1998**, *44* (1), 217.

30. Harrick, N. J. *Anal. Chem.* **1964**, *36* (1), 188.

31. Harrick, N. J. *Appl. Opt.* **1966**, *5* (7), 1236.

32. Harrick, N. J. *Internal Reflection Spectroscopy*; Harrick Scientific Corp.: Ossining, New York, 1987.

33. Lodge, A., 1886.

34. Smirnow, I. *Berliner Kinische Wochenschrift* **1892**, *32*, 645.

35. Hjerten, S.; Jerstedt, S.; Tiselius, A. *Anal. Biochem.* **1965**, *11* (2).

36. Virtanen, R. *Acta Polytechnica Scandinavica-Chemical Technology Series* **1974**, 123, 1-67.

37. Jorgenson, J. W.; Lukacs, K. D. *J. Chromatogr.* **1981**, *218* (1-3), 209-216.

38. Jorgenson, J. W.; Lukacs, K. D. *Anal. Chem.* **1981**, *53* (8), 1298-1302.

39. Jorgenson, J. W.; Lukacs, K. D. *Science* **1983**, *222* (4621), 266-272.

40. Li, S. F. Y. *Capillary Electrophoresis: Principles, Practice, and Applications*; Journal of Chromatography Library; vol. 52: Elsevier, 1992.

41. Chankvetadze, B. *Capillary Electrophoresis in Chiral Analysis*; John Wiley & Sons, Ltd.: New York, NY, 1997.

42. Landers, J. P. In *Handbook of Capillary Electrophoresis*; Landers, J. P., Ed.; CRC Press: Boca Raton, 1994, pp 625-633.

43. Regnier, F. E. a. W., D. In *Capillary Electrophoresis Technology*; Guzman, N. A., Ed.; Chromatographic Science Series; vol. 64; Marcel Dekker, Inc.: New York, 1993, pp 287-310.

44. Mazzeo, J. R. a. K., I. S. In *Handbook of Capillary Electrophoresis*; Landers, J. P., Ed.; CRC Press: Boca Raton, 1994, pp 495-512.

45. Green, J. S.; Jorgenson, J. W. *J. Chromatogr.* **1989**, *478* (1), 63-70.

46. Bushey, M. M.; Jorgenson, J. W. *J. Chromatogr.* **1989**, *480*, 301-310.

47. Huang, X. H.; Coleman, W. F.; Zare, R. N. *J. Chromatogr.* **1989**, *480*, 95-110.

48. Swedberg, S. A. *Anal. Biochem.* **1990**, *185* (1), 51-56.

49. Emmer, A.; Jansson, M.; Roeraade, J. *J. High Resolut. Chromatogr.* **1991**, *14* (11), 738-740.

50. Liu, J. P.; Dolnik, V.; Hsieh, Y. Z.; Novotny, M. *Anal. Chem.* **1992**, *64* (13), 1328-1336.

51. Schure, M. R.; Lenhoff, A. M. *Anal. Chem.* **1993**, *65* (21), 3024-3037.

52. Dougherty, A. M. a. S., A. R. In *Capillary Electrophoresis Technology*; Guzman, N. A., Ed.; Chromatographic Science Series; vol. 64; Marcel Dekker, Inc.: New York, 1993, pp 435-472.

53. Olesik, J. W.; Kinzer, J. A.; Olesik, S. V. *Anal. Chem.* **1995**, *67* (1), 1-12.

54. Sutton, K. L.; B'Hymer, C.; Caruso, J. A. *Journal of Analytical Atomic Spectrometry* **1998**, *13* (9), 891.

55. B'Hymer, C.; Day, J. A.; Caruso, J. A. *Appl. Spectrosc.* **2000**, *54* (7), 1040-1046.

56. Vuorensola, K.; Kokkonen, J.; Siren, H.; Ketola, R. A. *Electrophoresis* **2001**, *22* (20), 4347-4354.

57. Todebush, R. A.; He L. T.; de Haseth, J. A. *Anal. Chem.* **2003**, *75* (6), 1393-1399.

58. Kolhed, M.; Hinsmann, P.; Svasek, P.; Frank, J.; Karlberg, B.; Lendl, B. *Anal. Chem.* **2002**, *74* (15), 3843-3848.

59. Schaumloffel, D.; Prange, A. *Fresenius' J. Anal. Chem.* **1999**, *364* (5), 452-456.

60. Kinzer, J. A.; Olesik, J. W.; Olesik, S. V. *Anal. Chem.* **1996**, *68* (18), 3250-3257.

61. Michalke, B.; Schramel, P. *Fresenius' J. Anal. Chem.* **1997**, *357* (6), 594-599.

62. Figeys, D.; Ducret, A.; Aebersold, R. *J. Chromatogr. A* **1997**, *763* (1-2), 295-306.

63. Tangen, A.; Lund, W.; Josefsson, B.; Borg, H. *J. Chromatogr. A* **1998**, *826* (1), 87-94.

64. Herring, C. J.; Qin, J. *Rapid Commun. Mass Spectrom.* **1999**, *13* (1), 1-7.

65. Tong, W.; Link, A.; Eng, J. K.; Yates, J. R. *Anal. Chem.* **1999**, *71* (13), 2270-2278.

66. Moini, M. *Anal. Chem.* **2001**, *73* (14), 3497-3501.

67. Deng, B. Y.; Chan, W. T. *J. Chromatogr. A* **2000**, *891* (1), 139-148.

68. Kelly, J. F.; Ramaley, L.; Thibault, P. *Anal. Chem.* **1997**, *69* (1), 51-60.

69. Barnidge, D. R.; Nilsson, S.; Markides, K. E. *Anal. Chem.* **1999**, *71* (19), 4115-4118.

70. Smith, A. D.; Moini, M. *Anal. Chem.* **2001**, *73* (2), 240-246.

71. Li, J. X.; Umemura, T.; Odake, T.; Tsunoda, K. *Anal. Chem.* **2001**, *73* (24), 5992-5999.

72. Huikko, K.; Kotiaho, T.; Kostiainen, R. *Rapid Commun. Mass Spectrom.* **2002**, *16* (16), 1562-1568.

73. Lu, G. H.; Bird, S. M.; Barnes, R. M. *Anal. Chem.* **1995**, *67* (17), 2949-2956.

74. Orberger, G.; Geyer, R.; Stirm, S.; Tauber, R. *Eur. J. Biochem.* **1992**, *205* (1), 257-267.

75. Fujii, T.; Miyahara, Y. *Appl. Spectrosc.* **1998**, *52* (1), 128-133.

76. Bousfield, G. R.; Baker, V. L.; Gotschall, R. R.; Butnev, V. Y.; Butnev, V. Y. *Methods-A Companion to Methods in Enzymology* **2000**, *21* (1), 15-39.

77. Stoolman, L. M. *Cell* **1989**, *56* (6), 907-910.

78. Brandley, B. K.; Swiedler, S. J.; Robbins, P. W. *Cell* **1990**, *63* (5), 861-863.

79. Watson, S. R.; Fennie, C.; Lasky, L. A. *Nature* **1991**, *349* (6305), 164-166.

80. Tsuzuki, A.; Tateishi, T.; Ohno, N.; Adachi, Y.; Yadomae, T. *Bioscience Biotechnology and Biochemistry* **1999**, *63* (1), 104-110.

81. Ooi, V. E. C.; Liu, F. *Current Medicinal Chemistry* **2000**, *7* (7), 715-729.

82. Talaga, P.; Bellamy, L.; Moreau, M. *Vaccine* **2001**, *19* (20-22), 2987-2994.

83. Riebe, D.; Thorn, W. *Electrophoresis* **1991**, *12* (4), 287-293.

84. Sakagami, H.; Takeda, M. *International Journal of Oncology* **1992**, *1* (3), 283-287.

85. Cohenford, M. A.; Qiao, L.; Rigas, B. *Gastroenterology* **1995**, *108* (4), 457A-457A.

86. Kennedy, J. F.; Pagliuca, G. *Carbohydrate Analysis: A Practical Approach*; Chaplin, M.; Kennedy, J., Eds.; Oxford: England, 1994, pp 43-68.

87. Thomas, A. G. A.; de Haseth, J. A. *To be submitted.* **2003**.

88. Thomas, A. G. A.; de Haseth, J. A. *To be submitted* **2003**.

89. Melkowits, R. B.; and de Haseth, J. A. *To be submitted.* **2003**.

90. Melkowits, R. B.; Levery, S. B.; and de Haseth, J. A. *To be submitted.* **2003**.

91. Huang, Y. P.; Mechref, Y.; Novotny, M. V. *Carbohydr. Res.* **2000**, *323* (1-4), 111-125.

92. Wang, C. Y.; Hsieh, Y. Z. *J. Chromatogr. A* **2002**, *979* (1-2), 431-438.

93. Militsopoulou, M.; Lamari, F. N.; Hjerpe, A.; Karamanos, N. K. *Electrophoresis* **2002**, *23* (7-8), 1104-1109.

94. Gennaro, L. A.; Delaney, J.; Vouros, P.; Harvey, D. J.; Domon, B. *Rapid Commun. Mass Spectrom.* **2002**, *16* (3), 192-200.

CHAPTER 2

MICELLAR ELECTROKINETIC CHROMATOGRAPHIC INVESTIGATIONS OF ENANTIOMERIC MICROBIAL DEGRADATION PATTERNS IN THREE CHIRAL PESTICIDES[1]

[1] Jarman, J. L.; A. W. Garrison; W. J. Jones, and J. K. Avants. To be submitted to *Journal of Chromatography A* for publication.

Abstract

Three chiral pesticides of environmental interest, imazaquin, fonofos, and metalaxyl, were analyzed using chiral capillary electrophoretic techniques. Methodology development included cyclodextrin and micellar compound optimization and calibration curve determination. Soil samples from three federal land plots in two geographical regions were spiked with each compound, and chiral separations were performed at various time intervals to determine degradation patterns. While the soil slurries were created identically, separation methods were optimized for each of the three pesticide compounds. Of particular interest were enantioselective microbial degradation patterns and the differences in these from site to site. Metalaxyl underwent chiral degradation in a single soil type, but did not exhibit degradation in either of the other soils. Imazaquin and fonofos exhibited only uniform degradation, although it cannot be concluded that overall loss of either compound was due to microbial populations present. It is expected, however, that all three compounds will eventually degrade enantioselectively due to various microbes present in the soil matrices.

Introduction

While the global view of pesticide application changes with the development of more environmentally friendly compounds, pesticides previously applied in mass quantities still present possible pollution and exposure problems. Three such compounds, imazaquin, fonofos, and metalaxyl, are chiral members of different pesticide classes commonly used in modern agriculture. Compound structures are shown in Figure 2.1.

Imazaquin, a relatively non-toxic and moderately persistent herbicide, is frequently used to control the growth of weeds in soybean crops, turf, and ornamentals.[1,2] Imazaquin, a member of the imidazolinone class, is highly water-soluble, has a relatively long half-life when solvated, and is primarily broken down through microbial degradation.[3] There is significant data available on imazaquin exposure effects, but all data pertain to exposure to the racemate, not to the individual enantiomers. Fonofos, a moderately persistent organophosphorus insecticide also known as Dyfonate, is primarily applied to corn crops.[4] This highly toxic and relatively water-insoluble compound has been known to cause death due to respiratory arrest and has been credited with at least 21 human poisonings.[4] Finally, metalaxyl is an acetanilide fungicide primarily applied to tobacco, ornamentals, conifers, and turf.[5] It has been shown to affect the liver in large doses and is under investigation as a carcinogenic compound.[6] Although non-toxic to freshwater fish, it has been shown to have adverse effects on freshwater aquatic invertebrates and is highly water-soluble.[7]

Even when pesticides are applied correctly, collection due to field run-off and multiple applications over a given area can easily concentrate such compounds in streams and low-lying areas. Increased concentrations lead to an increased probability of adverse

Figure 2.1. Structures of the chiral pesticides Imazaquin, Metalaxyl, and Fonofos. Chiral centers are denoted by *.

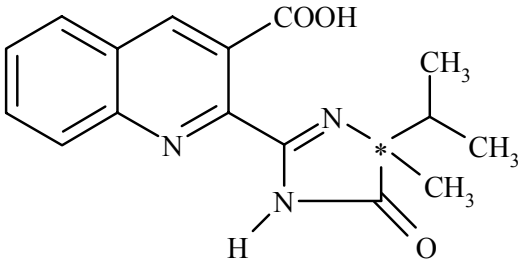

Imazaquin

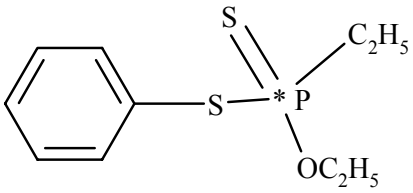

Fonofos

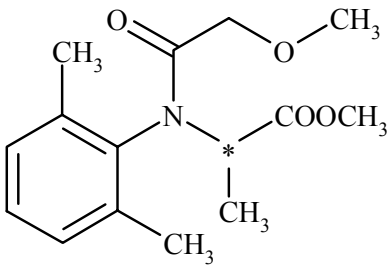

Metalaxyl

exposure effects. As has been shown in the case of the infamous pesticide DDT, the pesticide degradation products or contaminants may be more harmful to biological systems or to the environment than the parent compound or compounds.[8,9] It is because of these possibilities that degradation studies on these and other pesticides are crucial.

Pesticide degradation can be caused by any number of factors including weather conditions, soil pH and composition, or microbial populations.[10] While many studies have been completed on overall pesticide degradation due to these processes, a noticeably smaller amount of data has been collected on enantioselective degradation patterns of chiral pesticides. In many cases, the enantiomers of these compounds have significantly different effects in the environment and in biological systems. For example, one isoform might be toxic to a particular species while the other may be innocuous.[11] In addition, characteristics of the enantiomer pair can lead to differences in compound effectiveness between different microbial populations.[12,13]

The microbial population present may preferentially increase the activity of one enantiomer due to enhanced or discouraged performance of either enantiomer. Preferential activity may, in turn, alter several characteristics such as toxicity, biological uptake, and degradation rates.[11,14-17] If the active enantiomer is degrading at a different rate than its counterpart, application and exposure information should be revised to reflect this aspect of pesticide use.

The *R* enantiomer of metalaxyl has been shown to be the active compound, and there are commercially available *R*-enriched products. These *R*-enriched products are twice as effective as racemic mixtures in real applications.[18] Through the increase in efficiency of the product, the total amount of pesticide released into the environment is

drastically reduced. Therefore, complete characterization of the enantioselective degradation of these molecules is essential in order to maximize the effectiveness of the compound, while a safe environmental contamination level is maintained.

Traditional methods for the analysis of chiral pesticides include high-performance liquid chromatography (HPLC) and gas chromatography (GC). Both of these techniques, however, require relatively expensive chiral columns that are specific to the analyte in question. In contrast, chiral analyses accomplished with traditional capillary electrophoresis (CE), also called capillary zone electrophoresis (CZE), and micellar electrokinetic chromatography (MEKC) require only micelle-forming compounds such as sodium dodecyl sulfate (SDS) and chiral selectors such as cyclodextrins (CDs) to achieve enantiomeric separations. These additives are easily incorporated into the existing electrolyte solutions, or running buffers. As a result, rapid chiral analyses are easy to complete and yield reliable, reproducible results.

Micellar electrokinetic chromatography (MEKC) was first introduced in 1984 as a means of separating neutral compounds. Traditional CE cannot accomplish neutral separations because the lack of self-electrophoretic ability in neutral compounds causes them to elute as one unresolved peak.[19] In this hybrid technique that combines the nature of traditional CE with the added partitioning phenomena of a stationary phase, a pseudo-phase is introduced in the form of a charged compound that possesses an electrophoretic mobility and can therefore retain the neutral compounds that would otherwise migrate at the same rate as the electroosmotic flow.[20]

Micellar-forming compounds, commonly called surfactants or detergents, are particularly attractive as separation aids because they increase the solubility of relatively

hydrophobic compounds. The surfactants, as shown in Figure 2.2, are typically long hydrophobic alkyl chains (tails) attached to a polar group (head). For each compound, there is a concentration above which the molecule forms aggregates in aqueous solutions, which are assumed to be spherical with the heads forming the outer surface and the tails pointed into the center.[21] These aggregates, also shown in Figure 2.2, are known as micelles; the concentration above which micelles form is referred to as the critical micelle concentration (CMC). The micelles typically have a different electrophoretic mobility from the surrounding aqueous phase, therefore corresponding to the stationary phase in a liquid chromatographic separation. As a result, a partitioning system is developed in which analyte molecules move selectively between the non-polar (micelle) phase and the polar (buffer) phase. However, when developing chiral separation techniques, it is crucial that the concentration of the surfactant exceed the CMC in order to ensure the formation of the pseudo-phase. The CMC is dependent on temperature, salt concentration, and buffer additives so that all other parameters should be optimized prior to micelle optimization. Other identifying features of micellar compounds are the aggregation number (n), defined as the number of molecules in a given micelle, and the Kraft point (K_p), or the temperature above which surfactant solubility rises dramatically due to increased micelle formation. According to Terabe, there are three general requirements for selecting an appropriate micellar compound for MEKC:[22]

1. The surfactant must have sufficient solubility in the buffer solution to form micelles.
2. The micellar solution must be homogeneous and compatible with the detector used, e.g. UV transparent for UV detection.

3. The micellar solution must have a low viscosity.

Additionally, the CMC and *n* values should easily be accommodated by the buffer system, and the pH must remain constant throughout the entire course of the analyses. Particulate matter must be filtered out from the buffer and analyte solutions, and the buffer should not be degassed due to problematic bubbling. MEKC is also much more temperature-sensitive than CE and high concentrations of cationic surfactants can reverse the EOF, which requires the reversal of the instrument polarity to facilitate analyte detection.[19,23-25] Perhaps the most common micellar compound used is SDS, which has a CMC of 0.008 M and an aggregate number of 58 at 25°C.[26]

During the course of a separation, there are three main interactions between the micellar compound and the analyte or other solutes, as shown in Figure 2.3. The solute can be adsorbed to the surface of the polar phase by electrostatic or dipole interactions, the solute can actually participate in the formation of the micelle, or the solute can be incorporated into the core of the micelle. The degree to which each of these actually occurs depends on the nature of both the solute and the surfactant. These interactions combined with the electrophoretic movement of the micelle toward an end of the column create separation of molecules, as shown in Figure 2.4.

In this example, an anionic surfactant is used and a positive voltage is applied to the inlet end of the capillary. Electroosmotic flow in neutral or alkaline conditions works against the electrophoretic pull of the micelle, which results in overall solution movement down the column. Some degree of retention occurs between those molecules with an affinity for the micellar phase. Larger affinities correspond to incorporation into the core of the micelle and lead to longer migration times. When an analyte is injected, a small

Figure 2.2. Structure and schematic of a typical micellar compound, SDS, showing **A**. individual and **B**. aggregated forms of the compound. The aggregate diagram shows only a few of the 58 actual molecules involved in the micelle formation.

A.

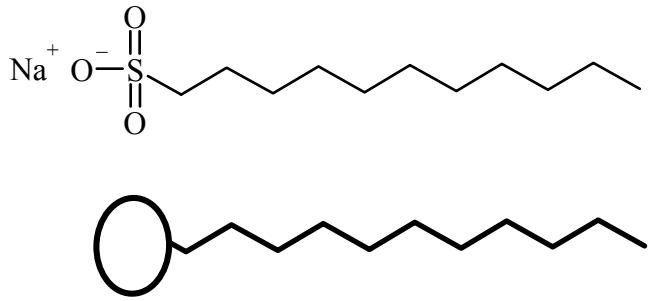

B

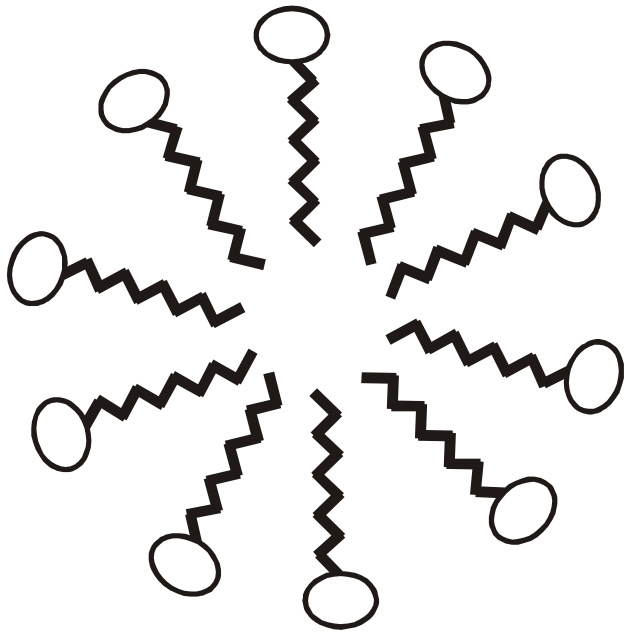

Figure 2.3. Schematic of the three possible interactions between any given solute and the micellar phase. **A.** Solute adsorbed to polar head group surface, **B.** Solute behaving as a co-surfactant and participating in forming the micelle, and **C.** Solute incorporated into the core of the micelle.

A.

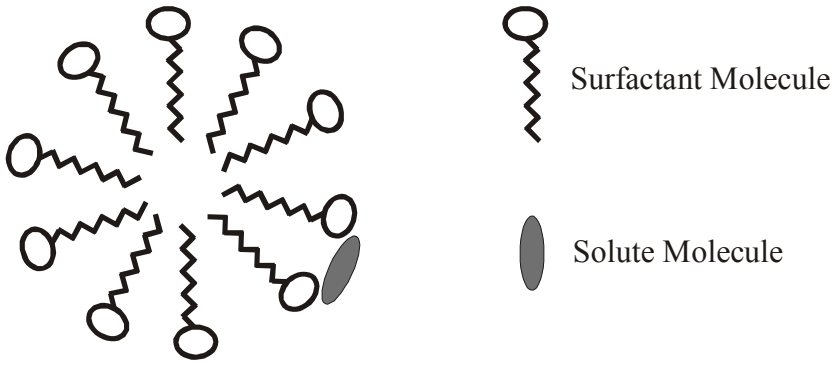

B.

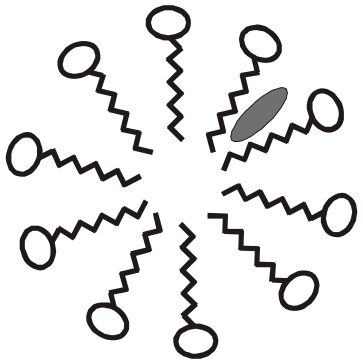

C.

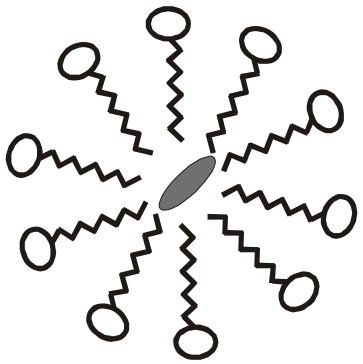

Figure 2.4. Schematic of the separation principle in MEKC showing the partitioning of the solute into the micellar phase. Migration patterns are shown for anionic surfactants such as SDS. The detector is assumed to be located near the negative electrode.

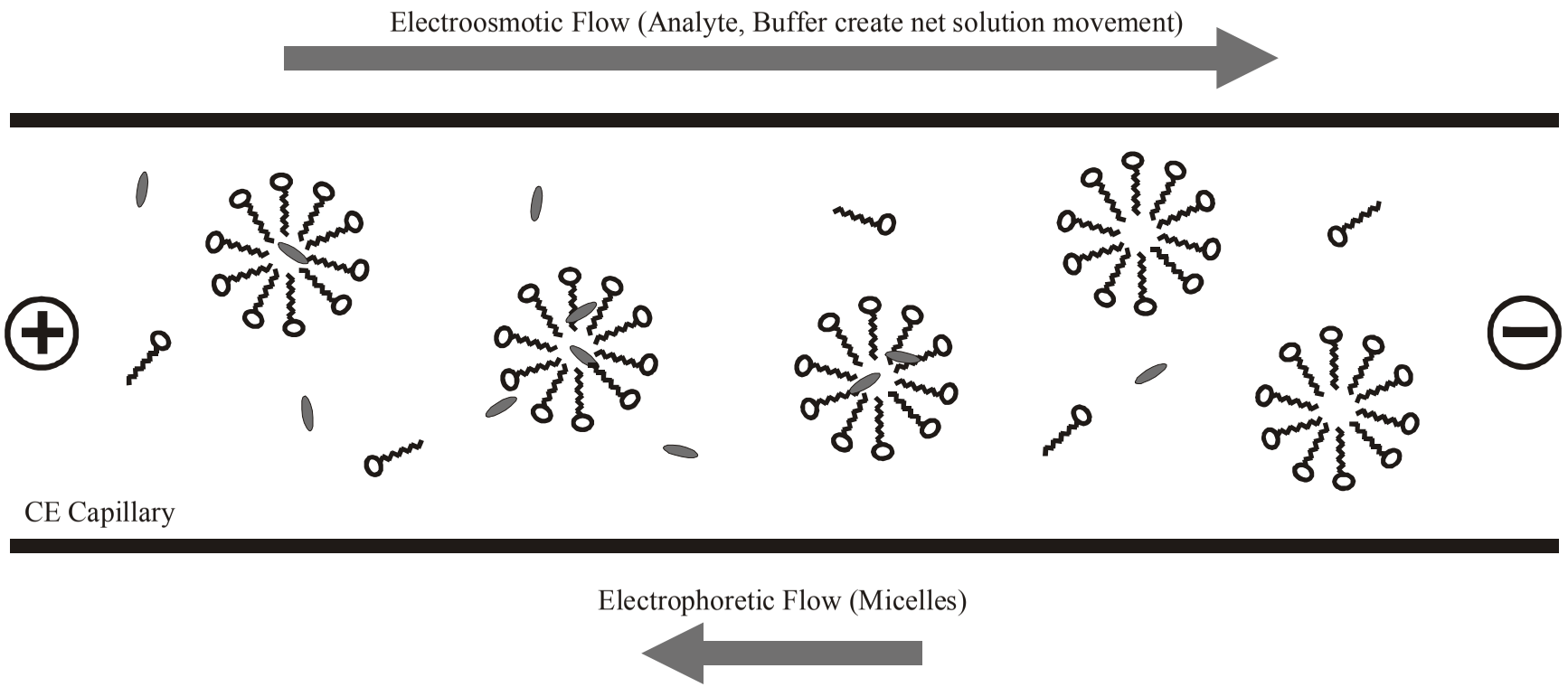
Electroosmotic Flow (Analyte, Buffer create net solution movement)
CE Capillary
Electrophoretic Flow (Micelles)
Surfactant molecule (shown as anionic) that aggregates to form micelles
Solute molecule

portion is integrated to some extent into the micelle and migrates at the same rate as a pure micelle. The remaining quantity remains in the buffer solution and migrates at the EOF rate, or the rate of all neutral compounds. Therefore, the overall rate of analyte migration depends on the distribution coefficient between the micelle and the aqueous phase. In order to detect analytes, the electrophoretic mobility must be between that of the micelle and that of any given neutral compound that does not have a large enough affinity to interact with the micelle. Generally, MEKC selectivity can be altered with the same parameters as in traditional CE, but the added properties of surfactant type and concentration yield more flexibility for optimization of the method.

CDs, the reagents of choice for chiral separations, are also used to create a partitioning environment within the capillary column. CDs are rings of glucose or glucose-derivative molecules in three sizes, referred to as α, β, and γ for 6, 7, and 8 unit rings, respectively. These highly characterized molecules, shown in Figure 2.5, were isolated from potato starch in 1891,[27] and are described as α-(1,4) oligomers of α-D-glucopyranose. Derivatized CDs contain extra functional groups in place of specific hydroxyl groups on the rim of the molecule. CDs were first used in 1988,[28] and are presently commercially available with native or derivative compositions and in all three sizes. While there are many available CD derivatives, they are not all used as chiral selectors; the most common derivative groups are methyl, hydroxyethyl, and hydroxypropyl.

Cyclodextrin molecules have a hydrophobic cavity and a hydrophilic outer surface, causing them to act much like a micelle.[29] They interact with analyte molecules by allowing them to enter and exit the cone area according to chemical affinity for

Figure 2.5. **A.** Structure of native β-cyclodextrin molecule and **B.** Physical dimensions of all native rings.

A.

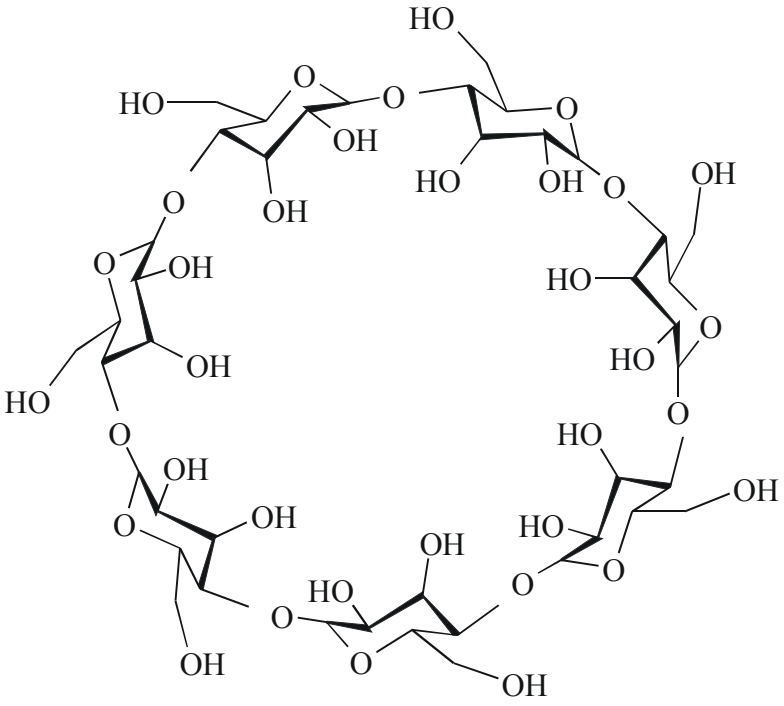
HO
O
HO
OH
O
OH
HO
OH
O
OH
O
OH
HO
O
HO
O
OH
HO
O
OH
HO
OH
O
OH
HO
O
OH
O
HO
O
OH

B.

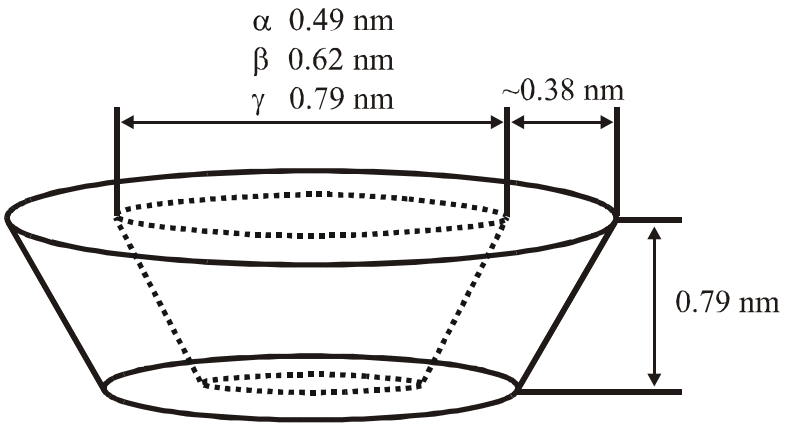
α 0.49 nm
β 0.62 nm
γ 0.79 nm
~0.38 nm
0.79 nm

complexation with the CD molecule. Two major interactions, hydrophobic inclusion within the CD and hydrogen bonding between the analyte and CD hydroxyl groups, are responsible for chemical affinity and therefore the enantiomeric separation. Replacement of these hydroxyl groups can increase hydrogen bonding and electrostatic or hydrophobic interaction sites, depending on the derivatization group. It has been shown that several properties of the CD itself can dramatically affect separation efficiency, such as the presence or absence of an overall charge on the CD, the degree of substitution, and the CD concentration. Of course, fixed experimental parameters such as pH, capillary size, and applied voltage can also be used to optimize analyte separation.

CE method development through the use of CD additives has many advantages. Although the CD library is quite large and can require significant time for method optimization, CDs are easily changed without disturbing other optimized buffer characteristics such as pH and electrolyte concentration. A distinct advantage of chiral CE using CDs is that multiple additives can be used in a single method in order to optimize enantiomeric separation. CDs can also be used to create a countercurrent system and enhance existing partial separations. Further, only small amounts of these compounds are required and it is possible to recover these quantities, which is advantageous due to the expensive nature of the more highly derivatized varieties. Finally, because minimal capillary conditioning is required between additives, analysis time is not greatly increased.[28]

Derivatization of the CD molecule is perhaps the most important consideration. While native CDs are typically more cost-effective, the additional functional groups found in commercial products have distinct advantages. For example, methylation is

known to increase the hydrophobicity of the β-CD cavity[30] and to actually increase the ring flexibility by eliminating some sites of hydrogen bonding.[31] In addition, substitution location has a large effect on the selectivity of the CD and has been extensively studied.[32-35]

Multiple studies have been completed in an effort to more accurately define the selectivity of CDs for specific classes of molecules, and while several small trends have been put forth in multiple review articles, an overall rule for selectivity does not exist. For example, it has been argued that native CDs do not exhibit the same level of selectivity as substituted CDs.[31,36] This property has been attributed to the regular polygon shaped cavity of native CDs, while the addition of larger functional groups causes the ring cavity to bend out of shape as revealed with X-ray crystallography. It was concluded that this alteration increases the steric properties of the molecule and therefore increases the chiral selectivity. In contrast, however, other researchers discovered that native CDs yielded the best separation for the molecules of interest.[37]

These characteristics of CDs, such as derivatization degree and type as well as cavity size, define the level of chemical affinity between CD molecules and analyte molecules. Ideally, only one enantiomer will have increased affinity for the CD, which facilitates chiral separation. Higher analyte affinity leads to increased migration times, but can also prevent separation. If a high analyte affinity is suspected, the CD concentration or type must be changed. It is also possible to introduce a size exclusion facet to the separation methodology if the goal is to separate chiral analytes from larger matrix components, such as examination of field samples that may contain soil residue or bacteria. Unfortunately, separation success with CD additives cannot be predicted, which

can cause methodology development to be quite difficult and expensive. Chemical behavior of CDs, however, has been extensively studied, and they have been found to resolve both neutral and charged molecules from many different compound classes.[38]

Increased separation success can be obtained by combining several components into the running buffer or by using a hybrid additive such as a chiral surfactant. For example, the inclusion of a surfactant and a CD into a moderately basic buffer allows the analyte molecules to interact with both pseudo-phase additives and further distinguish them from one another chemically. Electroosmotic flow (EOF) modifiers such as neutral hydrophilic polymers or alkylammonium cations may be utilized to decrease the EOF and therefore slow analyte movement through the column or to reverse the EOF. At times, an organic modifier such as acetonitrile is needed to increase either analyte or CD solubility in the aqueous buffers or to alter the electrolyte conductivity, which alters the EOF.[20]

The combination of MEKC and CD-CE is commonly referred to as cyclodextrin modified micellar electrokinetic capillary electrophoresis, or CD-MEKC. The technique, introduced by Terabe *et al.*,[39] was developed as a method for CE analysis of highly hydrophobic compounds. In traditional MEKC, extremely non-polar analytes are entirely incorporated into the micellar phase and cannot be separated. Because CDs have hydrophilic rims, they are soluble in the aqueous phase and are not incorporated into the micelles. There are possible interactions between CDs and the surfactants, usually loose surfactant molecules partitioning into the cavity of the CD.[40] The presence of surfactant molecules inside the CD alters the partitioning rates of the analyte molecules. Many different combinations of the three "phases" are possible, and they differ according to the type of charge on the surfactant and CD molecules.

The affinity of analyte molecules for hydrophobic and hydrophilic environments creates distribution coefficients among the micellar phase, the CD phase, and the aqueous phase. Neutral CDs migrate with the EOF, which is different from the charged micellar phase migration rate. This difference indicates that solute partitioned into the CD or micellar phases will have different mobilities and therefore will separate. Due to the stereochemistry of enantiomers, it is likely that they will partition into each phase differently. A schematic for this separation principle is shown in Figure 2.6. The method of analysis for each of the three pesticides in question was chosen to achieve the best results with respect to hydrophobic properties of each compound. Imazaquin, being highly water-soluble, was analyzed with CD-CE. The high hydrophobicity of fonophos and metalaxyl, however, led to the optimization of CD-MEKC methods. In order to increase compound solubility and slightly slow the EOF, a small amount of organic modifier was also added.

Chiral separations are commonly judged by enantiomeric ratios (ER) in order to determine the level of success. These ratios are calculated by dividing the area of the first peak by the area of the second peak. A truly racemic mixture, completely separated, should yield an ideal ER of 1. When this quantity is to be considered, experimental parameters should be optimized to avoid any changes in analyte elution order that can occur when instituting countercurrent processes. For the purposes of chiral degradation studies such as the work presented here, this ratio should increase or decrease over time according to some mathematical relationship that can be used to describe the rate kinetics of the degradation. It is crucial that the separation and degradation be evaluated with this procedure, as opposed to with simple area comparisons, to discount the high variability

Figure 2.6. Separation principle of CD-MEKC. Again, migration directions are indicated for anionic surfactants and the detector is assumed to be near the negative electrode. The cyclodextrin is shown as a neutral or cationic species.

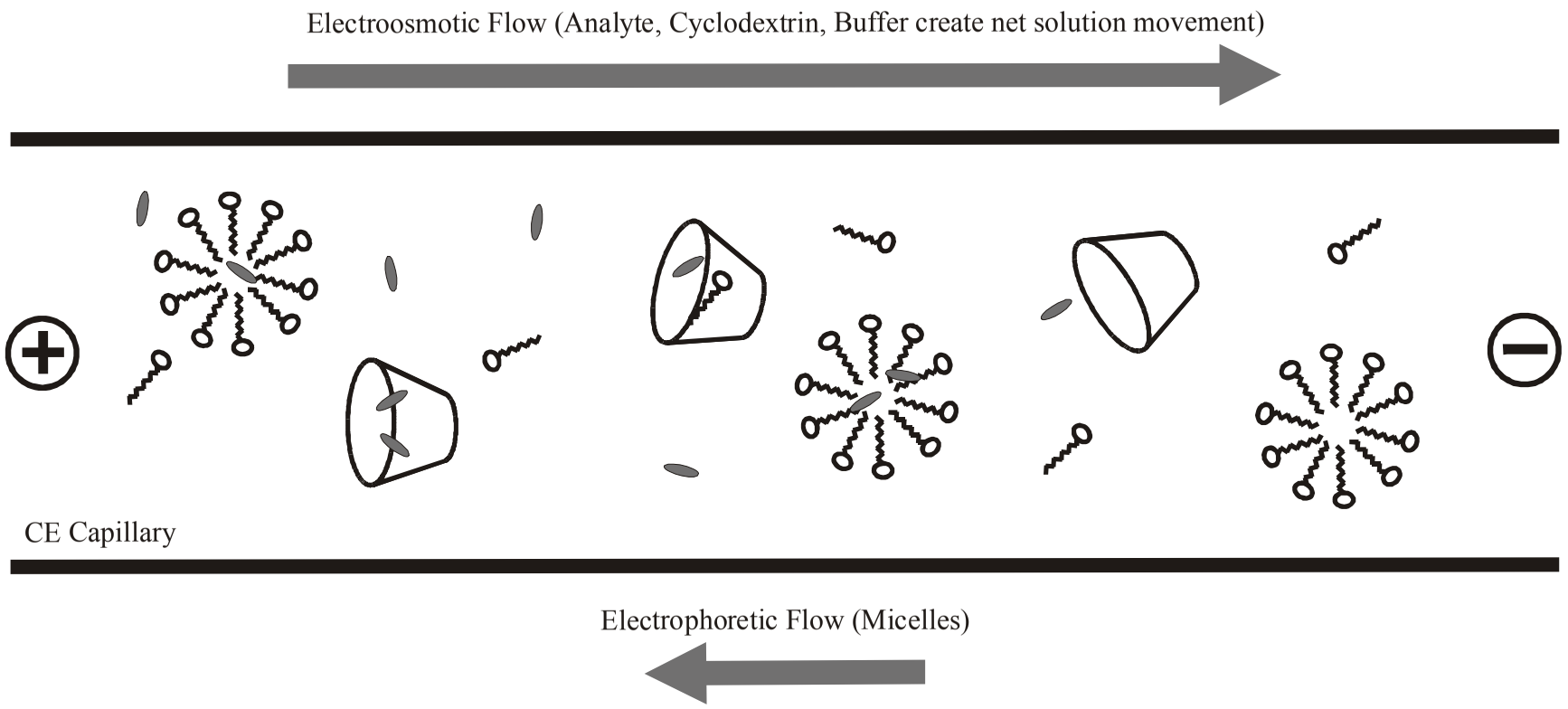
Electroosmotic Flow (Analyte, Cyclodextrin, Buffer create net solution movement)
CE Capillary
Electrophoretic Flow (Micelles)
Surfactant molecule (shown as anionic) that aggregates to form micelles
Solute molecule
Cyclodextrin molecule

between capillary electrophoretic runs due to soil matrix or buffer conditions, column efficiency, daily instrument variations, and other experimental parameters. Additionally, a standard from a previously established calibration curve should be analyzed daily prior to any sample analysis for the most direct concentration determination.

Despite wide use in chiral drug analyses, application of CE or MEKC to pesticide analysis is relatively new.[41] In past investigations, chiral pesticides such as dichloroprop, bromochloroacetic acid, and ruelene have exhibited asynchronous enantiomeric degradation rates.[11,42,43] In order to study these rates under a variety of conditions, a capillary electrophoretic separation method was developed for several compounds of interest. Of these compounds, three were chosen to investigate further using a soil slurry study. Imazaquin, fonofos, and metalaxyl were used to spike soil slurries from a federal site in Ohio as well as two sites in Athens, Georgia. Enantiomeric microbial degradation patterns were then determined with CD-CE and CD-MEKC by periodically sampling and analyzing the slurries over four months.

Experimental

All work described herein was completed at the United States Environmental Protection Agency (US EPA) National Exposure Research Laboratory in the Ecosystems Research Division located in Athens, Georgia under the direction of Dr. A. Wayne Garrison and in conjunction with Dr. W. Jack Jones. The work was accomplished between August 2000 and July 2001.

Chemical Reagents. Sodium tetraborate (Na-TB), sodium dodecyl sulfate (SDS), gamma-cyclodextrin (γ-CD), dimethyl beta-cyclodextrin (DMB-CD), and HPLC

grade acetonitrile (AcN), sodium acetate, hydrochloric acid (HCl), and acetic acid were purchased from Sigma-Aldrich (St. Louis, MO, USA). All were used as received. Imazaquin, fonophos, and metalaxyl standards were obtained from Chem Service (West Chester, PA, USA) and diluted with methanol to make spiking solutions. Acetate buffer was made with sodium acetate and glacial acetic acid, while borate buffer was made from sodium borate and deionized water. The borate buffer pH was adjusted with dilute HCl. Imazaquin CD-CE analyses were carried out in 50 mM acetate buffer, pH 4.5, with 15 mM DMB-CD. Fonofos was analyzed with CD-MEKC with a running buffer composed of 20 mM Na-TB, 100 mM SDS, 15% AcN, at pH 8.5 with 25 mM γ-CD. Metalaxyl was analyzed, also with CD-MEKC, in a 30 mM Na-TB, 100 mM SDS, pH 8.5 buffer with 15% AcN and 40 mM γ-CD added prior to analysis.

Soil Slurries and Sampling Procedure. Approximately two pounds of soil were collected from each of the three federal sites, two in Athens, Georgia and one in Ohio, known to be free of pesticide residues in question. Approximately half of the soil was autoclaved in order to eliminate the microbial population and serve as control samples. Each 200-mL amber serurm bottle was spiked with a known amount of pesticide by adding enough pesticide/methanol solution to achieve 30 mg/L total concentration and allowing the solvent to evaporate from the otherwise empty bottles. The soil was sieved to remove large particles, divided into small aliquots, and placed in the bottles. Water was added and the bottles were sealed and placed on an agitation tray. The entire system was allowed to mix continuously for three days to ensure total compound distribution and desorption from the glass bottles. The bottles were continuously agitated over the course

of the investigation. The investigation required a total of 15 bottles, which included three active samples and two autoclaved samples for each of the three soils under investigation.

Every second day the bottle caps and septa were removed, the bottles were flushed gently with fresh air to maintain an aerobic environment, and the bottles were recapped. Sampling was performed approximately once every five days and was accomplished by withdrawing 1 mL of slurry from the bottle with an insulin syringe. The caps were not removed during the sampling process. The 1-mL aliquots were centrifuged to separate the remaining soil particles and frozen until CE and MEKC analyses could be performed. Upon analysis, 80 µL of the supernatant was withdrawn with an automatic pipette and the pellet was saved for possible future analyses. In cases where analyses revealed that the majority of the analyte was adsorbed to the solid material, the soil was extracted using an in-house procedure, and the resulting extract was analyzed in the same manner as the supernatant.

Instrumentation. All CE and MEKC analyses were carried out on a Beckman P/ACE 5500 or P/ACE 5000 CE (Beckman Instruments, Fullerton, CA, USA) system at 23°C with UV detection at 200 nm (fonophos, metalaxyl) or 230 nm (imazaquin). Applied voltages were 15 kV (metalaxyl), 25 kV (fonophos), and 30 kV (imazaquin). Uncoated fused silica columns (25-µm i.d., 300-µm o.d., 57 cm total length, 40 cm effective length) were used as purchased from MicroSolv Technology Corporation (Long Branch, NJ, USA). Columns were designated for use with either borate or acetate buffer systems in order to preserve electrophoretic resolution and migration times. Data was collected and analyzed with Beckman Gold™ software and Microsoft Excel™.

Results and Discussion

Determination of enantioselective degradation patterns is necessary in order to more accurately develop proper use and exposure regulations, as well as to aid in identification of appropriate pesticides to use in various locations. It was expected that the findings of the work described here would indicate different degradation rates for each pesticide, and further, unique degradation rates for the same pesticide under varying conditions. Autoclaved samples were not expected to show degradation at the same rate as the live counterparts, and any decreases in concentration can be attributed only to hydrolysis as photochemical reactions and microbial processes have been eliminated. In addition, enantiomeric ratios may be dependent upon the microbial population present.

Initial work to determine calibration curves and detection limits indicated that residues could be quantified at levels as low as 1-2 ppm. Therefore, the spiked slurries were expected to yield several months of quality data. Half-life values for the three analytes in soil were listed as 4-6 months for imazaquin,[1,3] 2-3 months for fonophos,[44] and approximately 70 days for metalaxyl.[45] Therefore, it was expected that metalaxyl and fonophos would rapidly begin to degrade while imazaquin degradation would only be detected some time later.

Analysis of the electropherograms for the three compounds reveals significant differences. As show in Figure 2.7, imazaquin enantiomers are easily and completely separated in under ten minutes, which is ideal for any chiral analysis. In contrast, fonofos analysis was considerably more difficult and eventually required an additional soil extraction to be performed. Initial analyses of the pesticide achieved separation efficiency equivalent to that found during the method optimization phase of the project

Figure 2.7. Typical electropherogram of the MEKC separation of imazaquin enantiomers. The ER was calculated as 0.97.

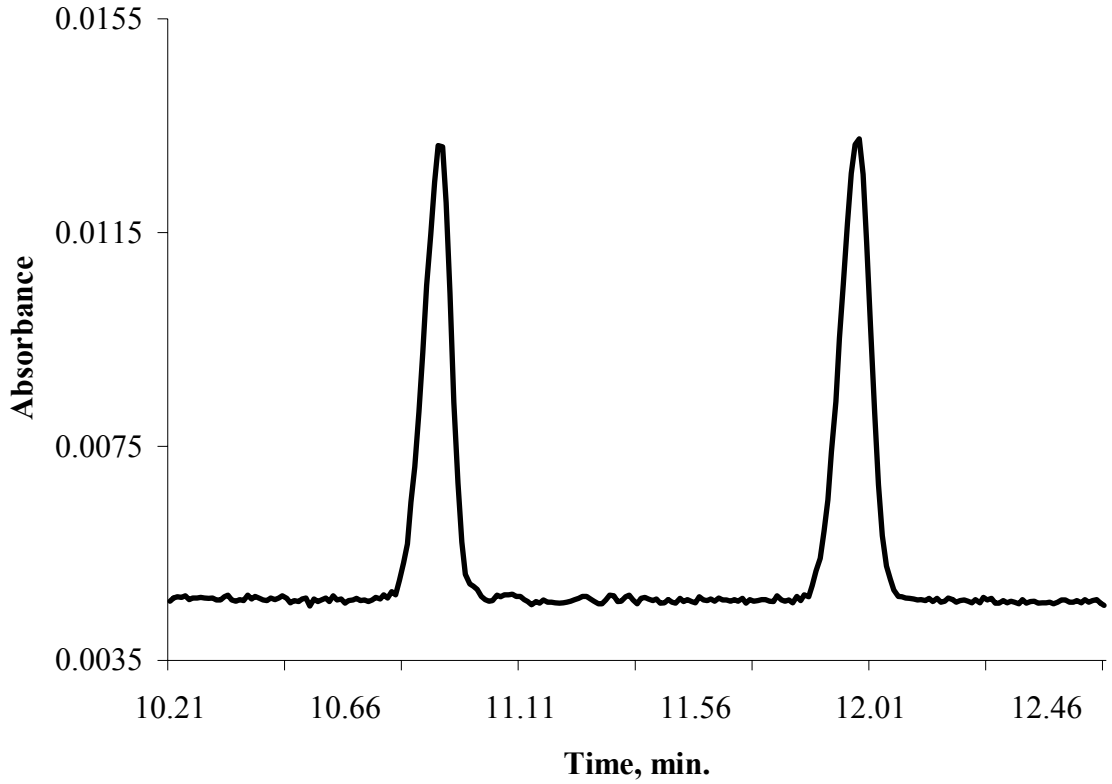
0.0155
0.0115
0.0075
0.0035
Absorbance
10.21
10.66
11.11
11.56
12.01
12.46
Time, min.

with peak areas in the aqueous and solid sample portions nearly identical. Analysis of the supernatant samples collected after 8 weeks, however, indicated either rapid degradation of both enantiomers or absence from the aqueous phase (Figure 2.8). When the soil pellets from the same samples were extracted and analyzed (Figure 2.9), it was apparent that most of the hydrophobic fonofos was adsorbed to the surface of the soil particles. As a result, supernatant portions were no longer analyzed, although they were saved for possible future analyses.

The most impressive results, however, were revealed in the analysis of metalaxyl. Although this particular compound was expected to degrade first, enantioselective degradation was not specifically anticipated. Samples from the Ohio soil slurry, however, exhibited marked differences in peak areas and decreasing ER values. As shown in Figure 2.10, the enantiomer that elutes from the column first was enantioselectively broken down while in the slurry. Figure 2.11 shows the calculated ER values and concentrations over time. The decrease in ER values is expected for those degradations in which the first enantiomer is selectively degraded. If the second enantiomer were to begin degrading instead, the ER values would approach infinity instead of approaching 0.

If the reaction is assumed to follow first order rate kinetics, the rate constant and the half-life of each enantiomer can be determined. The disappearance rate constants were calculated as 0.063 day^{-1} and 0.011 day^{-1} for enantiomers A and B, respectively, which correspond to half-life values of 11 and 63 days. The data appears to follow a linear trend, although more data are necessary to conclude definitively linear degradation. Because metalaxyl is one of the few pesticides available in a formula enriched with one

Figure 2.8. CD-MEKC electropherogram of the separation of fonofos enantiomers from the supernatant portion of a 1-mL aliquot. The aliquot was collected from a slurry of USDA site soil, fonophos, and water. Approximately 8 weeks had passed since the initiation of the degradation study. The ER is 0.84, but concentrations extrapolated from the calibration standard were only 1.2 and 1.3 ppm, respectively.

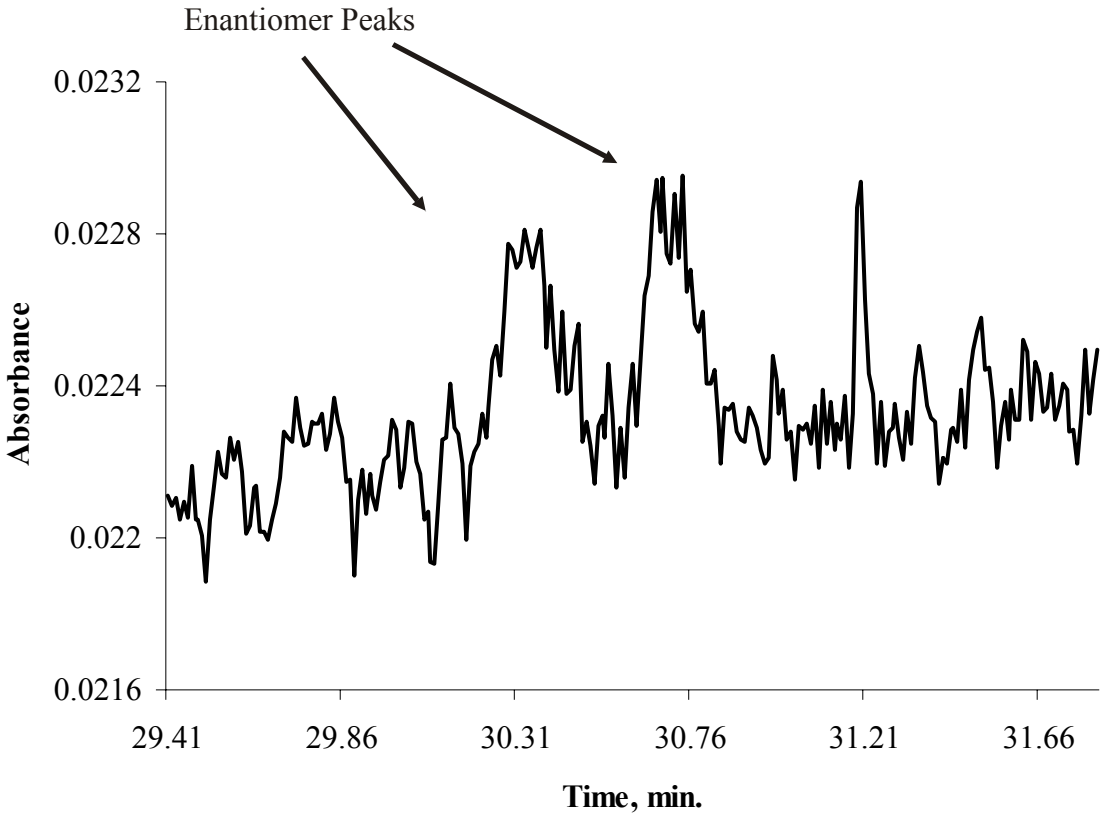
Enantiomer Peaks
0.0232
0.0228
0.0224
0.022
0.0216
Absorbance
29.41
29.86
30.31
30.76
31.21
31.66
Time, min.

Figure 2.9. CD-MEKC electropherogram of the corresponding soil pellet extract from the 5/31/2001 slurry sample. The ER for this separation is 0.88. A significant increase in absorbance and signal level is evident, indicating that future analyses of this particular soil should first examine the soil pellet and, if necessary, follow with the supernatant. Areas indicated corresponding concentrations of 21 and 23 ppm, respectively

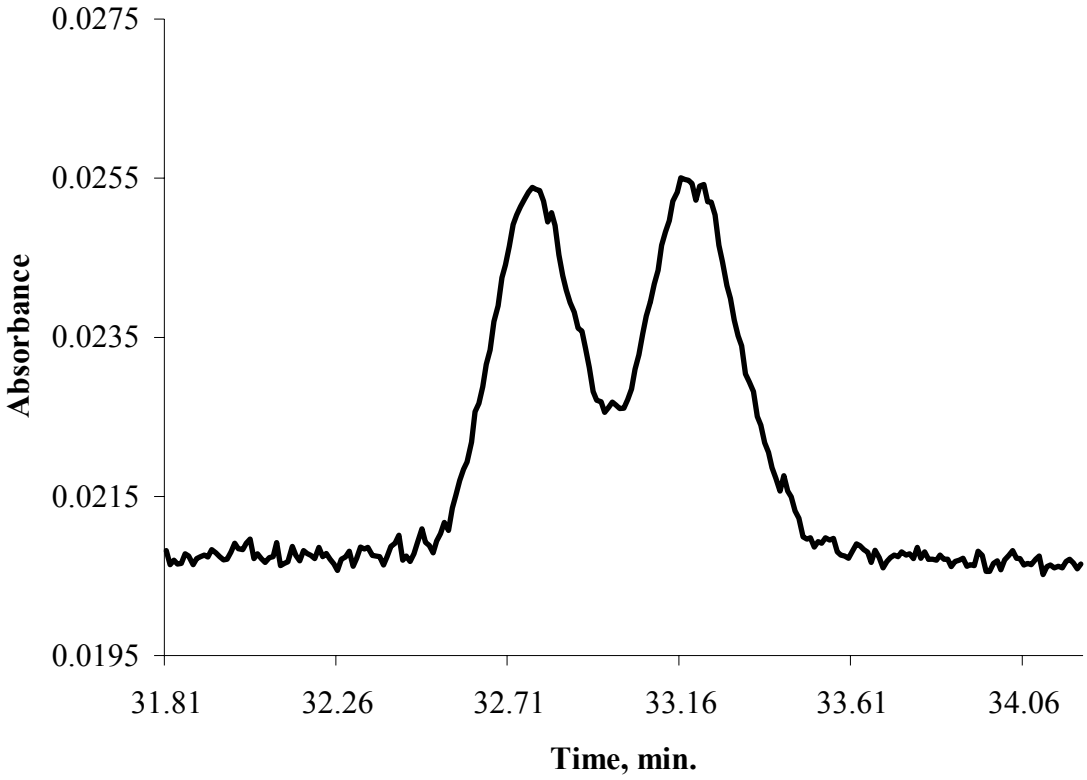
0.0275
0.0255
0.0235
0.0215
0.0195
Absorbance
31.81
32.26
32.71
33.16
33.61
34.06
Time, min.

Figure 2.10. Electropherograms of metalaxyl analyses from each collected slurry sample revealing enantioselective degradation patterns.

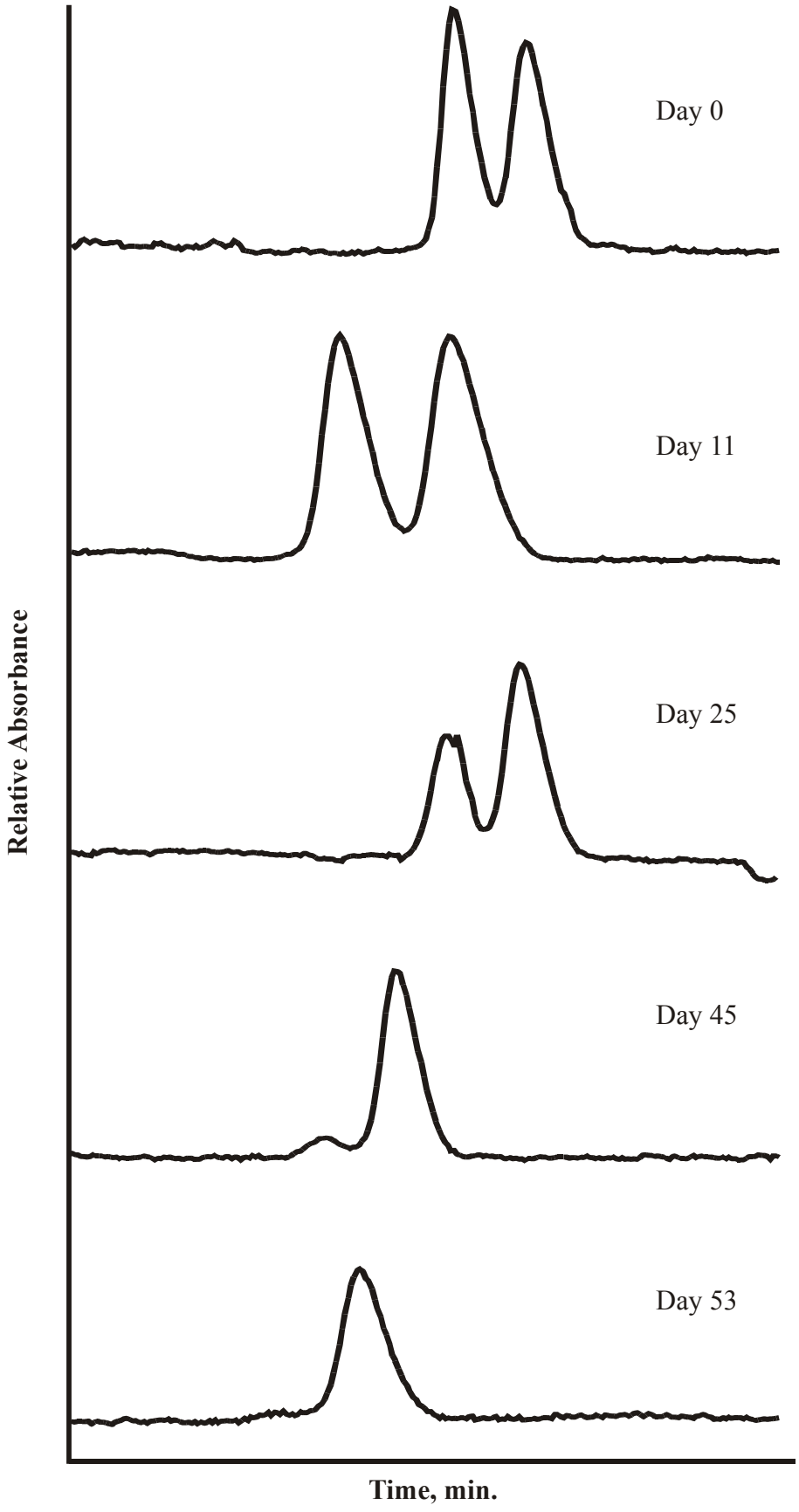
Day 0
Day 11
Day 25
Day 45
Day 53
Relative Absorbance
Time, min.

Figure 2.11. Graphical representation of the numerical results for the enantioselective degradation of metalaxyl as shown in Figure 2.10. The concentrations and ER values plotted are the average values of the three collected samples. The degradation trend follows first order rate kinetics.

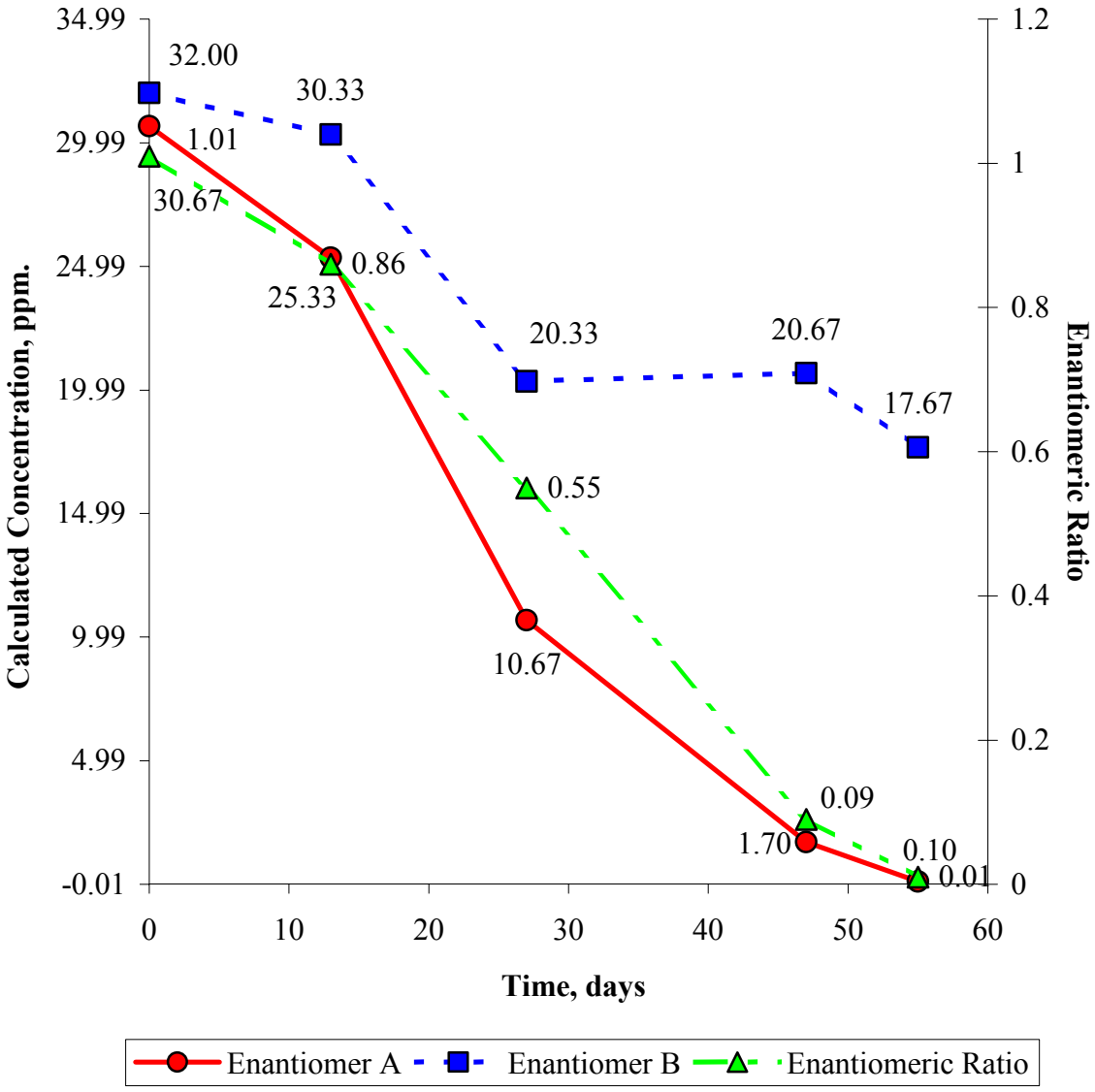
34.99
29.99
24.99
19.99
14.99
9.99
4.99
-0.01
1.2
1
0.8
0.6
0.4
0.2
0
0
10
20
30
40
50
60
Calculated Concentration, ppm.
Enantiomeric Ratio
Time, days
32.00
30.33
1.01
30.67
0.86
25.33
20.33
20.67
17.67
0.55
10.67
0.09
1.70
0.10
0.01
Enantiomer A
Enantiomer B
Enantiomeric Ratio

enantiomer, consumers in areas where this phenomenon is observed can tailor application and spending to target the appropriate enantiomer. For example, if the *S* enantiomer is degrading, expensive enriched *R* formulations may not be necessary. In contrast, if the active *R* enantiomer is disappearing, costs can increase due to decreased effectiveness.

Further conclusions can be drawn as to the mechanism of metalaxyl degradation, of which possibilities include photolysis, hydrolysis, and microbial degradation. Photolytic processes can be eliminated due to the use of amber vials and the fact that the slurries were kept in a dark area throughout the course of investigation. Hydrolytic processes or degradation due to intrinsic soil characteristics such as pH and composition would occur in both live and autoclaved slurries. Therefore, autoclaved samples were periodically analyzed and compared with live samples to determine the rate of these processes. Comparison of metalaxyl-spiked Ohio samples revealed faster overall degradation rates with a definitive enantioselective degradation process occurring in the live samples. Figure 2.12 shows the analytical results of the initial and final autoclaved samples collected. Initially, the autoclaved sample had an ER of 1.03 and concentrations at the spiking concentration. The same autoclaved sample, when analyzed exactly 6 weeks later, has an ER of 1.04, which indicates very little difference in peak areas, and corresponding concentrations of 25 and 26 ppm, which indicate very little overall degradation. In comparison, the live sample from the same sampling date as the final autoclaved sample shows an ER of 0.09 and concentrations of 1.8 and 20. ppm, indicating a large difference in enantiomeric concentrations in the sample. One additional sample was collected approximately 1 week later in which the first enantiomer has degraded below the detection limit.

By examining initial and final results from the other two field sites, shown in Figures 2.13 and 2.14, it is even more apparent that the observed degradation is site-specific. Due to the relatively close locations of the other sites, however, it could be argued that the degradation is somewhat geographically specific. Future studies should endeavor to include soil from a wider variety of geographical locations.

Although the other two compounds investigated in this particular study did not exhibit enantioselective degradation in the first 4 months, other processes of degradation were evident. As shown in Figure 2.15, imazaquin was observed degrading with no enantiomeric preference. When compounds exhibit this type of degradation, it is important to account for losses of overall concentration due to other processes. Because use of amber bottles prevented photolytic processes, the concentration decreases are most likely due to hydrolytic processes. An additional possibility, and one that is much harder to isolate, is that the microbial population present degrades both enantiomers at approximately the same rate. In order to rule this possibility out, the autoclaved samples should be examined at each sampling interval. Unfortunately, however, the autoclaved samples were not sampled unless evidence of enantioselective degradation was discovered. Therefore, specific causes of the overall decreases in concentration as in imazaquin and fonophos samples, and in the remaining metalaxyl samples, cannot be determined.

Figure 2.12. Comparison of autoclaved Ohio soil spiked with metalaxyl **(A)** at study initiation and **(B)** near study completion. A slight decrease in calculated concentration is observed (approximately 34 and 25 ppm for each enantiomer, respectively) but ER values are nearly identical at 1.03 and 1.04, indicating that there is no enantioselective degradation evident.

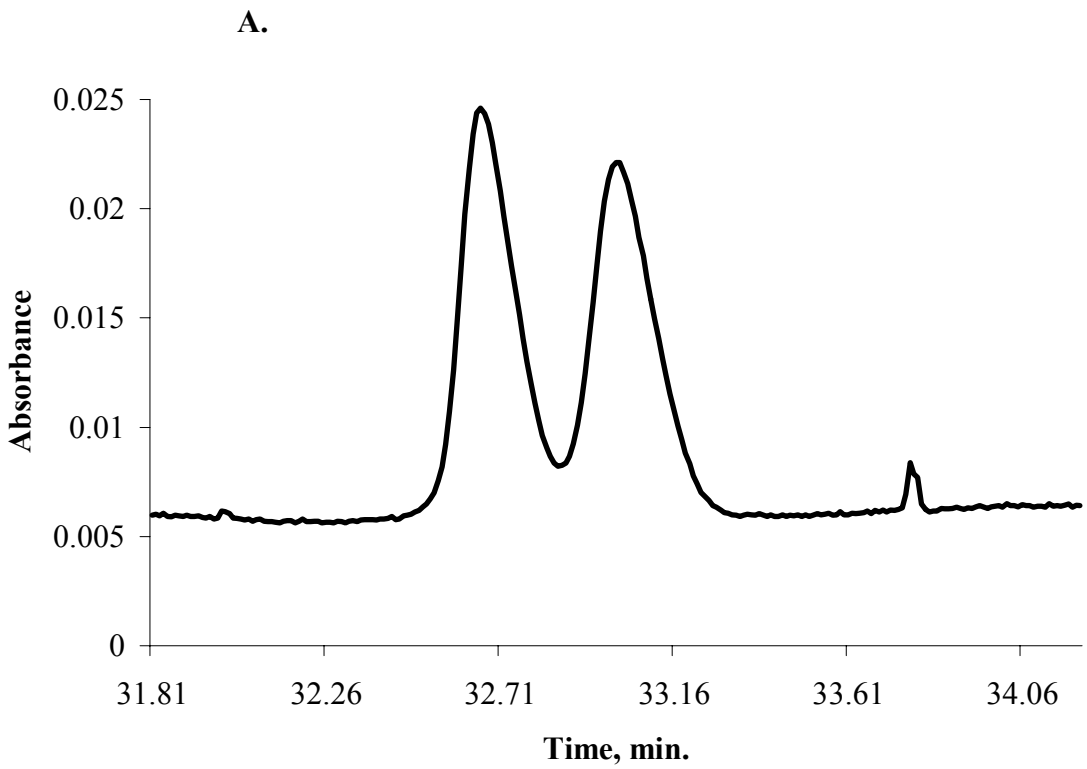
A.
0.025
0.02
0.015
0.01
0.005
0
Absorbance
31.81
32.26
32.71
33.16
33.61
34.06
Time, min.

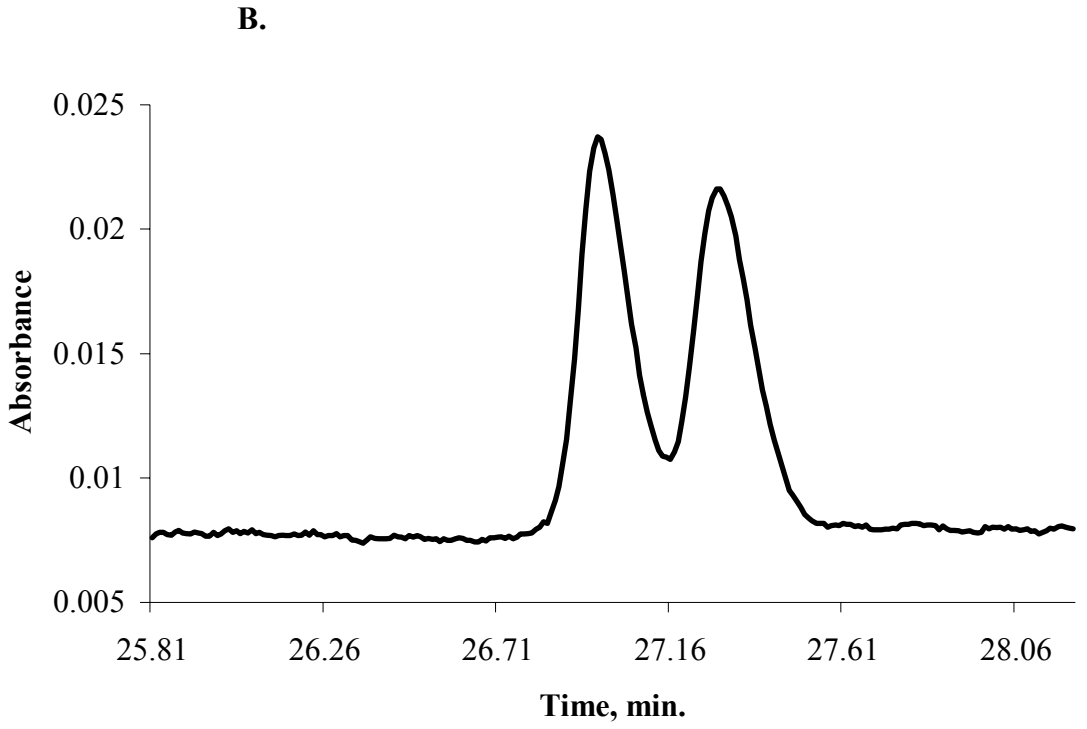
B.
0.025
0.02
0.015
0.01
0.005
Absorbance
25.81
26.26
26.71
27.16
27.61
28.06
Time, min.

Figure 2.13. Comparison of electropherograms from Horseshoe Bend (Athens, GA) soil samples spiked with metalaxyl. Samples were collected on **(A)** the first and **(B)** final days of analysis and have ER values of 0.92 and 0.96, respectively, with relative concentrations decreasing by approximately half the initial value.

A.

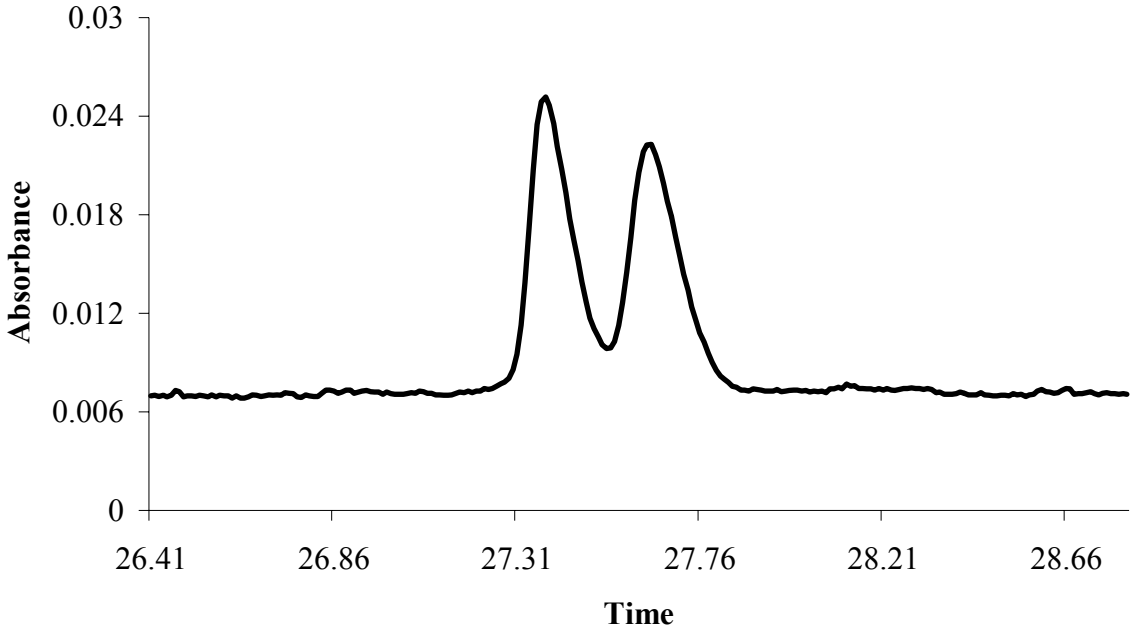
0.03
0.024
0.018
0.012
0.006
0
Absorbance
26.41
26.86
27.31
27.76
28.21
28.66
Time

B.

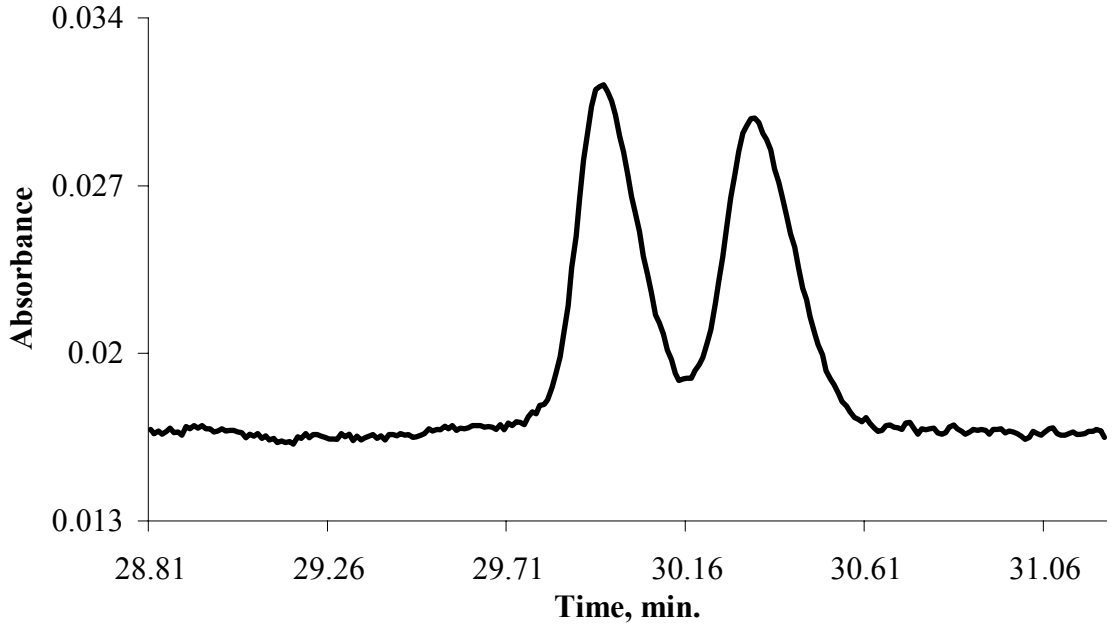
0.034
0.027
0.02
0.013
Absorbance
28.81
29.26
29.71
30.16
30.61
31.06
Time, min.

Figure 2.14. Comparison of electropherograms from USDA (Athens, GA) soil samples spiked with metalaxyl. Samples were collected on **(A)** the first and **(B)** final days of analysis and have ER values of 1.04 and 1.11, respectively, with relative concentrations decreasing by approximately one half.

A.

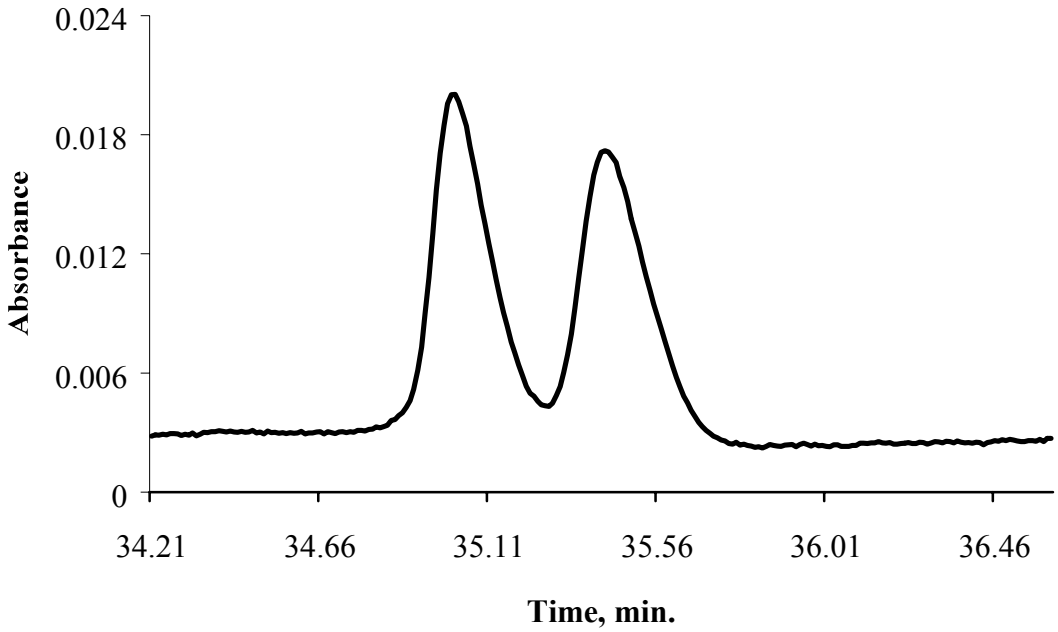
0.024
0.018
0.012
0.006
0
Absorbance
34.21
34.66
35.11
35.56
36.01
36.46
Time, min.

B.

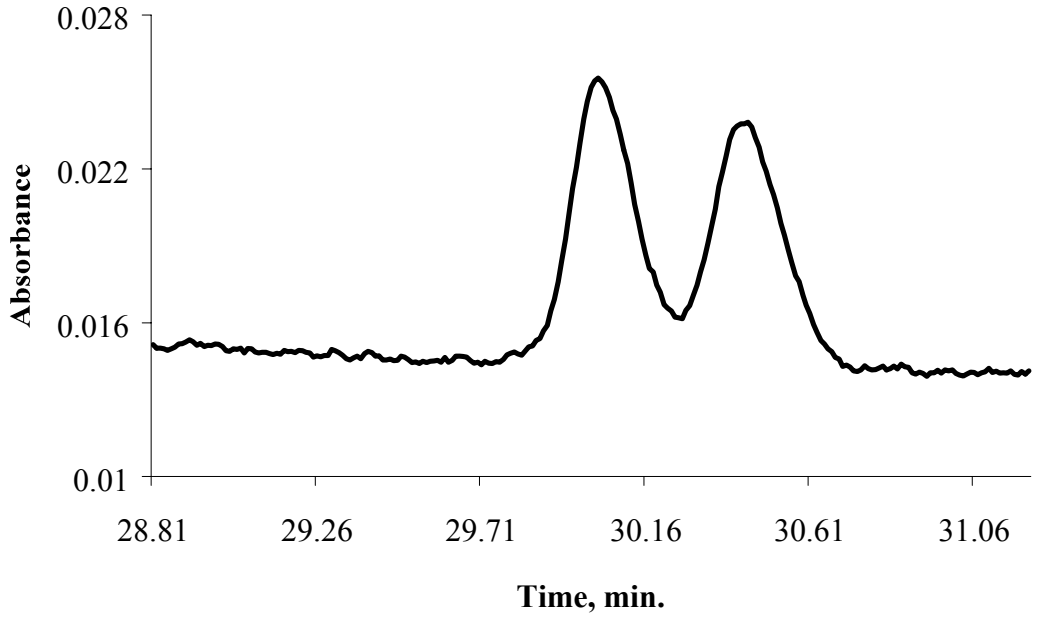
0.028
0.022
0.016
0.01
Absorbance
28.81
29.26
29.71
30.16
30.61
31.06
Time, min.

Figure 2.15. Comparison of electropherograms from Horseshoe Bend soil slurries spiked with imazaquin. Differences from initial (**A.**) and final (**B.**) concentrations are evident but cannot be definitively assigned to a specific degradation mechanism.

A.

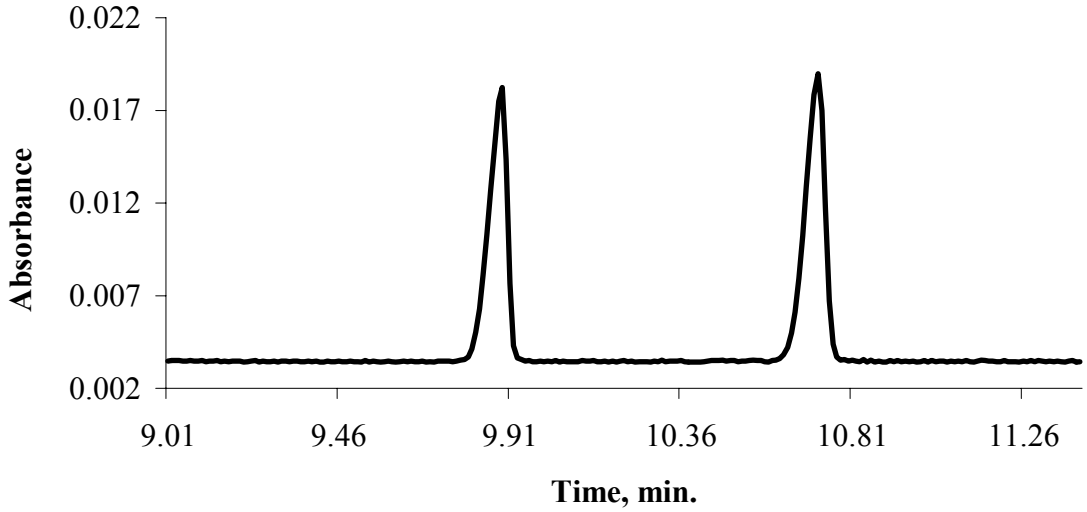
0.022
0.017
0.012
0.007
0.002
Absorbance
9.01
9.46
9.91
10.36
10.81
11.26
Time, min.

B.

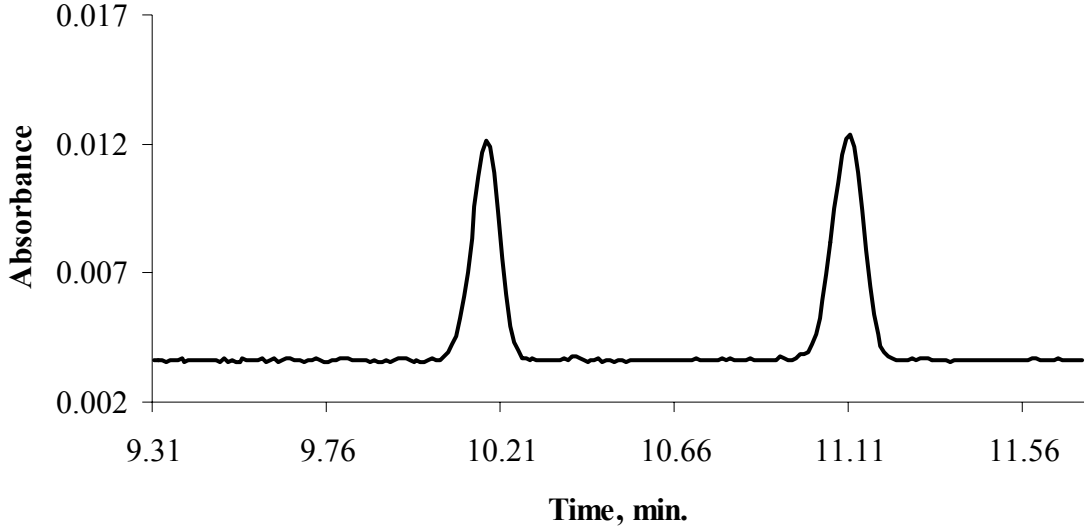
0.017
0.012
0.007
0.002
Absorbance
9.31
9.76
10.21
10.66
11.11
11.56
Time, min.

Conclusions

Pesticides are under constant scrutiny from various agencies concerned with environmental exposure, pollution, and maximum crop output. As a result, analyses of environmental degradation are crucial in order to determine actual field levels, effectiveness, and persistence of these applied compounds. Chiral pesticides introduce a new facet into the determinations, in that often only one of the enantiomers of a given compound produces the desired result, and the second may or may not be as effective. In many cases, the active enantiomer may actually degrade before the "effective" period of the compound has lapsed, or the inactive enantiomer can cause other types of environmental effects.

In an effort to better characterize these processes, three common pesticides were analyzed using specialized capillary electrophoretic techniques. The addition of micellar compounds or cyclodextrins into the running buffer of CE introduced different dimensions of separation and enabled the analysis of fonophos, a relatively hydrophobic compound. The three compounds were spiked into soil slurries from three different sites in both live and autoclaved conditions. It was expected that enantioselective degradation would be apparent, and could then be attributed to the microbial populations present in the various soil samples. Through these analyses, Ohio soil spiked with metalaxyl was observed to undergo enantioselective degradation and consequential concentration decreases.

In contrast, metalaxyl in the other two soils showed only uniform degradation during this particular time period. Fonofos and imazaquin did not exhibit enantioselective degradation, although a decrease in total concentration is evident. The

study is continuing, however, as it is expected that these two compounds as well as the other metalaxyl slurries eventually will degrade enantioselectively. As evidenced by the shift in fonophos concentrations, it is crucial that studies of this nature account for all possible phases in which the pesticide may have a greater affinity. It is also important, however, for both autoclaved and live samples to be examined at each sampling interval to prevent possibly erroneous conclusions from being drawn for the degradation of imazaquin.

Future Studies

There are several potential sources of information in this particular degradation study. Primarily, the study should be carried out for a longer time period to observe degradation in imazaquin and fonophos samples. Additionally, soils from other geographical regions with varying concentrations of sand, clay, and organic matter should be highly characterized and used to make slurries. In this manner, more general trends in microbial degradation may be observed. Finally, it is possible to determine which metalaxyl enantiomer is degrading at a faster rate, which is an economically valuable piece of information. In order to accomplish this, pure enantiomer solutions should be used to spike a slurry sample. Increased peak area indicates higher enantiomeric concentration and reveals the optical identity of both analyte peaks. In this manner, metalaxyl application can be better tailored to optimize its effectiveness.

Acknowledgements

The author would like to thank Drs. A. Wayne Garrison and W. Jack Jones for guidance in experimental procedures, and Jimmy Avants for assisting with the data collection for this work and for performing all soil extraction prodecures. Funding was provided by the U.S.E.P.A. and by the National Network for Environmental Management Studies.

References

1. *Herbicide Handbook of the Weed Science Society of America*: Champaign, IL, 1989.
2. *Farm Chemicals Handbook*; Meister Publishing Co.: Willoughby, Ohio, 1995.
3. U.S. Environmental Protection Agency, Office of Pesticide Programs. *Pesticide Fact Sheet* **1986***83*; USEPA: Washington, D.C.
4. <http://pmep.cce.cornell.edu/profiles/extoxnet/dienochlor-glyphosate/fonofos-ext.html>.
5. Food and Drug Adminstration, Bureau of Foods, Department of Commerce. *The FDA Surveillance Index*; National Technical Information Service: Springfield, VA, 1986.
6. National Research Council. *Regulating Pesticides in Food*; National Academy Press: Washington, D.C., 1987.
7. Walker, M. M. a. K., Lawrence H. *U.S. Environmental Protection Agency's Pesticide Fact Sheet Database*; Lewis Publishers: Chelsea, MI, 1992.
8. Foreman, W. T.; Gates, P. M. *Environmental Science & Technology* **1997**, *31* (3), 905-910.
9. Heberer, T.; Dunnbier, U. *Environmental Science & Technology* **1999**, *33* (14), 2346-2351.
10. Ragnarsdottir, K. V. *Journal of the Geological Society* **2000**, *157*, 859-876.
11. Garrison, A. W.; Schmitt, P.; Martens, D.; Kettrup, A. *Environmental Science & Technology* **1996**, *30* (8), 2449-2455.

12. Ludwig, P.; Gunkel, W.; Huhnerfuss, H. *Chemosphere* **1992**, *24* (10), 1423-1429.

13. Tett, V. A.; Willetts, A. J.; Lappinscott, H. M. *Fems Microbiology Ecology* **1994**, *14* (3), 191-199.

14. Muller, M. D.; Schlabach, M.; Oehme, M. *Environmental Science & Technology* **1992**, *26* (3), 566-569.

15. Armstrong, D. W.; Reid, G. L.; Hilton, M. L.; Chang, C. D. *Environmental Pollution* **1993**, *79* (1), 51-58.

16. Huhnerfuss, H.; Faller, J.; Kallenborn, R.; Konig, W. A.; Ludwig, P.; Pfaffenberger, B.; Oehme, M.; Rimkus, G. *Chirality* **1993**, *5* (5), 393-399.

17. Buser, H. R.; Muller, M. D. *Environmental Science & Technology* **1995**, *29* (3), 664-672.

18. Buser, H. R.; Muller, M. D.; Poiger, T.; Balmer, M. E. *Environmental Science & Technology* **2002**, *36* (2), 221-226.

19. Terabe, S.; Otsuka, K.; Ichikawa, K.; Tsuchiya, A.; Ando, T. *Anal. Chem.* **1984**, *56* (1), 111-113.

20. Chankvetadze, B. *Capillary Electrophoresis in Chiral Analysis*; John Wiley & Sons, Ltd.: New York, NY, 1997.

21. Terabe, S. *J. Pharm. Biomed. Anal.* **1992**, *10* (10-12), 705-715.

22. Terabe, S.; Miyashita, Y.; Ishihama, Y.; Shibata, O. *J. Chromatogr.* **1993**, *636* (1), 47-55.

23. Terabe, S.; Matsubara, N.; Ishihama, Y.; Okada, Y. *J. Chromatogr.* **1992**, *608* (1-2), 23-29.

24. Terabe, S.; Katsura, T.; Okada, Y.; Ishihama, Y.; Otsuka, K. *Journal of Microcolumn* **1993**, *5* (1), Separations, 23-33.

25. Terabe, S.; Ozaki, H.; Otsuka, K.; Ando, T. *J. Chromatogr.* **1985**, *332* (SEP), 211-217.

26. Li, S. F. Y. *Capillary Electrophoresis: Principles, Practice, and Applications*; Journal of Chromatography Library; vol. 52: Elsevier, 1992.

27. Villiers, A. *COMPTES RENDUS HEBDOMADAIRES DES SEANCES DE L ACADEMIE DES SCIENCES* **1891**, *112*, 536-538.

28. Fanali, S.; Sinibaldi, M. *J. Chromatogr.* **1988**, *442*, 371-377.

29. Baker, D. R. *Capillary Electrophoresis*; John Wiley & Sons, Inc.: New York, 1995.

30. Tanaka, M.; Miki, T.; Shono, T. *J. Chromatogr.* **1985**, *330* (2), 253-261.

31. Harata, K.; Uekama, K.; Otagiri, M.; Hirayama, F. *Acta Crystallographica Section a* **1984**, *40*, C110-C110.

32. Tanaka, M.; Asano, S.; Yoshinago, M.; Kawaguchi, Y.; Tetsumi, T.; Shono, T. *Fresenius' J. Anal. Chem.* **1991**, *339* (1), 63-64.

33. Yoshinaga, K.; Rikitake, M.; Kito, T.; Yamamoto, Y.; Eguchi, H.; Komatsu, M. *Chemistry Letters* **1991**, 7, 1129-1132.

34. Tanaka, M.; Yoshinaga, M.; Asano, S.; Yamashoji, Y.; Kawaguchi, Y. *Fresenius' J. Anal. Chem.* **1992**, *343* (12), 896-900.

35. Yoshinaga, M.; Tanaka, M. *J. Chromatogr. A* **1994**, *679* (2), 359-365.

36. Harata, K.; Hirayama, F.; Imai, T.; Uekama, K.; Otagiri, M. *Chemistry Letters* **1984**, 9, 1549-1552.

37. Kuhn, R.; Stoecklin, F.; Erni, F. *Chromatographia* **1992**, *33* (1-2), 32-36.

38. Weinberger, R. *Practical Capillary Electrophoresis*. Academic Press, 2000.

39. Terabe, S.; Miyashita, Y.; Shibata, O.; Barnhart, E.; Alexander, L.; Patterson, D.; Karger, B.; Hosoya, K.; Tanaka, N. *J. Chromatogr.* **1990**, *516* (1), 23-31.

40. Funasaki, N.; Yodo, H.; Hada, S.; Neya, S. *Bulletin of the Chemical Society of Japan* **1992**, *65* (5), 1323-1330.

41. Penmetsa, K. V.; Leidy, R. B.; Shea, D. *J. Chromatogr. A* **1997**, *790* (1-2), 225-234.

42. Garrison, A. W., Jones. ; U.S. Environmental Protection Agency: National Meeting of the Society of Environmental Toxicology and Chemistry, November, 2001.

43. Cash, T. L. Masters Thesis. University of Georgia: Department of Chemistry/Franklin College of Arts and Sciences, 2001, pp 35-47; University of Georgia Main and Science Libraries.

44. Rao, P. S. C., and Davidson. In *Environmental Impact of Nonpoint Source Pollution*; Overcash, M. R., and Davidson, Ed.: Ann Arbor Science, 1980.

45. Kimmel, E. C.; Casida, J. E.; Ruzo, L. O. *J. Agric. Food Chem.* **1986**, *34* (2), 157-161.

CHAPTER 3

GLASS NEBULIZER INTERFACE FOR

CAPILLARY ELECTROPHORESIS–FOURIER TRANSFORM INFRARED SPECTROMETRY[1]

[1]Reprinted from *Journal of Chromatography A*, 976, Jessica L. Jarman, Richard A. Todebush, and James A. de Haseth, "Glass Nebulizer Interface for Capillary Electrophoresis-Fourier Transform Infrared Spectrometry," 19-26, 2002, with permission from Elsevier.

Abstract

A capillary electrophoresis system has been successfully interfaced to a Fourier transform infrared spectrometer. The design of the interface is a custom-designed glass microconcentric nebulizer. Typical deposit characteristics include reproducible circular deposits of uniform thickness that lack any splatter as found in earlier designs. Interface performance is demonstrated in that there is no loss of electrical current during operation and spectra of analytes can be readily produced. Furthermore, it has been shown that the interface maintains the plug flow characteristic of capillary electrophoresis.

Keywords:

Interfaces, CE–FT-IR; Instrumentation; Nebulization

Introduction

Interfaces between spectrometry and chromatographic techniques have yielded highly reliable and informative analytical methods. Regrettably, the potential of infrared spectrometry as an interface method is still being realized. Infrared spectrometry, especially conventional Fourier transform infrared (FT-IR) spectrometry, is a rapid method of analysis that may reveal unequivocal structural information about analyte molecules. The typical spectrum collected has a high signal-to-noise ratio and can be collected in approximately 50 to 200 ms on most commercial instruments. Additionally, FT-IR spectrometry is highly sensitive and detection limits have been reported in the picogram range.[1] Attempts to interface FT-IR spectrometry and chromatographic techniques include gas chromatography (GC),[2-11] liquid chromatography (LC),[12-16] and supercritical fluid chromatography (SFC).[17-19] GC–FT-IR spectrometric techniques have been available for well over thirty years while LC–FT-IR methods were developed within the last twenty years, and SFC–FT-IR has been commercialized in the last few years. Capillary electrophoresis (CE), however, has only recently been successfully interfaced to FT-IR spectrometry.[20]

Capillary electrophoresis (CE) is a separations technique that uses an electrical current to separate charged species. A typical CE apparatus includes two buffer reservoirs, a high voltage supply, a fused silica capillary, and a detector. The high voltage is applied across the column, which causes both electrophoretic and electroosmotic flow to occur within the column. Analyte molecules are carried along in the electroosmotic flow of the electrolyte "buffer" and elute according to their charge-to-mass ratio. The analytes separate due to different electrophoretic mobilities in a given

buffer system. Separations are carried out quite rapidly and require only nanoliters of sample. The resolution from the electrophoretic properties of the system is very high and separations of complex mixtures, such as fragments from protein digests, are common practice.[12,21-23] Temperature can be widely varied which allows for a large number of applications, and separations are carried out at near ambient pressure, which adds to the ease of the analyses. Typically, detection is performed on column with UV-Vis or laser induced fluorescence (LIF) detectors, but neither of these methods provides structural information and analyte identification is accomplished only with migration time comparisons. Several successful CE–Mass Spectrometry (MS) interfaces[24-26] have been developed in an effort to obtain more analyte information, but MS is sample-destructive and is therefore not suited for samples that require further analysis after the CE separation. Furthermore, the strength of mass spectrometric analysis lies in the identification of homologues but does not readily lend itself to the identification of isomers. Due to the high degree of structural information found in analyte infrared spectra, an ideal detection method for CE is FT-IR spectrometry. This information, combined with the high resolving power of CE, creates a highly sensitive and informative analysis technique that is performed quickly and allows sample recovery for further analyses.

Successful CE interfaces have three main requirements.[27] First and foremost, a stable electrical contact must be maintained throughout the course of the analyses. Interfaces meet this requirement with a variety of methods that include sheath liquids,[28] coupled columns,[27,29,30] pierced or cracked columns,[24] wires that surround or are inserted into the column,[31] and metal coatings.[32] The interface described in this paper is a metal

coating interface in which a thin layer of a conductive paint is used to coat the end of the column and is connected to electrical ground. The capillary is inserted into a glass nebulizer to complete the interface. The second main requirement is that the extremely low flow rates of CE systems (~100 nL/min) are adapted to the higher flow requirements of the sample nebulization system. Some interfaces use "make-up" liquids,[27] to account for the extra volume needed for a nebulizer, while others choose to accept the consequential losses in resolution and increased migration times in lieu of a volume equalizing system. This method of approach leads to the third and final concern. Laminar flow is induced when the flow rate of the CE system is not matched in some way to the flow rate of the nebulization system. Currently, there are no commercially available nebulizers designed to operate at typical CE flow rates.[29] During sample nebulization and introduction into the interface, the flow profile inside the column should remain plug-like. Laminar flow in a CE column, while it still allows for rapid separation, decreases the high resolving power of the technique and leads to migration time shifts, peak broadening, and loss of resolution. Some methods of laminar flow prevention include those that allow the nebulizer to pull through a separate liquid that never enters the capillary column,[27] the application of a negative pressure to the inlet vial to counteract the pull of the aspiration system,[33] and minimization of the nebulization gas or liquid flow.[24]

The development of a CE–FT-IR spectrometric interface involves two additional concerns. Capillary electrophoresis uses electrolytic solutions, commonly referred to as CE buffers, to conduct electrical current and facilitate analyte separation. Many of these electrolytes exhibit high absorbances in the IR region and may mask any analyte

identification information. Even spectral subtraction cannot completely remove the masking bands, and solvents that do not rapidly evaporate can become trapped in the sample matrix. Therefore, a successful interface must employ either an electrolytic solution which is not IR active, or must include a solvent and buffer elimination step. Secondly, because the sample is deposited directly onto an infrared transparent window, there must be a method of sample containment. CE–MS interfaces require complete sample introduction into a closed chamber during which ionization and desolvation steps are accomplished. To accomplish this, a complete sample aerosol is necessary. In a CE–FT-IR interface, the nebulization must produce deposits of neat analyte in a confined area. Furthermore, the deposit should be of uniform thickness and not "splattered." The concentration of as much analyte as possible into a single deposit allows for highly sensitive IR analyses. Deposits should therefore be contained in as small an area as possible and should not show splatter patterns.

Previously, we reported the first successful CE–FT-IR interface with a metal nebulizer used in the interface design.[20] This design successfully addressed many difficulties typically encountered in a CE interface while it also overcame obstacles specific to CE–FT-IR interfaces: constant electrical contact, absence of buffer interferences in the IR spectra, and sample containment to maximize spectral sensitivity. The newer improvement on this design is described herein and uses a custom designed microconcentric glass nebulizer to accomplish sample deposition onto calcium fluoride or zinc selenide IR crystals for off-line spectral collection with an FT-IR microscope.

Experimental

Chemical Reagents. The following electrolytic solutions were used in separate experiments: ammonium acetate (NH_4Ac, Fisher Scientific, Atlanta, GA, USA); sodium borate ($Na_2B_4O_7 \cdot 10\ H_2O$, Sigma, St. Louis, MO, USA); and sodium hydroxide (NaOH, Fisher Scientific). All were used as received.

Electrolyte solution concentrations varied from 1.0 to 5.0 x 10^{-2} M depending on experimental parameters. Higher electrolyte concentrations were used in an attempt to decrease separation time and obtain larger currents. All solutions were prepared with 18.0 MΩ deionized water purified with a Barnstead Nano Ultrapure water system and had a pH of 8.5.

The following samples were used to test the stability and separation ability of the interface: caffeine and salicylic acid (Baker, Phillipsburg, NJ, USA), and N-Acetylglucosamine (GlcNAc, Sigma). Solutions of each compound were made with 18 MΩ water to final concentrations of 5.0 x 10^{-3} M.

The samples were deposited onto 25-mm diameter x 6-mm thick zinc selenide (ZnSe) or calcium fluoride (CaF_2) windows (Spectral Systems, Hopewell Junction, NY, USA).

Capillary Electrophoresis and FT-IR Spectrometric Microscope. Two capillary electrophoresis systems were used to separate samples of interest and discern the success of the interface. A Beckman P/ACE 5000 CE instrument (Beckman, Fullerton, CA, USA) equipped with a P/ACE UV absorbance filter detector was used in addition to an Agilent ^{3D}CE instrument (Agilent Technologies, Palo Alto, CA, USA) equipped with a UV-Vis diode array detector. The system was controlled with ^{3D}CE

Chemstation software. Results presented herein are from the Agilent CE system unless otherwise noted. CE–FT-IR spectra were collected with a Perkin-Elmer Spectrum 2000 FT-IR spectrometer coupled with a Perkin-Elmer *i*-series FT-IR microscope with an adjustable limiting aperture (Perkin-Elmer). The microscope detector was a liquid nitrogen cooled mercury-cadmium-telluride (MCT) detector (Perkin-Elmer). The aperture allows for the beam size to be set from 10 to 400 μm in diameter to allow for variations in sample size. The spectra were collected with PEImage software. Spectral manipulation such as digital subtraction, baseline correction, and normalization, were calculated with the use of GRAMS/32 AI v.6.00 software (Thermo Galactic, Salem, NH, USA).

Uncoated fused silica capillaries (Agilent Technologies, Wilmington, DE and Polymicro Technologies, Phoenix, AZ, USA), with an outer diameter of 360 μm and inner diameters of 50 and 75 μm were used. Capillary length varied from 40 to 120 cm and the distance from the inlet to the UV-Vis detector was 22 cm for extended capillaries. This length could be varied somewhat, but it was found to be unnecessary for the investigations described here. Analyses were carried out at 25°C with an applied voltage of 25-30 kV and simultaneous UV-Vis detection at 195 nm as a back-up for the IR detection method. Injection was accomplished by applying 50 mbar of pressure to the sample vial for 5 sec.

Glass Interface. The glass interface, shown in Figure 1, was designed with the use of a female tee (Upchurch Scientific, Oak Harbor, WA, USA) and a standard sidearm fitting (J.E. Meinhard, Santa Ana, CA, USA). The last 20 cm of the extended fused silica

Figure 3.1. (A) A schematic representation of the interface with the PTFE tee and microconcentric glass nebulizer. Helium and nitrogen ports are open to the capillary and shell, respectively. The resulting aerosol is deposited directly onto a calcium fluoride or zinc selenide IR window. (**B)** Cross-section of interface tip showing the layers of capillary, helium, nitrogen, and glass.

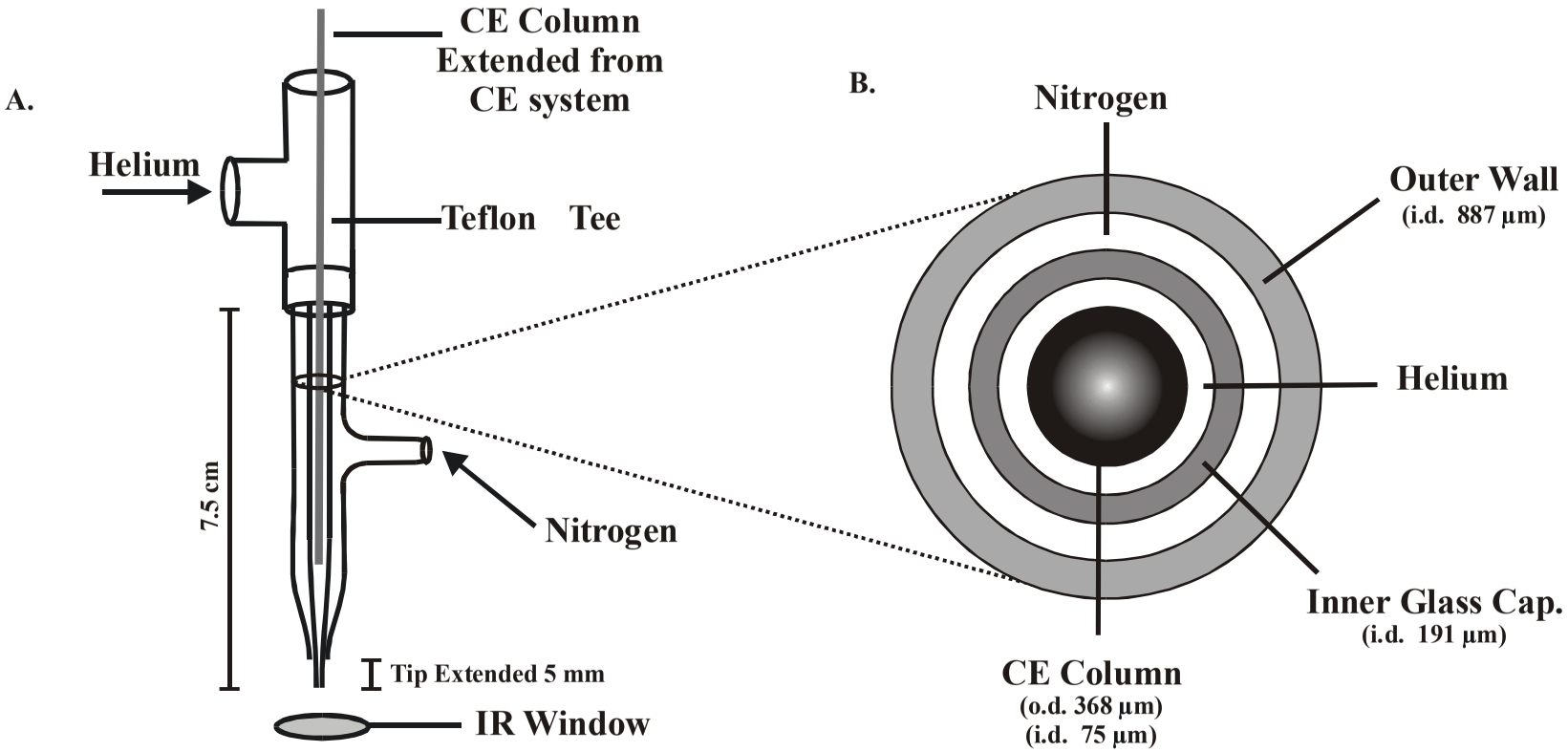
A.
CE Column
Extended from
CE system
Helium
Teflon Tee
7.5 cm
Nitrogen
Tip Extended 5 mm
IR Window
B.
Nitrogen
Outer Wall
(i.d. 887 µm)
Helium
Inner Glass Cap.
(i.d. 191 µm)
CE Column
(o.d. 368 µm)
(i.d. 75 µm)

capillary was coated with silver paint (Fullam, Latham, NY, USA) and threaded through a metal clamp to maintain electrical contact. The capillary was then passed through the tee and fitting and inserted into the capillary of a custom-designed microconcentric glass nebulizer (J.E. Meinhard). A helium flow was introduced through the tee while a nitrogen flow was introduced through the outer shell of the nebulizer. The tip of the nebulizer capillary extended 5 mm past the outer shell and the inner diameter of the glass capillary was large enough to accommodate the painted silica column when inserted just to the narrowing point. At the narrowest point, the tip is 191 μm I.D. These dimensions are variable to accommodate a variety of systems and produce somewhat different results with respect to deposit shape and size. All gas flows were controlled manually with the aid of metered needle valves. Deposits were visualized and photographed with an ausJENA stereomicroscope (Jenavert, Germany) and a Hitachi digital camera (Hitachi, Denshi America, Woodbury, NY, USA).

Results and Discussion

The interface design described above was chosen to satisfy the requirements discussed earlier. The use of a nebulizer with an extended tip of extremely small inner diameter allows the flow rates of the nebulizer and the capillary electrophoretic system to be more closely matched. Additionally, the aerosol is more easily contained. The helium introduced between the column and the nebulizer capillary aids in solvent evaporation and nebulization while the outer flow of nitrogen is used to help contain the deposit in a small area. This apparatus allows suitable deposits to be made in as little as 1 s, although for very dilute samples it is more advantageous to deposit multiple layers to increase

spectral sensitivity. Therefore, the width of the analyte peak can determine the optimal deposition time. Detection with the diode array detector was performed simultaneously with interface operation due to the off-line characteristics of the system and to verify true analyte deposition. The new glass interface was compared with the previously described metal interface through examination of the deposit characteristics of both apparatuses. Deposits from the metal interface exhibited a significant amount of splatter patterns and interference patterns, which indicate regions of variable thickness. The glass nebulizer exhibited neither of these undesirable artifacts, thus, the glass interface is an improved design.

A typical deposit from the glass nebulizer, shown in Figure 2 and obtained on the Beckman instrument, is round in shape and has a diameter between 200 and 400 μm. The deposit is an aqueous solution of caffeine and sodium borate electrolyte (5 and 50 mM, respectively) that has been allowed to dry as completely as possible to obtain a deposit of the solute and electrolyte mixture. In this case, the nonvolatile electrolyte molecules cannot be eliminated from the analyte matrix. Through visualization under an optical microscope, rings of variable thickness are not evident and there is even distribution of analyte molecules instead of a ring of high concentration on the outer edge. For the purposes of visualization, the deposit image has been digitally enhanced hence there is an artificial ring around the deposit. The original deposit was completely transparent and did not display any evidence of uneven thickness. It should also be noted that all the analyte has been concentrated into a single deposit, which is optimal for high spectral sensitivity.

Figure 3.2. A typical deposit from the CE–FT-IR spectrometric interface of 5 mM caffeine in 50 mM sodium borate buffer is shown. (The deposit is digitally enhanced to show its clear boundary.) Deposits are of relatively uniform thickness and no splatter droplets are evident which indicates the concentration of all the analyte is confined to a small volume.

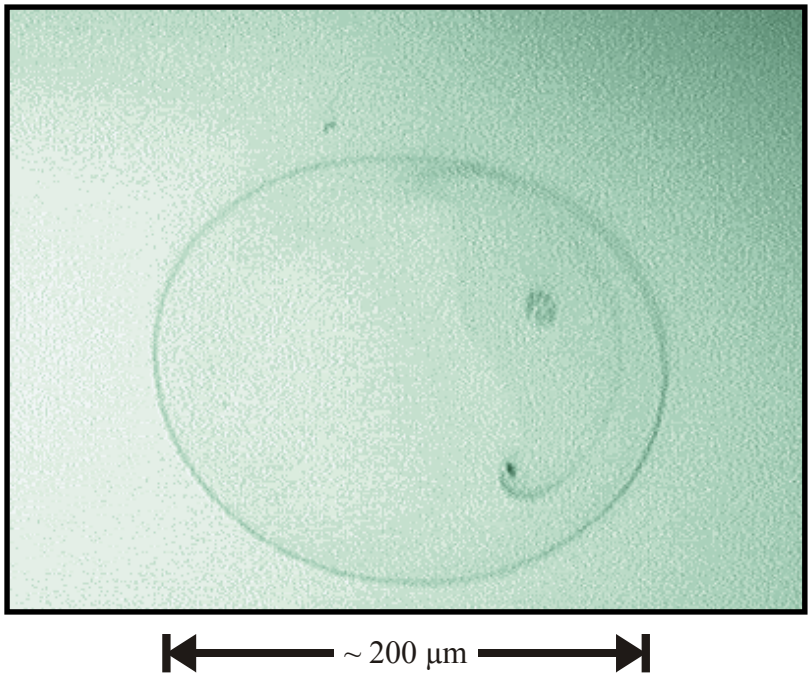
~ 200 μm

To examine the thickness characteristics of a typical interface deposit further, a second deposit of an aqueous solution of sodium borate buffer was characterized using the FT-IR spectrometric microscope. After setting an aperture of 30 μm on the microscope, sequential spectra were collected for the center of the deposit, a 300 X 400-μm area. The maximum characteristic absorbance was then recorded and plotted in relation to the area of the deposit that was sampled. The resulting contour map, shown in Figure 3, reveals a relatively uniform deposit thickness with sufficient absorbance to achieve a high quality infrared spectrum. Additionally, the slight gradient in thickness follows a circular pattern, which indicates that the liquid is evenly deposited onto the window's surface. This deposit is larger than normally created, as the larger size was necessary to map the deposit accurately.

Several properties of the successful CE–FT-IR spectrometric interface were characterized. The primary concern was that stable electrical contact was well maintained throughout the entire course of a separation. Coating interfaces in general have had limited success with electrical contact due to the fragile nature of the metal coating when columns are threaded through tight fittings or clamps. Our interface, however, has demonstrated remarkable durability. In order to verify the stable contact, the electrical current through the column is monitored throughout a normal analysis. Any instability in the current is revealed as sharp dips or spikes in the recorded trace. Figure 4 shows a typical electropherogram obtained during the separation of a 50:50 (v/v) mixture of caffeine and salicylic acid. The current trace has been overlaid on the electropherogram. This current trace, monitored throughout the entire separation, does

Figure 3.3. Contour map of a sodium borate deposit with absorbance indicated on each contour line. Deposit is revealed to be only slightly variable in thickness and more than sufficient for high quality spectral analysis. Circular thickness regions indicate even deposition onto the infrared transparent window as opposed to weighted or skewed deposition as can be caused by uneven air flow or interface set up.

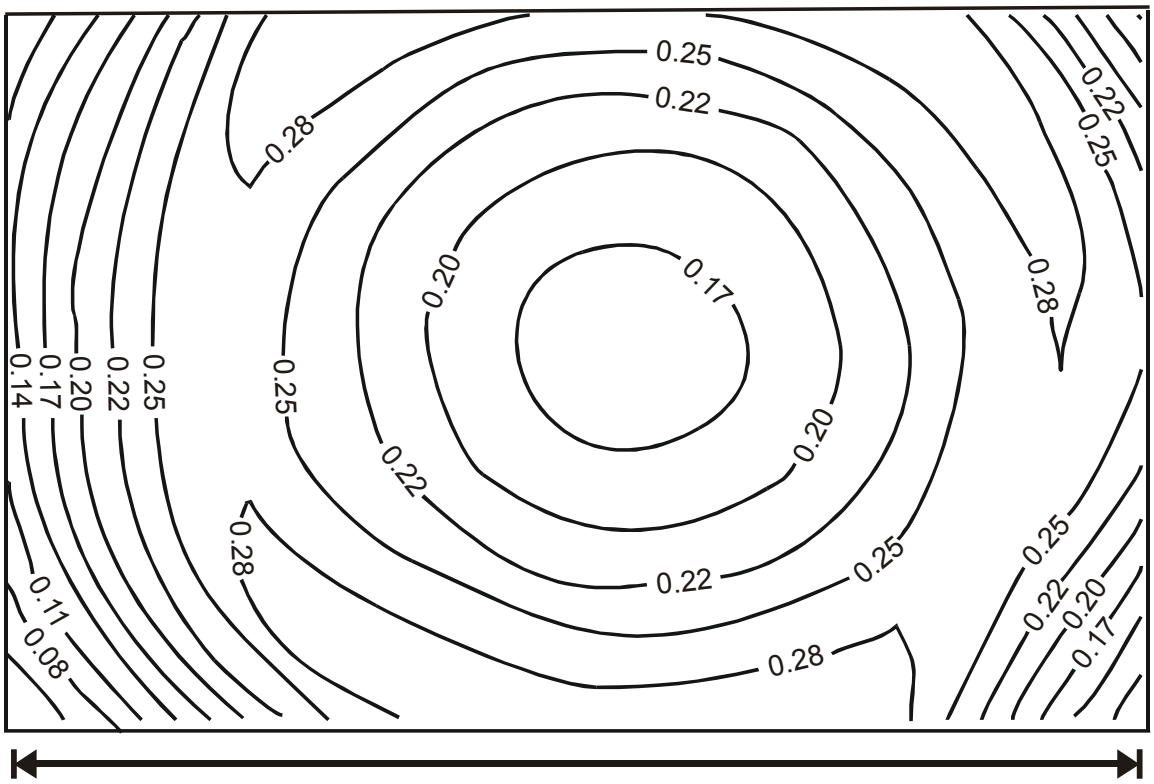
0.25
0.22
0.28
0.22
0.25
0.20
0.17
0.28
0.25
0.14
0.17
0.20
0.22
0.25
0.22
0.20
0.28
0.22
0.25
0.25
0.22
0.20
0.17
0.11
0.08
0.28
~ 400 μm

Figure 3.4. CE–FT-IR separation of 5 mM caffeine and 5 mM salicylic acid in 50 mM borate buffer with 15 kV at 25°C with a bare fused silica column (103.5 cm X 75 μm I.D.). The stable current trace overlaid on the electropherogram indicates constant electrical contact was maintained throughout the course of the separation.

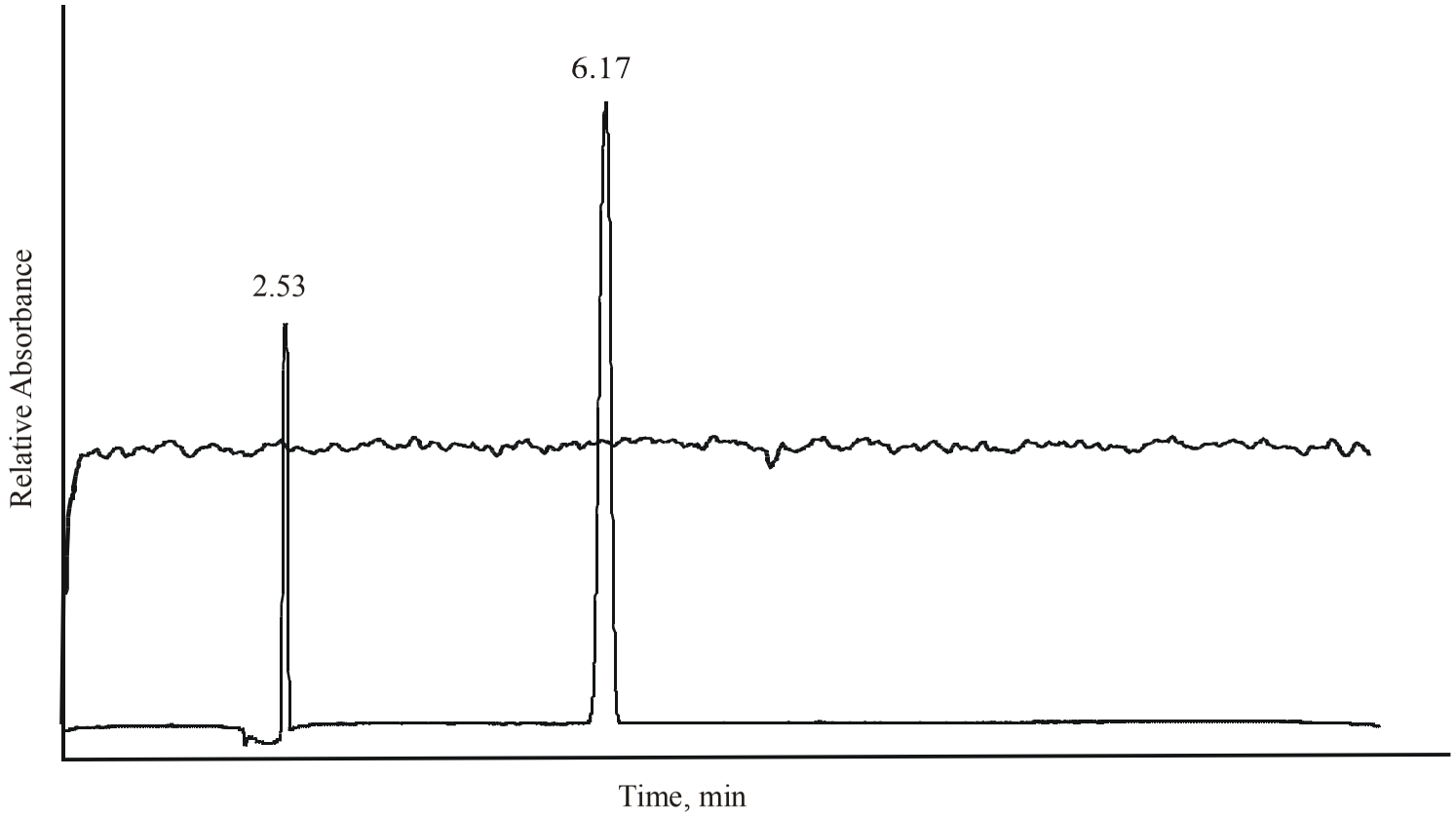
6.17
2.53
Relative Absorbance
Time, min

not exhibit any dips or spikes. The conclusion can then be made that stable electrical contact is maintained throughout the course of the CE analysis.

Adaptation of low CE flow rates has posed a problem for several other interface designs, which includes earlier attempts at CE–FT-IR interfaces as well many currently used CE–MS interfaces. The usual result is a compromise between mismatched flow-rates and a loss of resolution. Because the nebulizer design used in this interface was created to accommodate lower flow-rates, and because the CE system used is capable of using external pressure to drive the electroosmotic flow at a slightly faster rate, we are able to match the flow-rate of the CE system more closely to that of the nebulizer. During the CE–FT-IR spectrometric analyses, an external pressure of 2 bar was applied to the inlet buffer vial. This pressure ensured that the liquid maintained contact with the silver paint that coats the outlet of the column. This pressure, however, is minimal and does not appear to alter the flow characteristics of the CE system.

A commonly encountered obstacle in capillary electrophoretic interfaces is alteration of the plug flow by the nebulization of the eluent. This distortion creates laminar flow inside the column. In order to determine the existence of laminar flow inside the capillary column, studies as described by Schaumlöffel and Prange,[27] were carried out. By subjecting the interface to these conditions, any suction from the nebulization process and its effect on the liquid inside the column are clearly evident. When favorable results are obtained, the conclusion can be drawn that the interface nebulization process is not having an adverse effect on the typical electrophoretic plug flow in CE separations. Therefore, the following studies were completed on the glass nebulizer CE–FT-IR interface:

1. The electric current of 30 μA at an applied voltage of 15 kV was measured again after the capillary had been left open to air at the inlet for 1 h while the nebulizer was operating. The presence of current indicates that air, which disrupts the current and breaks electrical contact, was not drawn into the capillary during 1 h of nebulization.
2. The capillary was flushed with water and placed in the inlet vial containing a 5 mM solution of caffeine in 50 mM borate buffer. The absence of analyte peaks or a solvent front after 1 h of continuous nebulization indicates that the solution was not drawn into the capillary as a result of the nebulization gas flow.

Additionally, the nebulizer did not emit any droplets or aerosols during either study.

In mass spectral interfaces, there are additional concerns due to the sample introduction into an evacuated chamber; that is, lower sample chamber pressures increase the possibility of introduction of laminar flow profiles in the CE system. The CE–FT-IR spectrometric interface, however, is operated at ambient pressure and temperature with a nebulizer designed to handle lower liquid flow rates. Therefore, with careful gas flow control, we are able to maintain the plug flow profile, which is a main advantage of CE.

It was determined that the deposits were of uniform thickness, as evidenced by the lack of ridges in the central area of the deposit and by the uniform appearance when visualized under a microscope. Because interference patterns are not visible, we can conclude that the deposits at the thickest point are still thinner than the wavelength of visible radiation. This average thickness, if the entire analyte volume is collected in a single deposit, can be calculated by likening the deposit to a cylinder. For a typical

Figure 3.5. CE–FT-IR spectra of pure borate buffer, N-acetylglucosamine (GlcNAc) in 50 mM borate and 50 mM ammonium acetate buffers, and of the pure monosaccharide. Borate absorbance bands completely mask the characteristic analyte bands, but the analyte spectrum is clearly evident when the volatile ammonium acetate buffer is used.

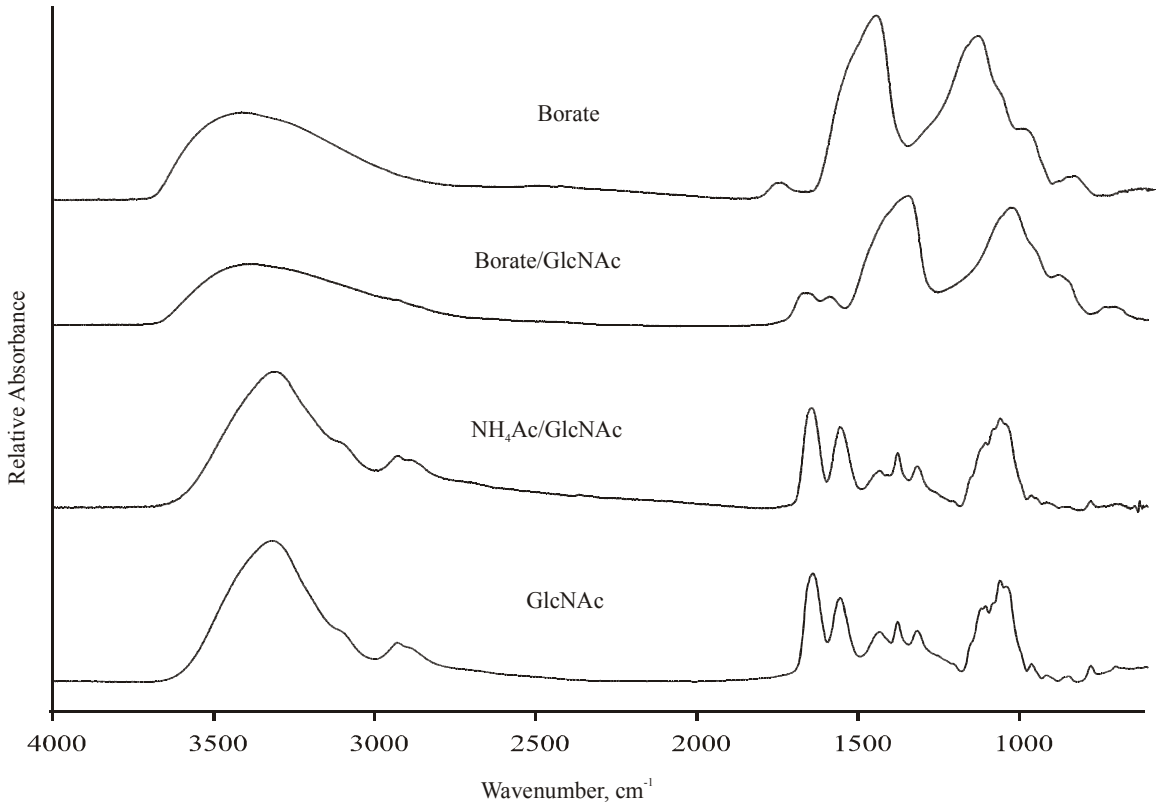
Borate
Borate/GlcNAc
NH4Ac/GlcNAc
GlcNAc
Relative Absorbance
4000
3500
3000
2500
2000
1500
1000
Wavenumber, cm-1

injection of 20 ng and a deposit size of 300 μm diameter, the thickness can be calculated as approximately 400 nm.

Finally, one major obstacle in the development of a successful CE–FT-IR interface is the interference of electrolyte absorbance bands in the analyte spectra. To determine the feasibility of alternative buffers that are not as electrolytic, but are more volatile, two solutions of N-Acetylglucosamine (GlcNAc), 5 mM in 50 mM Borate and 50 mM ammonium acetate, were analyzed with the interface on the Beckman instrument. Spectra of the pure buffer solution and the pure compound were also collected. The results, shown in Figure 5, reveal the spectral improvements gained with a more volatile buffer. Spectra of a deposit of pure ammonium acetate could not be collected as it is too volatile to leave a deposit.

Conclusions

The interface as described proved to be successful in a number of areas. Three main requirements of CE interfaces were satisfied which indicates that the system functions as a working interface. The apparatus has proven successful on two separate capillary electrophoresis systems, which attests to its flexibility and sturdy design.

Future projects are aimed at improvement of the interface design and further characterization its analytical properties. Although the interface is currently designed for off-line FT-IR analyses, an on-line design is in progress, and precise metering valves will be added to obtain a more accurate measure of actual helium and nitrogen gas flows. In order to address the problem of solvent absorption in the IR region, the interface was designed to accomplish solvent elimination concurrent with eluent nebulization. This

step requires a relatively volatile buffer, which is a problem in most capillary electrophoretic analyses. More specifically, the electrolyte itself must be relatively volatile. Typical CE analyses involve aqueous electrolyte solutions. Water is easily removed from the sample deposit through simple evaporation. Any remaining electrolyte molecules, however, are much more problematic and can be trapped in the sample matrix so that buffer removal is not always possible and spectral identification may be significantly impaired. The difficulties with weaker (more volatile) electrolytes arise when high volatility buffers are incapable of carrying the current needed for reliable, reproducible separations. Common CE electrolytes are sodium borate and sodium phosphate but more volatile alternatives currently under investigation include ammonium phosphate, ammonium formate, and ammonium acetate.

Acknowledgments

The authors wish to thank Dr. John L. Stickney and Lindell C. Ward (UGA, Athens, GA, USA) for the use of the optical microscope. The authors also wish to thank the National Institutes of Health for a National Research Resource grant (number 2P41-RR-05351) for the Resource Center for Biomedical Complex Carbohydrates.

References

1. Norton, K.; Griffiths, P. *J. Chromatogr. A* **1995**, *703* (1-2), 392.
2. Bartz, A.; Ruhl, H. *Anal. Chem.* **1964**, *36* (10), 1892.
3. Griffiths, P.; de Haseth, J.; Azarraga, L. *Anal. Chem.* **1983**, *55*, 1316A-1387A.
4. Visser, T.; Vredenbregt, M.; de Jong, A.; Somsen, G.; Hankemeier, T.; Velthorst, N.; Gooijer, C.; Brinkman, U. T. *J. Mol. Struc.* **1997**, *408-409*, 97.
5. Rodriguez, I.; Bollain, M.; Cela, R. *J. Chromatogr. A* **1996**, *750* (1-2), 341.
6. Rodriguez, I.; Bollain, M.; Garcia, C.; Cela, R. *J. Chromatogr. A* **1996**, *733* (1-2), 405.
7. Norton, K. L.; Griffiths, P. R. *J. Chromatogr. A* **1995**, *703* (1-2), 383.
8. Huilian, H.; Minghua, Z.; Yihua, H.; Kefu, S. *J. Chromatogr. A* **1991**, *547*, 494.
9. Wurrey, C. J. *TrAC* **1989**, *8* (2), 52.
10. Henry, D.; Giorgetti, A.; Haefner, A.; Griffiths, P.; Gurka, D. *Anal. Chem.* **1987**, *59* (19), 2356.
11. Gurka, D.; Titus, R.; Griffiths, P.; Henry, D.; Giorgetti, A. *Anal. Chem.* **1987**, *59* (19), 2362.
12. Issaq, H.; Chan, K.; Janini, G.; Muschik, G. *Electrophoresis* **1999**, *20* (7), 1537.
13. Geiger, J.; Korte, E.; Schrader, W. *J. Chromatogr. A* **2001**, *922* (1-2), 99.
14. Karami, A.; Balke, S.; Schunk, T. *J. Chromatogr. A* **2001**, *911* (1), 27.
15. Somsen, G.; Gooijer, C.; Brinkman, U. *J. Chromatogr. A* **1999**, *856* (1-2), 213.
16. Turula, V.; Bishop, R.; Ricker, R.; de Haseth, J. *J. Chromatogr. A* **1997**, *763* (1-2), 91.

17. Smith, S.; Jordan, S.; Taylor, L.; Dwyer, J.; Willis, J. *J. Chromatogr. A* **1997**, *764* (2), 295.

18. Yang, J.; Griffiths, P. R. *J. Chromatogr. A* **1997**, *785* (1-2), 111.

19. Amador-Hernandez, J.; Luque De Castro, M. *J. Biochem. Biophys. Meth.* **2000**, *43* (1-3), 329.

20. Todebush, R.; He, L.; de Haseth, J., 2002; *Anal. Chem.* **2003**, *75* (6), 1393-1399.

21. Bonneil, E.; Waldron, K. *Talanta* **2000**, *53* (3), 699.

22. Issaq, H.; Chan, K.; Janini, G.; Muschik, G. *J. Liq. Chromatogr. Rel. Tech.* **2000**, *23* (1), 154.

23. Cao, P.; Moini, M. *J. Am. Soc. Mass Spectrom.* **1998**, *9* (10), 1088.

24. Moini, M. *Anal. Chem.* **2001**, *73* (14), 3501.

25. Zhang, B.; Foret, F.; Karger, B. *Anal. Chem.* **2001**, *73* (11), 2681.

26. McComb, M.; Perreault, H. *Electrophoresis* **2000**, *21* (7), 1362.

27. Schaumlöffel, D.; Prange, A. *Fresenius' J. Anal. Chem.* **1999**, *364*, 452-456.

28. B'Hymer, A.; Day, J.; Caruso, J. *Appl. Spectrsc.* **2000**, *54* (7), 1040-1046.

29. Tangen, A.; Lund, W.; Josefsson, B.; Borg, H. *J. Chromatogr. A* **1998**, *826*, 87-94.

30. Figeys, D.; Ducret, A.; Aebersold, R. *J. Chromatogr. A* **1997**, *763*, 295-306.

31. Deng, B.; Chan, W.-T. *J. Chromatogr. A* **2000**, *891*, 139-148.

32. Barnidge, D.; Nilsson, S.; Markides, K. *Anal. Chem.* **1999**, *71*, 4115-4118.

33. Lu, G.; Bird, S.; Barnes, R. *Anal. Chem.* **1995**, *67* (17), 2949-2956.

CHAPTER 4

CHARACTERIZATION AND APPLICATION OF FOURIER TRANSFORM INFRARED SPECTROMETRIC DETECTION IN CAPILLARY ELECTROPHORESIS[1]

[1] Jarman, J. L.; J. A. de Haseth. To be submitted to *Analytical Chemistry* for publication.

Abstract

Capillary electrophoresis/Fourier transform infrared (CE/FT-IR) spectrometric interfaces, while still in the developmental stages, have many advantages over traditional CE methods for analyte identification. Both CE and FT-IR spectrometry are relatively inexpensive, highly efficient, and sensitive techniques that can be used for a wide variety of samples. In traditional CE, analyte identification is achieved through non-specific information collected, including migration time, laser-induced fluorescence (LIF) and ultraviolet-visible (UV-vis) absorption. FT-IR spectrometry, however, is a structurally specific technique often used for structural determinations. One major advantage of a CE/FT-IR interface is the use of traditional detection and the exploitation of the structural specificity of the infrared region, which adds a much more reliable identification technique. Presented here are significant improvements and continued characterization of our existing successful CE/FT-IR interface. Results from studies on electrical stability, column robustness, and analyte recoverability are presented.

Introduction

One persistent criticism of chromatographic separations is that analyte identification is often accomplished by non-specific means, such as comparing migration times or peak areas.[1] Detection methods such as ultraviolet-visible (UV-Vis) absorption reveal only limited information while other methods such as laser-induced fluorescence (LIF) require either compound labeling or the presence of a native fluorescent group within the molecule.[2,3] As a result, several attempts have been made to interface traditional chromatographic systems with more powerful identification techniques such as mass spectrometry (MS), Raman spectroscopy,[4,5] and Fourier transform infrared (FT-IR) spectrometry. Until relatively recently, these interfaces have been restricted to liquid[6-9] or gas chromatography[6,10] (LC or GC). Increased use of capillary electrophoretic (CE) separation methods has increased the demand for identification of minute sample quantities and led to the development of a CE/FT-IR spectrometric interface.

CE is a separations technique that utilizes an electrical current in order to separate charged species. CE is considered a highly valuable technique in multiple areas of scientific interest due to its high resolving capabilities and minute sample requirements. A typical CE system includes two electrolyte, or running buffer, reservoirs, a high voltage supply, a capillary column, a sample reservoir, and a detector.[11-13] Although early CE systems used modified LC detectors, commercially available detection methods now include UV-vis absorption, LIF, and pulsed amperometric detection (PAD). Separation is achieved with the application of a high voltage applied across the silica column, which are commercially available in a wide variety of types. The applied

voltage creates two types of flows within the column, electroosmotic and electrophoretic. The electroosmotic flow (EOF) is responsible for moving analyte molecules past the detection window and toward the outlet of the column while charged analyte molecules are separated according to individual electrophoretic mobilities directly related to the charge-to-mass ratio. Sample introduction is accomplished with pressure or electrokinetically, and net flow rates within the column are approximately 100 nL/min.

Although separation of neutral particles requires slight modifications or optimization in electrolyte systems,[14] CE separations are characterized by sharp narrow peaks and relatively short migration times. Additionally, traditional CE columns are uncoated, fused silica and are therefore easy to flush and can be used with varied conditions. Minimal operational costs and highly automated systems have greatly increased the applicability and attractiveness of CE, and the literature base for reliable CE method development continues to increase rapidly.[15,16] CE is also an easily hyphenated technique, and has resulted in several successful configurations, including a wide variety of MS interfaces as well as CE-Raman interfaces.

Fourier transform infrared (FT-IR) spectrometry is a highly sensitive vibrational spectrometric technique that has the added advantages of being non-destructive and structurally specific. Although FT-IR interfaces with various separations techniques such as LC[17-21] or GC[22-25] are quite common and reliable, the true potential of infrared (IR) spectrometry has not yet been realized. One of the main advantages of IR spectrometry is the flexibility it offers for spectral collection. Materials in almost any form can be spectrally interrogated, regardless of chemical and physical characteristics including crystallinity, solubility, and phase at room temperature. Techniques used for analysis

include single and multiple reflection attenuated total reflection (ATR), diffuse reflection, transmission, flow cells, and transmission or reflection microspectrometry. In addition, spectral analyses are carried out in minutes and have been shown to have detection limits as low as the picogram range.[26-29]

The combination of CE and FT-IR spectrometry, therefore, results in a system for the separation of a large number of compounds that has more powerful identification abilities than migration time comparisons and UV-vis spectra. Recent advances in CE/FT-IR interfaces include on-column[30,31] and off-column[32,33] interfaces, which add to the versatility of the technique. Interfaces have been shown to be much more robust and reliable than it was originally believed possible.

Common criticisms of CE interfaces in general include lack of stable electrical contact, difficulty in accommodation of low CE flow rates, and difficulty in prevention of laminar flow within the column. As a result, many CE interfaces utilize make-up buffers or negative pressure application to enable efficient nebulization without induction of laminar flow.[34-37] One additional difficulty associated with FT-IR spectrometric interfaces is overcoming strong solvent or buffer absorbance bands in the IR spectra. In this case, CE buffers should either be completely eliminated from the dried deposit, or should be suitable for spectral subtraction. Ideally, dry deposits from the interface consist of pure analyte in an amorphous form in order to eliminate spectral shifts associated with polymorphic crystalline forms and loss of sensitivity due to scattered radiation. Traditional CE buffers such as sodium borate are involatile such that complete buffer elimination is not possible, and spectral subtraction is unsuccessful due to analyte

band shifts from the complexation. Buffer interferences, however, are easily overcome with the use of more volatile buffers such as ammonium acetate and ammonium formate.

Traditional CE systems require the column and electrodes to be immersed in two electrolyte vials: an inlet vial and an outlet vial. In order to successfully interface the instrument, the outlet vial must be rendered unnecessary such that the electrical circuit is completed in another manner. CE interfaces maintain electrical contact in a variety of ways, including sheath liquids,[34,36-38] pierced or cracked columns,[39] or what are known as "metal coating" interfaces.[33,40-42] The interface described here and shown in Figure 4.1 is a metal coating interface, with a thin layer of conductive paint applied to a portion of the end of the column. Electrical contact is made when the liquid eluting from the column comes in contact with the silver paint along the column edge. The painted portion of the column extends far enough down the length of the column to be in contact with a metal clamp that is connected to the instrument ground wire. Therefore, it is important that the coating remains solid, without flaking or peeling, and that the liquid flow remains constant. Further, the paint must not block the end of the column and should be hardy enough to be fitted through relatively tight fittings and to endure storage conditions, and flexible enough to allow for column manipulation.

While flow accommodation and electrical stability have been successfully demonstrated,[33] the interface has now been characterized for performance under much more strenuous conditions, including column condition after an extended storage period, high voltage application, and stability of column and interface after multiple subsequent analysis runs. Standards such as caffeine and a mixture of carbohydrates are analyzed under normal CE conditions, which include minute sample injection volumes and low

Figure 4.1. Schematic depiction of a microconcentric glass nebulizer apparatus for a CE/FT-IR spectrometric interface.

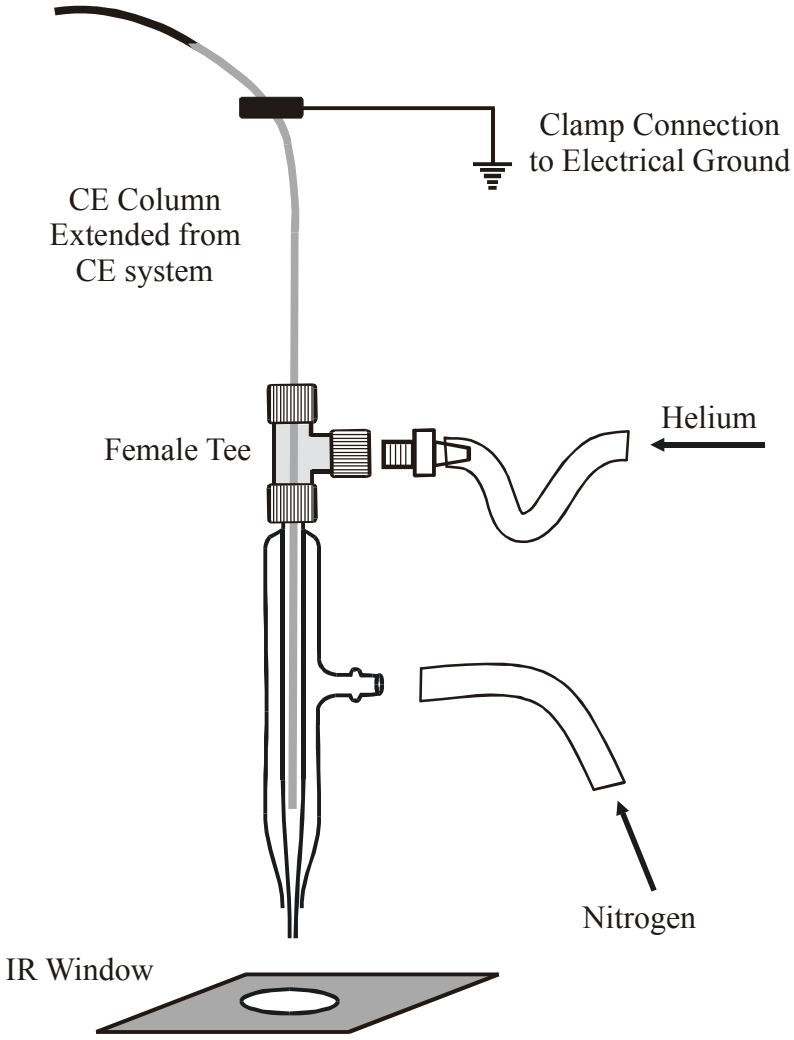
Clamp Connection
to Electrical Ground
CE Column
Extended from
CE system
Female Tee
Helium
Nitrogen
IR Window

solution concentrations. Collection of single-component deposits from these minute injections has been shown, despite relatively low peak resolution at the time of reference detection. Furthermore, injected analytes are reliably deposited and have been shown to be recoverable in quantities great enough for single reflection ATR analyses. Spectral identification of the collected compounds is accomplished without reliance upon migration time comparison or spiked solution verification.

Experimental

Chemical Reagents. The primary electrolytic solution used was ammonium acetate (NH_4Ac, Sigma, St. Louis, MO, USA); ammonium hydroxide (NH_4OH) and sodium hydroxide (NaOH) were purchased from Fisher Scientific (Atlanta, GA, USA) and used as needed. All were used as received.

Running buffer consisted of an aqueous ammonium hydroxide solution adjusted to the desired pH with ammonium hydroxide.[43] Electrolyte concentration was 5.0×10^{-2} M at 6.98, 10.0 or 12.0 pH unless otherwise stated. All solutions were prepared with 18.0 MΩ deionized water purified with a Barnstead Nano Ultrapure water system (Boston, MA, USA).

The following samples were used to test the stability and separation ability of the interface: caffeine (Baker, Phillipsburg, NJ, USA), sucrose (Fisher Scientific) and N-Acetylglucosamine (GlcNAc, Sigma, St. Louis, MO, USA). Solutions of each compound were made with 18 MΩ water to final concentrations of 5.0×10^{-3} M.

The samples were deposited onto 25-mm diameter x 6-mm thick zinc selenide (ZnSe) or calcium fluoride (CaF_2) windows (Spectral Systems, Hopewell Junction, NY,

USA). Analyte recovery was accomplished with a small volume of water being used to solvate the dry deposit, after which the water was drawn up with a 1-μL microcapillary (Drummond Scientific, Broomall, PA, USA) and deposited onto an internal reflection element. The solvent was allowed to evaporate prior to spectral interrogation.

CE and FT-IR Spectrometry. CE analyses were performed with an Agilent ^{3D}CE instrument (Agilent Technologies, Palo Alto, CA, USA) equipped with a UV-Vis diode array detector. The system was controlled with ^{3D}CE Chemstation software.

Uncoated fused silica capillaries (Agilent Technologies, Wilmington, DE and Polymicro Technologies, Phoenix, AZ, USA), with an outer diameter of 360 μm and inner diameters of 50 and 75 μm were used. The extended capillary was 21.5 cm to the reference UV-vis detection window and 103.5 cm total length. Column conditioning was accomplished with 0.1 M sodium hydroxide, ultrapure water, and running buffer rinses prior to each analytical run. Analyses were carried out at 20°C with an applied voltage of 17-25 kV and simultaneous UV-vis detection at 214 nm as a back-up for the IR detection method. Injection was accomplished by applying 10-50 mbar of pressure to the sample vial for 2-5 sec.

CE/FT-IR spectra were collected with a Perkin-Elmer Spectrum 2000 FT-IR spectrometer coupled with a Perkin-Elmer *i*-series FT-IR microscope with an adjustable limiting aperture (Perkin-Elmer). The microscope detector was a liquid nitrogen cooled mercury-cadmium-telluride (MCT) detector (Perkin-Elmer). The aperture allows for the beam size to be set from 10 to 400 μm in diameter to allow for variations in sample size. The spectra were collected with PEImage software. Spectral processing such as digital

subtraction, baseline correction, and normalization, was performed with the use of GRAMS/32 AI v.7.00 software (Thermo Galactic, Salem, NH, USA).

Recovered deposits were analyzed with a Bio-Rad FTS 4000 spectrometer fitted with a single reflection silicon Harrick SplitPea™ ATR accessory. The internal reflection element had an active area 250 μm in diameter and a 45° angle of incidence. The spectrometer detector was a deuterated tri-glycine sulfate (DTGS) detector (Digilab LLC, Randolph, MA). Both microspectral analyses and ATR analyses involved the collection of 100 scans co-added at a resolution of 4 cm^{-1}.

Glass Interface. The interface shown in Figure 4.1 and used here was fashioned from a custom-designed microconcentric glass nebulizer with an extended tip (J.E. Meinhard, Santa Ana, CA, USA). The extended tip was designed to accommodate low CE flow rates and serves to guide effluent toward the IR window. A female tee (Upchurch Scientific, Oak Harbor, WA, USA) is fitted to the top of the nebulizer. The CE column is partially coated with silver paint (Fullam, Latham, NY, USA) and threaded through the tee into the nebulizer where it remains during all analyses. A clamp is attached to the column such that the silver paint remains at electrical ground. The tip of the column is placed just to the narrowing point of the inner capillary for the nebulizer. Helium flow, which serves to aid in solvent evaporation and liquid expulsion from the nebulizer, is introduced through the tee and nitrogen is introduced through the outer shell of the nebulizer. Nitrogen flow can be eliminated with more volatile buffer concentrations in order to optimize deposition and prevent solute crystallization within the nebulizer. A more detailed description is found elsewhere.[33]

Results and Discussion

Previously reported results included separations performed in sodium borate buffer solutions, which provided excellent separation ability but was unsuitable for IR analyses. It was determined that a change was warranted in which weaker, more volatile electrolyte systems are used. These solutions created some concern with regard to the electrical stability of the interface system. Less volatile buffers such as sodium tetraborate have high conductivity, are widely used to separate neutral species, and have proven success in interfaced systems. Low volatility, however, can lead to co-deposition of the buffer and complexation with neutral molecules changes analyte spectra from those collected from corresponding pure solutions. More volatile buffer solutions such as ammonium formate and ammonium acetate have lower conductivity and therefore result in a loss of electrophoretic resolution. In addition, the potential for a break in electrical contact is increased. It has been shown that high quality FT-IR spectra can be collected of analytes in low concentration ammonium acetate solutions. Therefore, this particular electrolyte was the primary focus of analyses presented here in the efforts to further awareness and applicability of the glass interface apparatus.

One major drawback to several CE interfaces is the lack of long-term stability in storage conditions. Particularly fragile interfaces such as pierced or cracked columns, or columns etched in-house to create a nebulizing nozzle often have to be remade, sometimes requiring several attempts before achieving a successful device.[44-46] The interface described here, however, has been shown to withstand tight fittings, clamps, and normal day-to-day use including removal from the interface for extended column flushing and nebulizer cleaning. In addition, all analyses presented here were completed

with a column that had been coated and stored for intervals of four months. The painted coating required minimal retouching, if any.

CE interfaces must overcome several obstacles in order to be successful. A feasible apparatus must be electrically stable for long periods of time, which means that the electrical current during a separation must remain constant. Therefore, twelve consecutive analytical runs were performed under various conditions in order to determine factors affecting current stability. Injection was varied from 5-10 mbar for 1-5 sec and included analyte solutions of 5 mM caffeine, a mixture of 0.1 M GlcNAc and 0.07 M sucrose (1:1, v/v), individual GlcNAc and sucrose solutions, and a mixture of oligosaccharides, all mixed to the desired concentrations in 50 mM ammonium acetate, pH 6.98. One major factor that often affects CE current stability is electrolyte depletion. For these runs, the electrolyte concentration remained constant at 50 mM, but the vial was replaced after the fifth and the tenth runs, such that a large variation in the degree of buffer depletion was allowed. Temperature was held constant at 20°C. The current during each analysis was recorded and Figure 4.2 shows twelve overlaid traces. The twelve current traces show remarkable stability throughout each 25 minute run and excellent run-to-run reproducibility. The most likely time for electrical contact to be broken is when the droplets exit the nebulizer and the eluent is no longer in contact with the rim of the coated capillary. Despite constant nebulization, however, the current remained stable between 36 and 38 μA with an applied voltage of 17 kV. A study was also completed to determine whether the interface could withstand voltages in the higher range of instrumentation limits. For the purposes of comparison, the same solution of GlcNAc and sucrose was used with an injection of 10 mbar for 2 sec, and the temperature

remained 20°C. The analysis was completed in fresh 50 mM ammonium acetate buffer, pH 6.98, with an applied voltage of 25 kV, and the recorded current is shown in Figure 4.3. It can be seen that the higher voltage did not adversely affect the electrical stability of the system and, in fact, the current remained stable at about 60 μA. It is possible that an increased current would prevent analyte separation in the short length to the reference detection window, which accounts for the single peak shown in the electropherogram. One of the most likely instances for current variation is when the sample plug exits the capillary due to the potential difference in conductivities. While the second analyte cannot be determined from the reference detection, the first analyte should exit the column at approximately 11 min. The current trace, however, remains constant throughout the entire analysis, which indicates that the sample plug did not adversely affect the electrical contact.

Once the electrical stability was demonstrated, CE analysis of a single analyte was performed in an attempt to successfully collect an analyte deposit. Because previous studies indicated the preservation of plug flow within the column, the flow rate can be considered constant throughout the course of an analytical run.[33] Therefore, the rate of analyte migration to the 21.5 cm UV-vis reference detection window is maintained to the end of the column and through the interface. In order to calculate the elution time, therefore, a simple ratio of the known column lengths and reference detection time is used. The necessary equation is:

$$\frac{L_1}{t_1} = \frac{L_2}{t_2} \qquad \text{or} \qquad t_2 = \frac{L_2 t_1}{L_1} \tag{4.1}$$

Figure 4.2. Overlaid current traces from twelve successive analyte runs. Runs were performed with a variety of buffer conditions, injection volumes, and analyte compounds, yet current remained stable at 36-38 μA with an applied voltage of 17 kV.

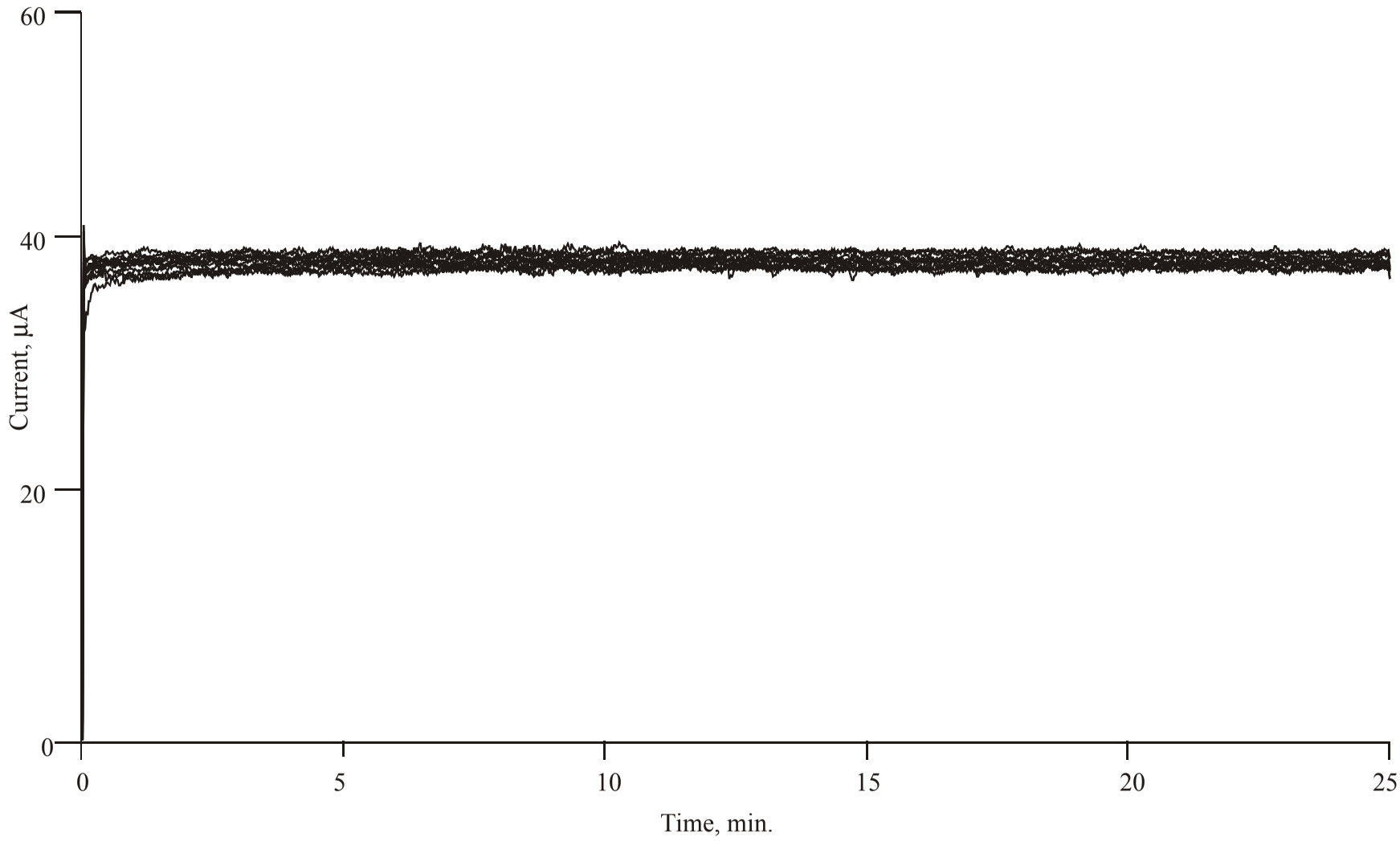
60
40
20
0
Current, µA
0
5
10
15
20
25
Time, min.

Figure 4.3. A single component analysis to demonstrate stability with application of higher voltages. Current remained stable at 60 μA with an applied voltage of 25 kV.

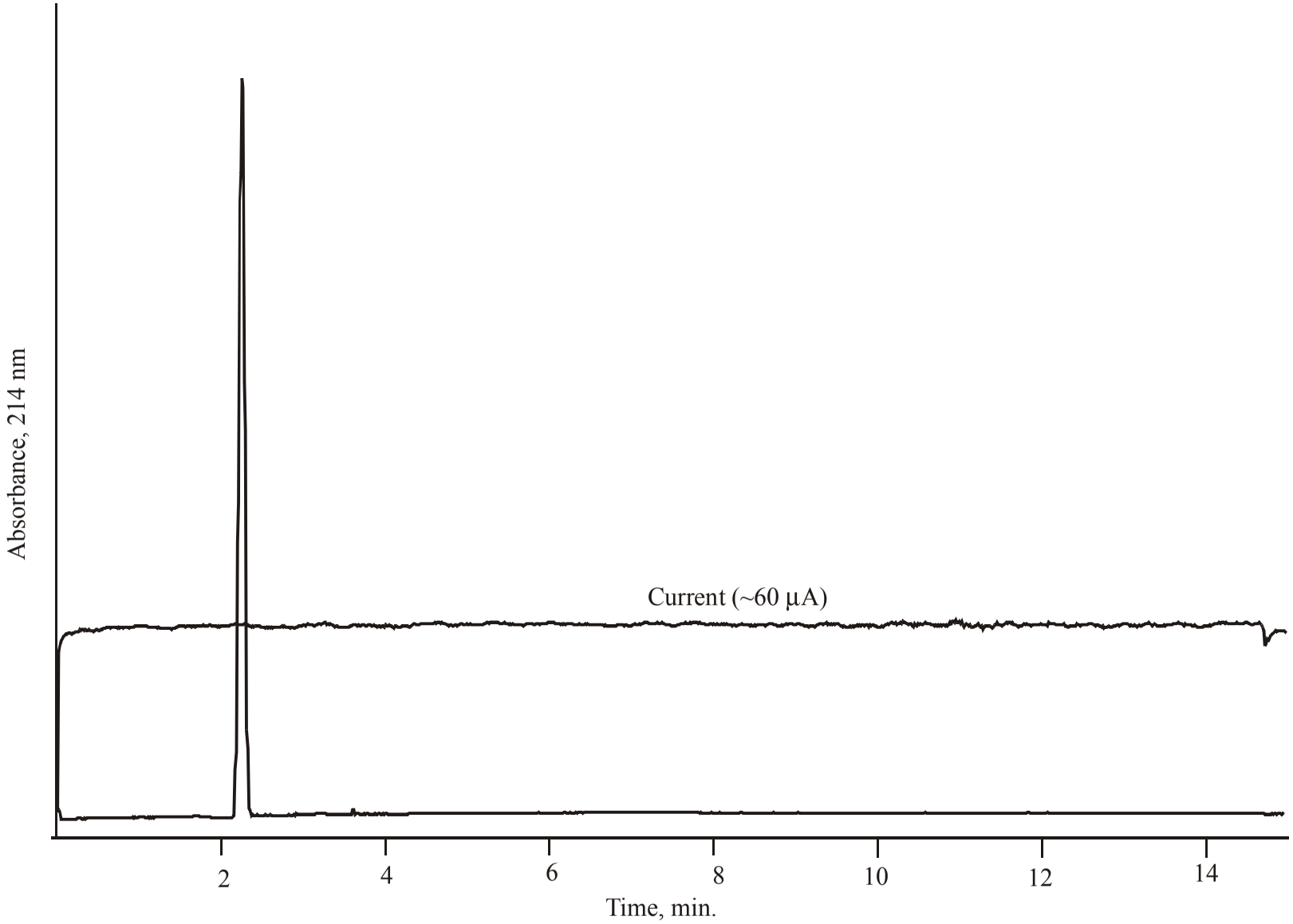
Absorbance, 214 nm
Current (~60 µA)
2
4
6
8
10
12
14
Time, min.

Figure 4.4. A single analyte run in order to demonstrate successful deposit collection. For this analysis, 5 mM caffeine (aq) was injected with 50 mbar pressure for 5 sec. Running buffer was 25 mM ammonium acetate, pH 12.0, and absorbance was recorded at 200 nm. Current was also recorded and remained stable at approximately 14 μA with an applied voltage of 17 kV at 20°C.

2.257
Current (~14μA)
Absorbance (200 nm)
0
Time, min.

in which L_1 is the column length to the detection window, L_2 is the total column length, t_1 is the time required to reach the detection window, and t_2 is the time required to migrate the total column length. For example, the caffeine plug shown in Figure 4.4 reached the on-column detection window at approximately 2.26 min. Therefore, with a column in which L_1 is 21.5 cm and L_2 is 103.5 cm, analyte elution is expected at 10.6 min. Because a large amount of analyte was injected, six deposits were collected between 9.6 and 11.6 min, four of which were found to contain caffeine. The spectrum collected from one of the deposits, shown in Figure 4.5a, has characteristics of both pure caffeine (Figure 4.5b) and the high pH ammonium acetate buffer (Figure 4.5c). When a spectral subtraction was performed (Figure 4.6), the characteristic caffeine bands became more apparent. However, there are residual spectral features in the region between 1600 and 1500 cm^{-1}, which cannot be accounted for. In an effort to eliminate possible contaminants from the CE system, spectra from pure caffeine and buffer solutions were collected on the microspectrometer and spectrally added. The result, shown in Figure 4.7, resembles the spectrum from the collected deposit although there is obvious discrepancy in the region of interest. One possible explanation for the residual features emerges with the analysis of ammonium acetate in the solid phase crystalline form. As shown in Figure 4.8, the band shifts in the crystalline form of ammonium acetate overlap more closely with the region in question. Upon further examination of the caffeine and buffer interface deposits (Figures 4.9a and 4.9b, respectively), ammonium acetate crystals are visible in both. Therefore, spectra from both the amorphous form and the crystalline form must be subtracted in order to produce a high quality spectral result and completely eliminate the possibility of impurities.

Figure 4.5. Spectral comparison of deposits of **A.** the collected interface deposit, **B.** caffeine stock solution, and **C.** ammonium acetate buffer stock solution. All deposits were allowed to dry completely prior to microspectrometric analyses.

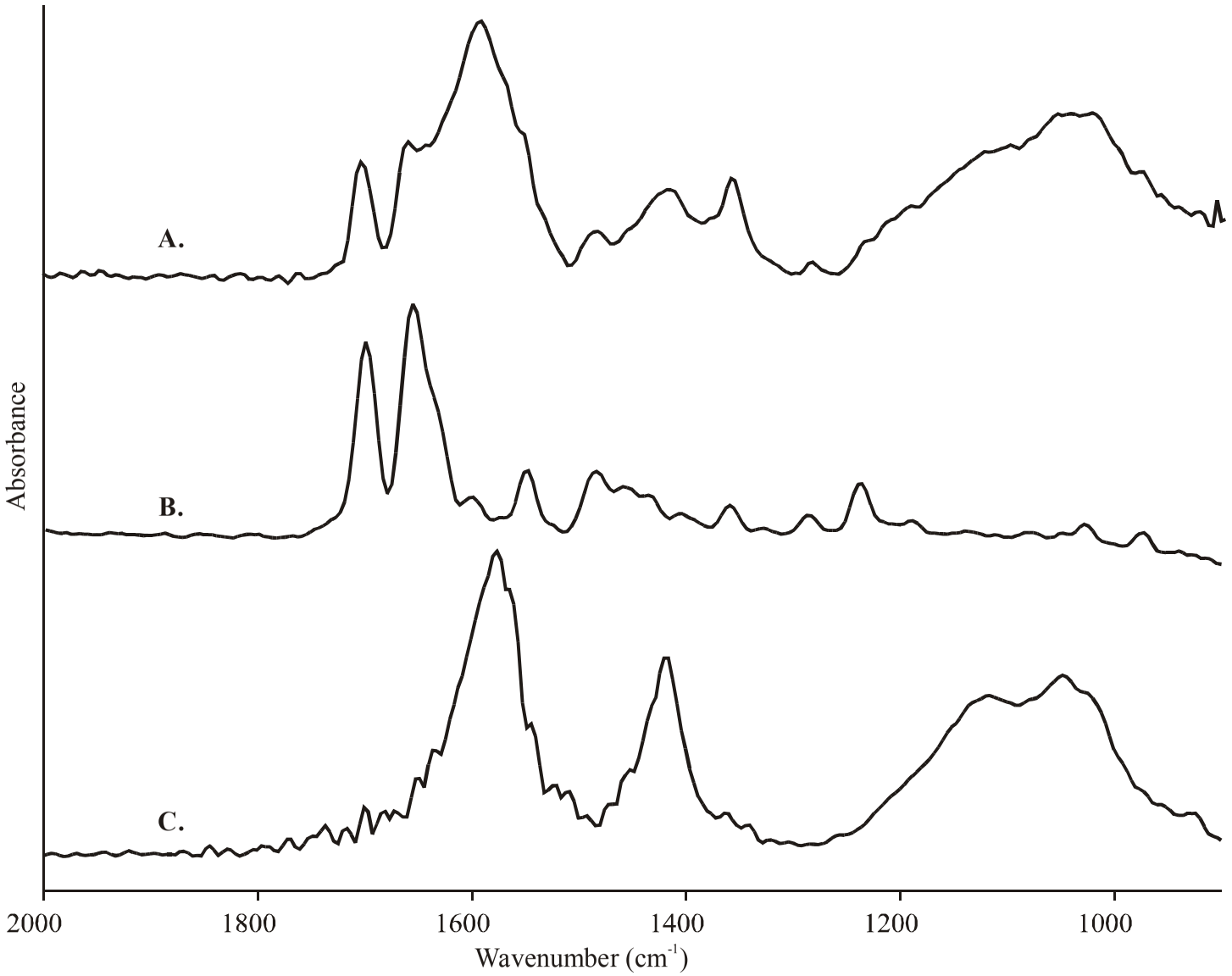
A.
B.
C.
Absorbance
2000
1800
1600
1400
1200
1000
Wavenumber (cm-1)

Figure 4.6. Results of a buffer subtraction to remove remaining spectral features of ammonium acetate. Caffeine bands became more apparent with the exception of the marked region between 1600 and 1500 cm^{-1}.

Absorbance
2000
1800
1600
1400
1200
1000
Wavenumber (cm-1)

Figure 4.7. Spectral comparison between the sum of stock caffeine and buffer solutions (dashed trace) and the deposit collected from the interface (solid trace). Good spectral correlation helps eliminate the possibility of contamination from introduction to the CE system.

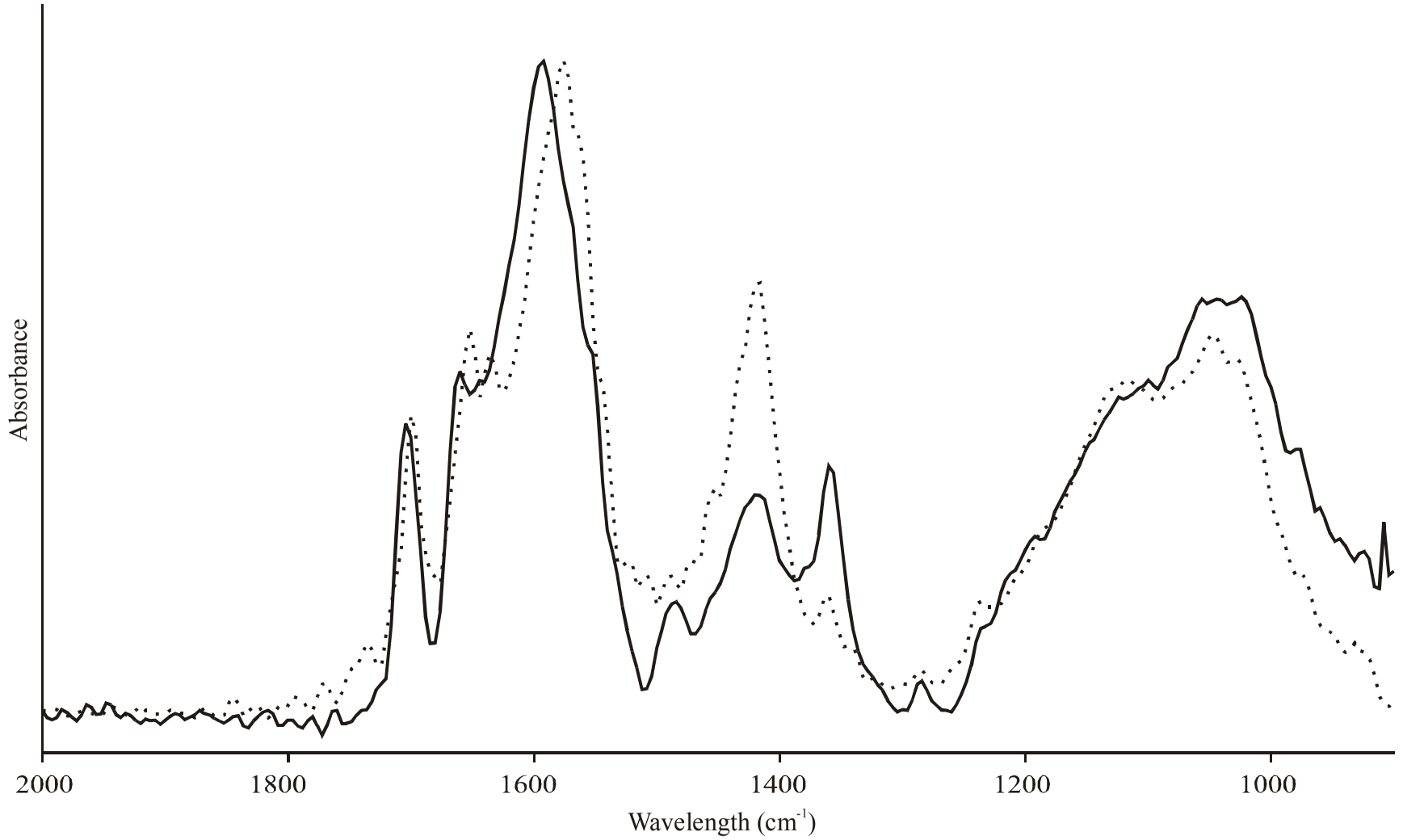
Absorbance
2000
1800
1600
1400
1200
1000
Wavelength (cm-1)

Figure 4.8. Spectral comparison of solid phase ammonium acetate (dashed trace) and the interface deposit (solid trace). Contributions in the interface spectrum due to crystallization of the buffer instead of amorphous deposition could account for region of inadequate buffer subtraction.

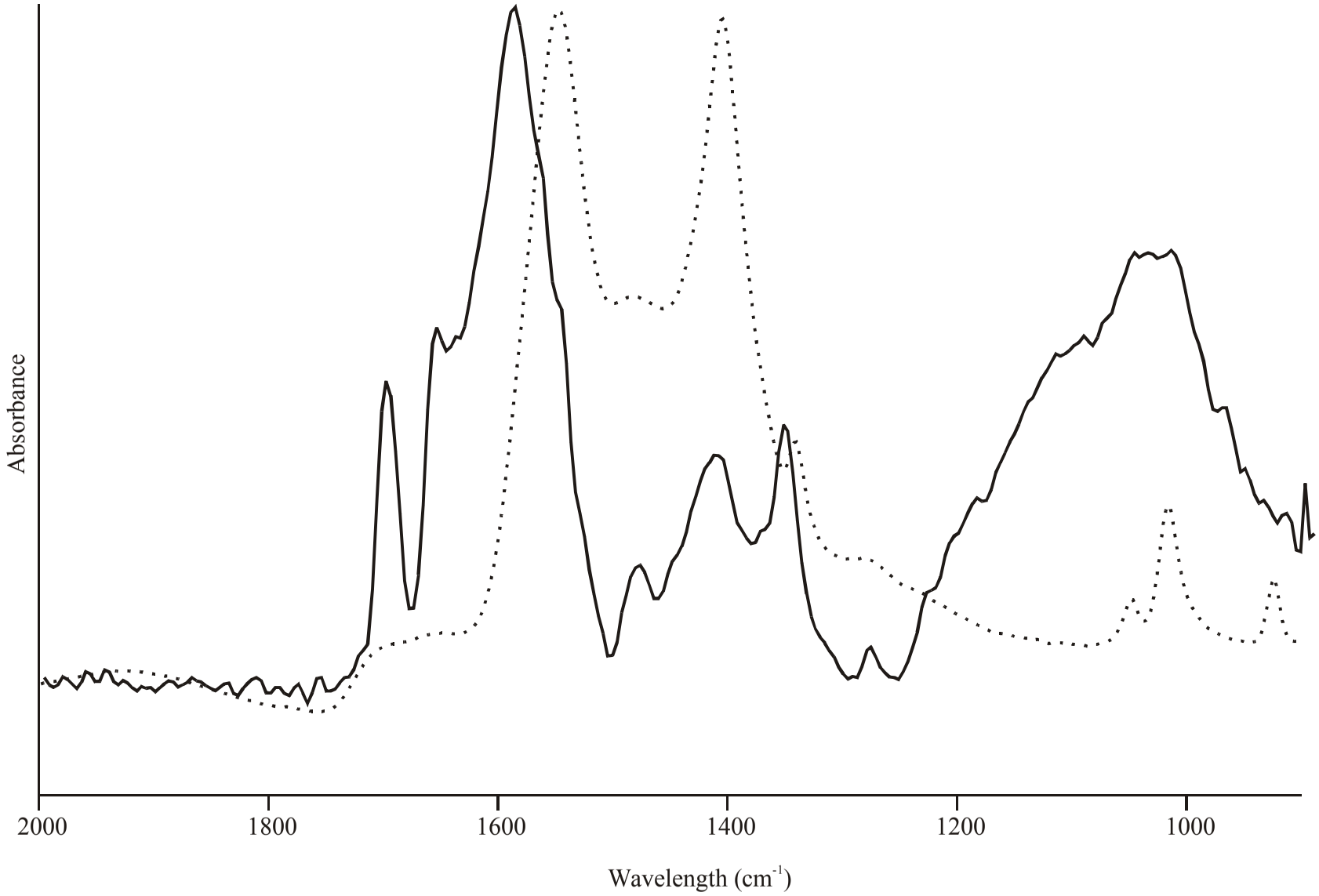
Absorbance
2000
1800
1600
1400
1200
1000
Wavelength (cm-1)

Figure 4.9. A. The collected and analyzed interface deposit. Needle-like caffeine crystals are clearly visible, as well as smaller, more round ammonium acetate crystals. **B.** A collected deposit of pure running buffer in which ammonium acetate crystals are more apparent.

A.

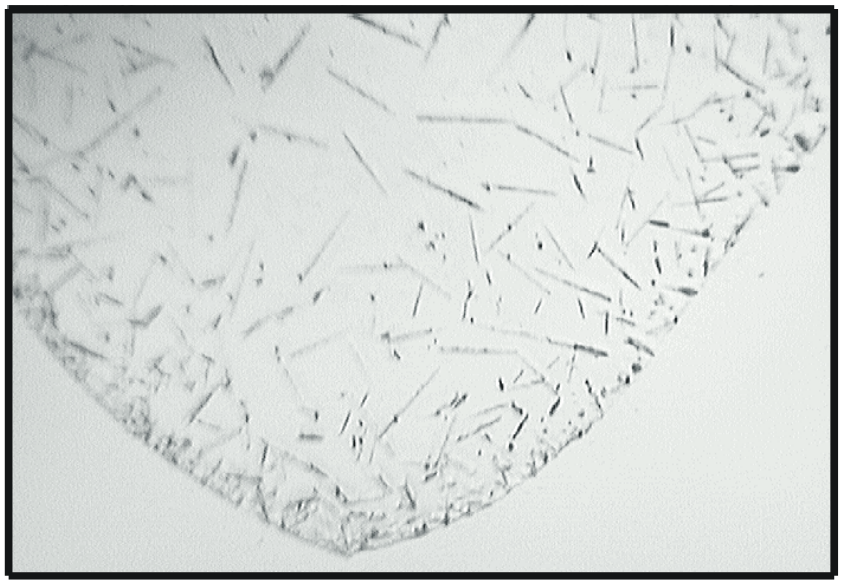

B.

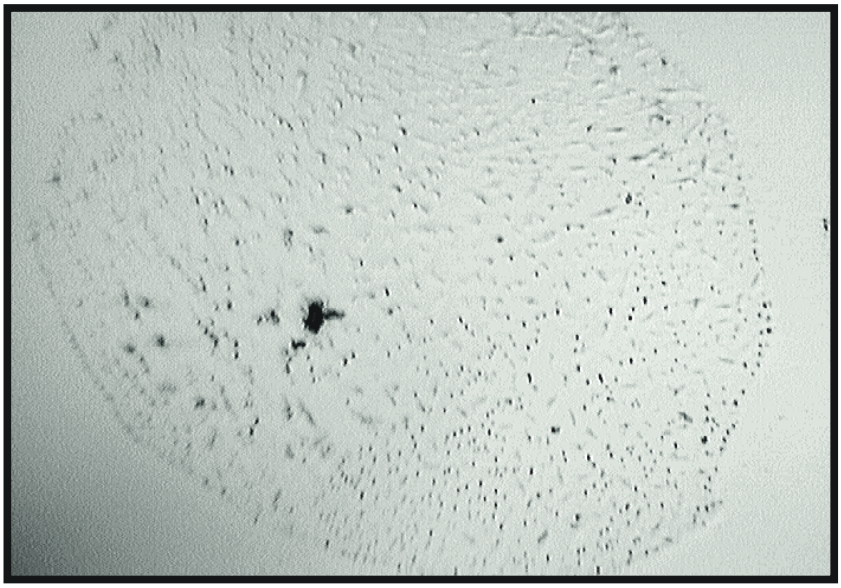

Ideally, interface deposits should contain only analyte molecules without crystallization of either analyte or solvent molecules. In this manner, the need for spectral processing is eliminated. In this case, however, the subtraction resulted in a spectrum suitable for analyte recognition through a spectral database and through visual comparison. The database returned caffeine as the top match from a library of 90,000 spectra. Neither deposit showed splatter patterns or evidence of large variations in thickness. Both of these attributes help to maximize spectral sensitivity by confining as much analyte as possible to a small, uniform area. In this manner, spectra can be obtained through analysis of any region of the deposit without encountering difficulties associated with regions of extremely high or low analyte concentrations.

Although previous studies showed analyte separations, collection of a single component from a multi-component analysis was necessary. It was unclear whether analytes eluting closely together could actually be deposited separately. Therefore, the separation of GlcNAc and sucrose shown in Figure 4.10 was performed and the first analyte peak was collected. A note of interest is that even though the analytes were not highly resolved at the reference detection window, use of Eq. 4.1 indicated that actual elution would occur almost two minutes apart. Therefore collection of single component deposits is easily accomplished. Because the electrolyte system used here was at pH 7.0 instead of >10 as in earlier analyses, the ammonium acetate was more volatile and the deposit was optically too thin for microspectrometric analysis. Therefore, the deposit was recovered with a small amount of water and re-deposited onto the single reflection ATR element of a Harrick SplitPea™. The ATR element has an active area of only 250 μm in diameter, which is well suited for such a small sample quantity. Sucrose and

GlcNAc spectra are shown in Figures 4.11a and 4.11b, and when they are compared with the analyte spectra from the collected deposit (Figure 4.11c), GlcNAc is the closest matching compound. Since buffer contributions are also evident, spectral subtraction of the buffer spectrum (Figure 4.11d) was performed, and the result is shown in Figure 4.11e.

Spectral band assignments can assist in determination of the chemical structure of the analyte as indicated in Figure 4.12. For example, the Amide I band usually found between 1640 and 1650 cm^{-1} shows up here at 1634 cm^{-1}, slightly lowered due to hydrogen bonding. The band commonly known as the Amide II is observed at 1553 cm^{-1}, which is well within the expected region. The band at 1411 cm^{-1} is most likely the in-plane bend of the hydroxide groups, although it is slightly raised from the usual 1350±50 cm^{-1}. This shift is known to occur with hydrogen-bonded compounds. Finally, the broad region around 1033 cm^{-1} can be attributed to the ether linkages in the four ring forms. Like other monosaccharides, GlcNAc exists at equilibrium between five forms (Figure 4.13) including a straight chain form and two different ring sizes. Therefore, it is reasonable to expect some degree of band shifting and band broadening. However, the analyte spectrum should mostly closely resemble that of the pure analyte since these spectral changes would not be induced by the CE system, and because the stock solution is already in ammonium acetate solution instead of water. Even without band assignment, analyte identification is easily accomplished with visual comparison of clear spectral features in the interface subtraction spectrum to the spectra of stock analyte solutions. For example, the sucrose reference spectrum is significantly different, so sucrose can be eliminated as the analyte of interest.

Figure 4.10. Electropherogram from the separation of GlcNAc (**A.**) and sucrose (**B.**) Structures are shown for reference. Analyte determination was not possible prior to spectral analysis due to peak tailing masking spiked signals. It is believed that the short distance to the reference detection window was partially responsible for difficulty in analyte determination. Separation conditions: 50 mM ammonium acetate buffer, pH 6.98, 20°C, 17 kV, mixture of 0.1 M GlcNAc in buffer and 0.07 M sucrose in buffer (1:1, v/v) injected with 5 mbar pressure for 2 sec.

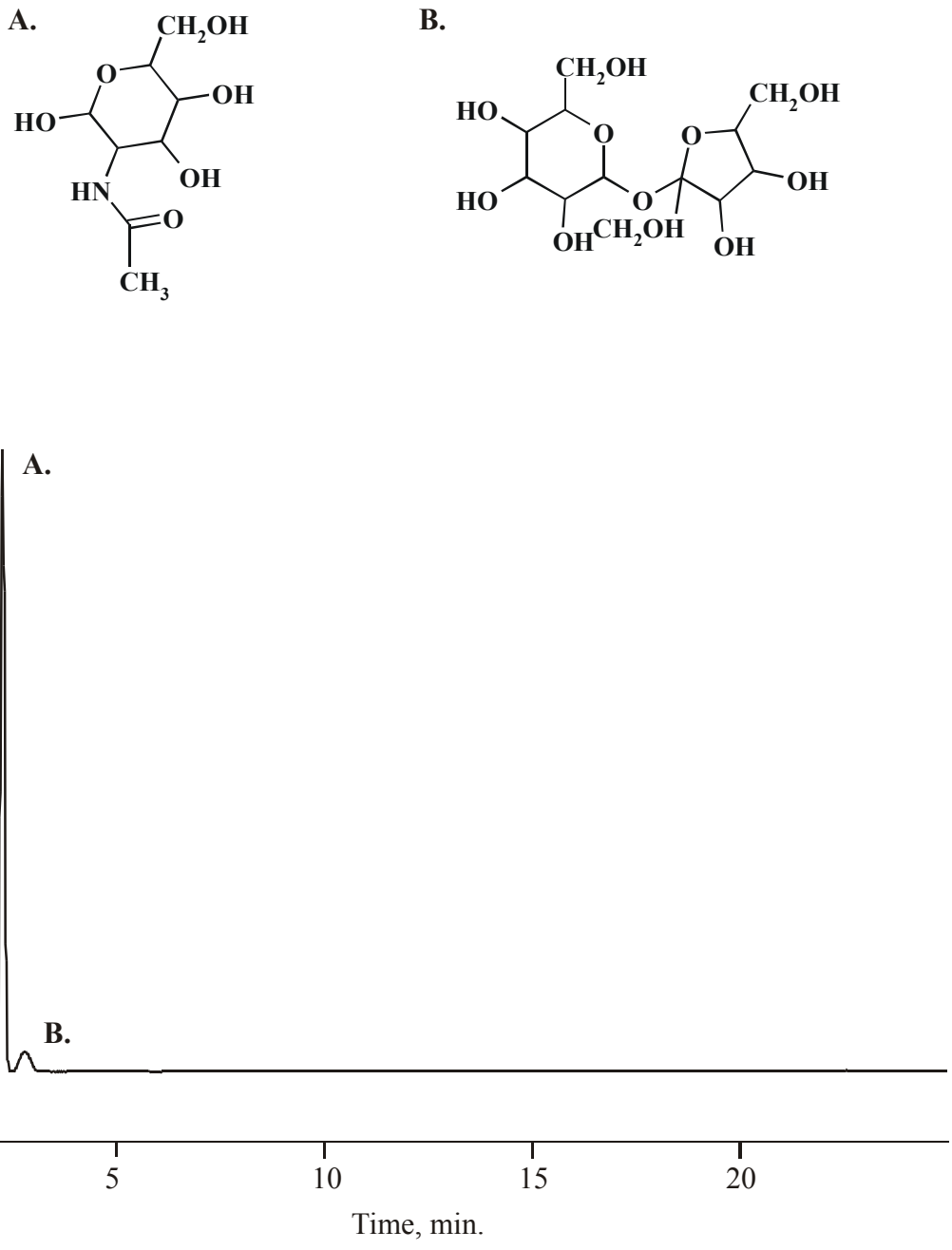
A.
CH2OH
O
OH
HO
OH
HN
O
CH3
B.
CH2OH
HO
O
CH2OH
O
HO
O
OH
OH
CH2OH
OH
A.
B.
Absorbance, 214 nm
5
10
15
20
Time, min.

Figure 4.11. Spectral comparison of deposits of **A.** sucrose stock solution, **B.** GlcNAc stock solution, **C.** collected interface deposit of the first peak in Figure 4.10, **D.** ammonium acetate buffer, and **E.** the result of a buffer subtraction from the interface deposit. Characteristic bands found in both the subtraction result and at least one reference analyte spectrum are marked

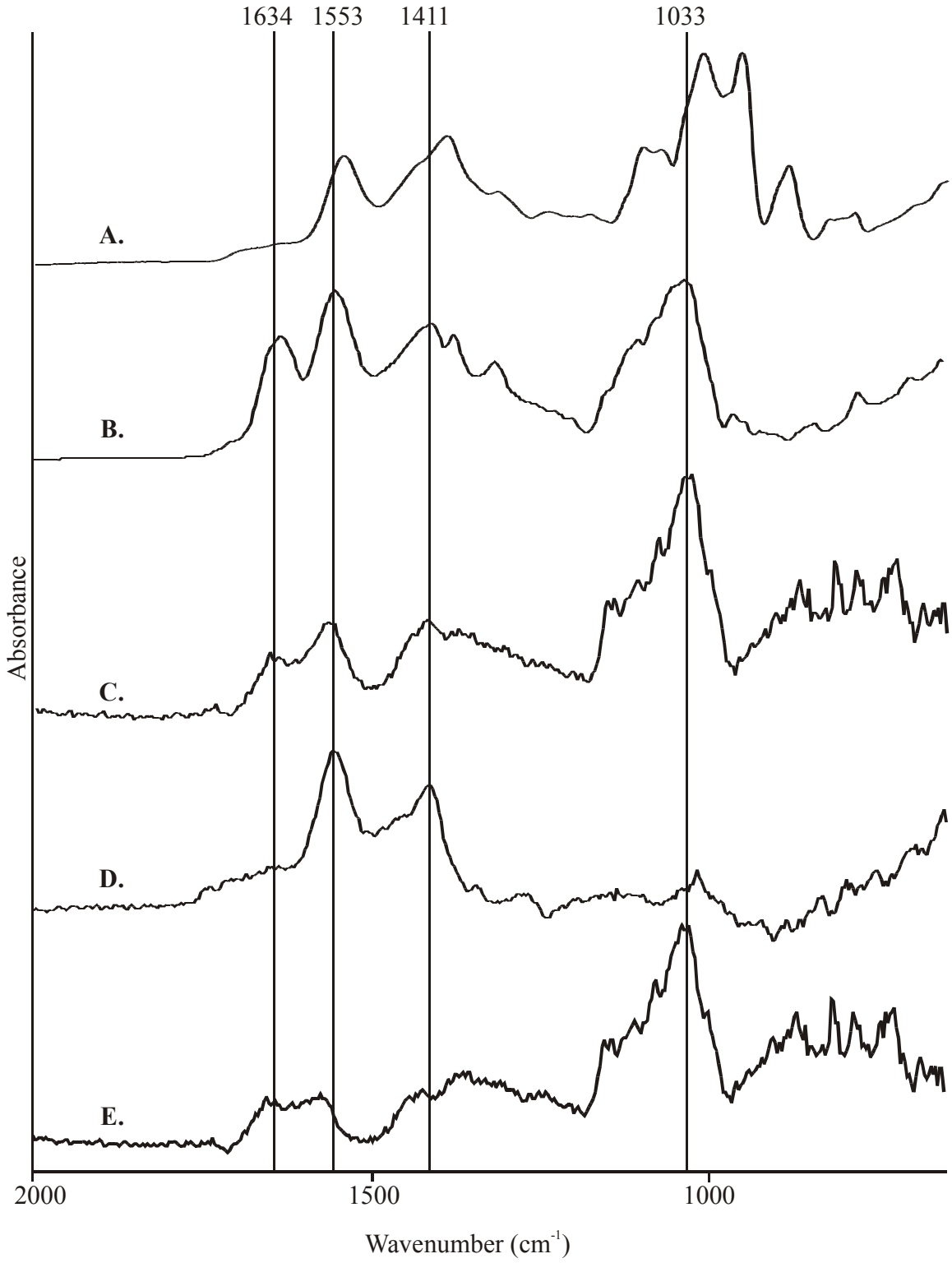
1634
1553
1411
1033
A.
B.
C.
D.
E.
Absorbance
2000
1500
1000
Wavenumber (cm-1)

Figure 4.12. Structural features of GlcNAc and their corresponding spectral assignments. Due to hydrogen bonding and the presence of different molecular configurations (see Figure 4.13), band broadening and shifting can be expected.

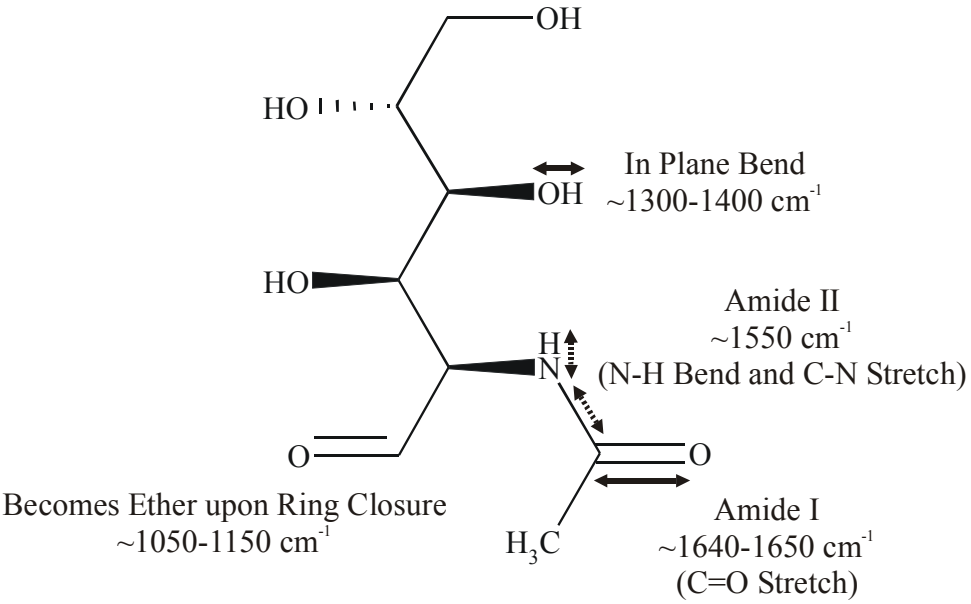
OH
HO
OH
In Plane Bend
~1300-1400 cm-1
HO
Amide II
~1550 cm-1
(N-H Bend and C-N Stretch)
H
N
O
O
Becomes Ether upon Ring Closure
~1050-1150 cm-1
H3C
Amide I
~1640-1650 cm-1
(C=O Stretch)

Figure 4.13. The five possible structures of GlcNAc, including two pyranose forms and two furanose forms. The carbon labeled with an (*) in the open chain conformation becomes an anomeric carbon in the ring forms. The stereochemical orientation of this carbon determines whether the ring is denoted as α or β.

Open Chain Form

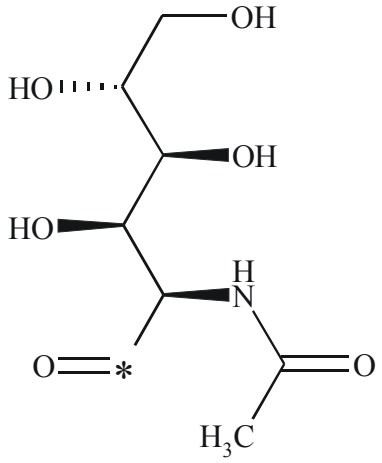

α-N-acetyl-D-glucosamine **β-N-acetyl-D-glucosamine**

Pyranose Forms

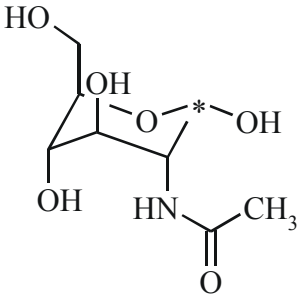

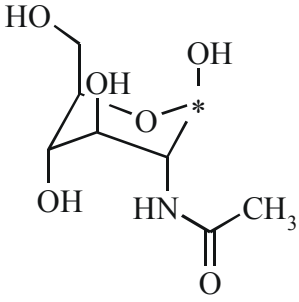

Furanose Forms

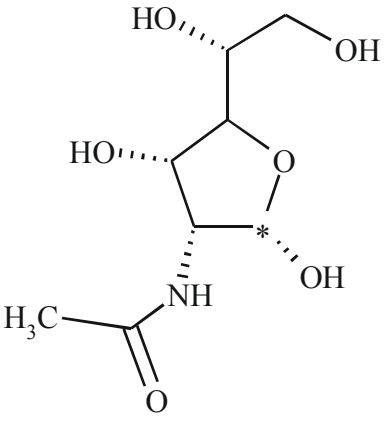

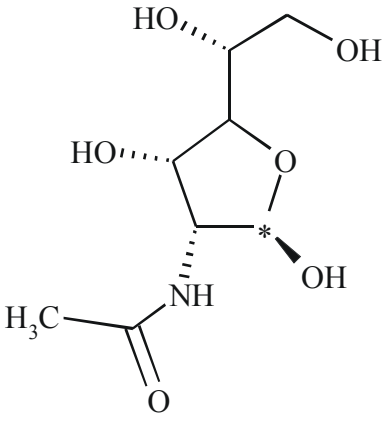

Conclusions

A CE/FT-IR interface has been presented that meets all criteria for CE interfaces and for IR analyses, in addition to offering analyte recoverability and highly stable characteristics. The interface described here has shown remarkable shelf life, electrical contact stability, and coating durability. These characteristics are at least partially responsible for its demonstrated ability to withstand demanding analysis conditions including high voltage applications and large numbers of consecutive analyses, both of which are vital for high quality analytical instrumentation.

These properties, however, are meaningless without the ability to reliably separate and conclusively identify analytes of interest. The interface has been shown to be a significant analysis system capable of performing high quality CE separations that culminate in analyte deposition. The deposition is carried out in such a way that the spectral sensitivity is maximized and analyte identification is easily accomplished though visual comparison, spectral interpretation, or database searching.

Finally, and perhaps most importantly, analyte deposits have been shown to be recoverable and suitable for additional analysis techniques. One of the most attractive features of FT-IR spectrometry is that it is a non-destructive technique well suited for areas of research in which a great deal of information must be gained from minute sample quantities. This interface facilitates separation of minute sample quantities, high quality UV-vis and IR spectrometric analyses, and still allows subsequent interrogation by other, possibly destructive, techniques such as MS.

In the future, it is important to be able to capture an entire CE trace such that compounds that may have separated after reference detection can be correctly resolved

and identified. Part of this undertaking requires a time-resolved on-line interface scheme, which is already in progress. Furthermore, regulation of gas flows is crucial to automation and to preserve nebulization quality.

Acknowledgements

The authors wish to thank the National Institutes of Health for a National Research Resource grant (number 2P41-RR-05351) for the Resource Center for Biomedical Complex Carbohydrates.

References

1. Hermentin, P.; Doenges, R.; Witzel, R.; Hokke, C. H.; Vliegenthart, J. F. G.; Kamerling, J. P.; Conradt, H.; Nimtz, M.; Brazel, D. *Anal. Biochem.* **1994**, *221* (1), 29-41.
2. Hempel, G. *Electrophoresis* **2000**, *21* (4), 698.
3. Wang, C. Y.; Hsieh, Y. Z. *J. Chromatogr. A* **2002**, *979* (1-2), 431-438.
4. Li, Z.; Wang, Y. J.; Liu, G. Q.; Chen, Y. *Chemical Journal of Chinese Universities-Chinese* **2001**, *22* (10), 1654-1657.
5. Seifar, R. M.; Dijkstra, R. J.; Gerssen, A.; Ariese, F.; Brinkman, U. A. T.; Gooijer, C. *Journal of* **2002**, *25* (13), 814-818.
6. Jeannot, R.; Sabik, H.; Sauvard, E.; Dagnac, T.; Dohrendorf, K. *J. Chromatogr. A* **2002**, *974* (1-2), 143-159.
7. Wehr, T. *Lc Gc* **2003**, 75-78.
8. Guan, X. M.; Hoffman, B.; Dwivedi, C.; Matthees, D. P. *J. Pharm. Biomed. Anal.* **2003**, *31* (2), 251-261.
9. Kim, H.; Han, S. B. *J. Pharm. Biomed. Anal.* **2003**, *31* (2), 341-349.
10. Lachenmeier, D. W.; Kroener, L.; Musshoff, F.; Madea, B. *Rapid Commun. Mass Spectrom.* **2003**, *17* (5), 472-478.
11. Jorgenson, J. W.; Lukacs, K. D. *J. Chromatogr.* **1981**, *218* (1-3), 209-216.
12. Jorgenson, J. W.; Lukacs, K. D. *Anal. Chem.* **1981**, *53* (8), 1298-1302.
13. Jorgenson, J. W.; Lukacs, K. D. *Science* **1983**, *222* (4621), 266-272.
14. Terabe, S.; Otsuka, K.; Ichikawa, K.; Tsuchiya, A.; Ando, T. *Anal. Chem.* **1984**, *56* (1), 111-113.

15. Fukushima, T.; Usui, N.; Santa, T.; Imai, K. *J. Pharm. Biomed. Anal.* **2003**, *30* (6), 1655-1687.

16. Riekkola, M. L. *Electrophoresis* **2002**, *23* (22-23), 3865-3883.

17. Bishop, R. T.; deHaseth, J. A. *Mikrochim. Acta* **1997**, 721-724.

18. deHaseth, J. A.; Turula, V. E. *Mikrochim. Acta* **1997**, 109-119.

19. Vonach, R.; Lendl, B.; Kellner, R. *J. Chromatogr. A* **1998**, *824* (2), 159-167.

20. Jones, J. C.; Littlejohn, D.; Griffiths, P. R. *Appl. Spectrosc.* **1999**, *53* (7), 792-799.

21. Geiger, J.; Korte, E. H.; Schrader, W. *J. Chromatogr. A* **2001**, *922* (1-2), 99-110.

22. Wilks, P. A. *Appl. Spectrosc.* **1968**, *22* (3), 237-238.

23. Hankemeier, T.; Brinkman, U.; Vredenbregt, M.; Visser, T. *Mikrochim. Acta* **1997**, 719-720.

24. Saferstein, R.; Manura, J. J. *Am. Lab.* **1978**, *10* (2), 125-129.

25. Brickhouse, M. D.; Creasy, W. R.; Williams, B. R.; Morrissey, K. M.; O'Connor, R. J.; Durst, H. D. *J. Chromatogr. A* **2000**, *883* (1-2), 185-198.

26. Filippelli, M. *Appl. Organomet. Chem.* **1994**, *8* (7-8), 687-691.

27. Smith, B. C. *Fundamentals of Fourier Transform Infrared Spectroscopy*; CRC Press: Boca Raton, FL, 1996.

28. Meyer, A.; Budzinski, H.; Powell, J. R.; Garrigues, P. *Polycyclic Aromatic Compounds* **1999**, *13* (3), 329-339.

29. Spectra-Tech. "Contaminant Analysis by FT-IR Microsocpy," 2 (1); Spec-Tech Inc.; 2 (1): Stamford, CT.

30. Kolhed, M.; Hinsmann, P.; Svasek, P.; Frank, J.; Karlberg, B.; Lendl, B. *Anal. Chem.* **2002**, *74* (15), 3843-3848.

31. Kolhed, M.; Hinsmann, P.; Lendl, B.; Karlberg, B. *Electrophoresis* **2003**, *24* (4), 687-692.

32. Todebush, R. A.; He L. T.; de Haseth, J. A. *Anal. Chem.* **2003**, *75* (6), 1393-1399.

33. Jarman, J.; Todebush, R.; de Haseth, J. *J. Chromatogr. A* **2002**, *976* (1-2), 26.

34. Kinzer, J. A.; Olesik, J. W.; Olesik, S. V. *Anal. Chem.* **1996**, *68* (18), 3250-3257.

35. Sutton, K. L.; B'Hymer, C.; Caruso, J. A. *Journal of Analytical Atomic Spectrometry* **1998**, *13* (9), 891.

36. Schaumloffel, D.; Prange, A. *Fresenius' J. Anal. Chem.* **1999**, *364* (5), 452-456.

37. B'Hymer, C.; Day, J. A.; Caruso, J. A. *Appl. Spectrosc.* **2000**, *54* (7), 1040-1046.

38. Michalke, B.; Schramel, P. *Fresenius' J. Anal. Chem.* **1997**, *357* (6), 594-599.

39. Moini, M. *Anal. Chem.* **2001**, *73* (14), 3497-3501.

40. Kelly, J. F.; Ramaley, L.; Thibault, P. *Anal. Chem.* **1997**, *69* (1), 51-60.

41. Barnidge, D. R.; Nilsson, S.; Markides, K. E. *Anal. Chem.* **1999**, *71* (19), 4115-4118.

42. Herring, C. J.; Qin, J. *Rapid Commun. Mass Spectrom.* **1999**, *13* (1), 1-7.

43. Zamfir, A.; Peter-Katalinic, J. *Electrophoresis* **2001**, *22* (12), 2448-2457.

44. Tangen, A.; Lund, W.; Josefsson, B.; Borg, H. *J. Chromatogr. A* **1998**, *826* (1), 87-94.

45. Tong, W.; Link, A.; Eng, J. K.; Yates, J. R. *Anal. Chem.* **1999**, *71* (13), 2270-2278.

46. Deng, B. Y.; Chan, W. T. *J. Chromatogr. A* **2000**, *891* (1), 139-148.

CHAPTER 5

SEMI-AUTOMATED DEPOSITOR FOR INFRARED MICROSPECTROMETRY[1]

[1] Jarman, J.L, Shelly I. Seerley, Richard A. Todebush, and James A. de Haseth. Submitted for publication to *Applied Spectroscopy* 03/27/03.

Abstract

The measurement of minute samples is desirable in many areas of research and analysis, including biological, environmental, and forensic sciences. The use of manual solution direct deposition, combined with surface evaporation, is a very useful and convenient method for the transfer of many analytes to a spectroscopic sampling window. For Fourier transform infrared (FT-IR) spectrometric analysis, high quality attenuated total reflection (ATR) and transmission analyses are possible with suitable solution deposits. If the sample area is very small, placement of the analyte deposit on the active area of the sampling accessory must be done carefully. To achieve this, a novel direct deposition system has been developed. This system, a series of valves attached to a glass nebulizer, generates deposits that are reproducible and placement of the deposits is precise. The valves allow for the sample to be loaded, helium airflow to expel the sample, and the nebulizer to be cleaned after deposition. To help contain the sample to a small area once deposition has taken place, a vacuum line is attached to the nebulizer. This simple semi-automated deposition system allows for higher sensitivity and run-to-run reproducibility for minute sample analysis.

Index Headings: Microspectrometry, Attenuated total reflection (ATR), Fourier transform infrared (FT-IR) spectrometry, Microconcentric nebulizer, Liquid deposition, Microsampling

Introduction

Infrared spectrometry is one of the most powerful analytical techniques in use today. With its growth, so has the need increased for rapid surface and bulk analyses with the use of internal reflection spectrometry.[1-16] A nondestructive, microsampling transmission or internal reflection method is attractive for many applications. An ideal sample for transmission analysis is optically flat and appropriately thin and internal reflection samples should have intimate contact with the internal reflection element. Many samples exist in a form inconvenient to microscopic analysis and such samples may be on a substrate unsuitable for analysis and require isolation to proceed. Once a sample has been isolated it may be dissolved and deposited onto a window or internal reflection element for spectral collection. To facilitate sample preparation and placement problems, a semi-automatic sample depositor has been developed that is suitable for nearly every non-volatile liquid or soluble solid sample. The depositor, fashioned from a microconcentric glass nebulizer, expels a minute volume of sample solution directly onto an infrared window or internal reflection element and alters the liquid evaporation pattern of the solvent to help ensure even analyte distribution. Non-volatile liquids are confined to the original droplet size due to a phenomenon known as the "pin line" which occurs at the point where the liquid first comes in contact with the surface.[17] The characteristics of the sample depositor allow the area covered by the droplet can be carefully controlled to optimize thickness and obtain high quality infrared spectra.

It could be argued that liquid chromatographic or electrokinetic systems are suitable sample introduction systems and that the sample depositor described here is simply a replacement. Due to the mechanisms of separation in both partitioning and

electrokinetic chromatographic systems, however, a large degree of sample dilution is observed. Therefore, already minute samples are increasingly difficult to detect and analyze further. Most chromatographic systems require significantly larger sample volumes than are required here, analyte concentrations in the mobile phase are extremely low, and chromatographic mobile phases may significantly interfere with infrared analysis. Finally, spectrometric analysis in chromatographic systems is often carried out in the UV-visible range, with a mass spectrometer, or with an infrared spectrometer. UV-visible radiation does not achieve the same high degree of structural information that is easily obtained with infrared spectrometry, and mass spectrometry is destructive to the sample, which prevents sample recovery or further analyses, and mass spectrometry does not easily answer questions of isomerism. In light of the drawbacks associated with chromatographic sample introduction, the sample depositor is a more ideal apparatus for minute sample manipulation and FT-IR spectrometric analysis.

The resulting samples are suited for transmission and internal reflection analyses and have better characteristics than is normally achieved with traditional methods. Because the sample is manipulated while in solution or in liquid form, a large degree of control is held over properties such as sample thickness, analyte distribution over a given surface area, and total sample volume used. Deposits from this system are of relatively even thickness and analyte distribution, which is favorable for transmission analyses. Deposits are also suitable for internal reflection analyses as the thickness is great enough to obtain high quality, reproducible spectra. In addition, sample volumes are minute, which makes the apparatus ideal for areas of investigation such as forensic sciences and

biochemical analyses in which sample material may be limited by either high cost or availability.

There has been much work done in the development of attenuated total reflection (ATR) accessories for use with infrared spectrometers, which has led to the development of single-reflection microsampling ATR accessories from a number of manufacturers. This technique allows for the analysis of samples that are in liquid, irregular solid, fiber, or powder form, as long as adequate contact between the sample and the internal reflection element (IRE) can be maintained. The sample is placed directly in contact with the IRE, which eliminates sample preparation steps such as pellet mixing or microtoming prior to transmission analysis. For solid samples, pressure may be applied to ensure sample contact and eliminate any gaps between the sample and the IRE. Analyses are often performed without the application of pressure if the sample has inherently good contact. In addition, ATR, especially single reflection ATR, requires only minute sample quantities. Because ATR spectrometry is non-destructive, further analyses can be performed with other, possibly destructive, techniques such as mass spectrometry.

There is a number of different designs used for internal reflection elements. The type of sample that is studied, e.g. liquid, solid, powder, or thin film, often determines which design is used. The designs fall into two categories: single and multi-reflection elements. The available geometries for single reflection elements are fixed angle triangular prisms and variable angle hemispheres. Multiple reflection elements are described in detail by Harrick and are not presented here.[18] The fixed angle single bounce element does not allow for the beam to be focused onto a very small area, thus the size of the beam entering the prism will be approximately equal to the size of the beam as

it enters the IRE. Fixed angle elements work well for relatively large samples that are at least 1 to 2 mm in diameter.[19] If the volume of the sample is small, however, then it cannot be distributed over a large area and still retain enough thickness to produce a good spectrum. Use of an IRE with a hemispherical design reduces the active area size by forcing a convergence of the beam.[20-23] Although many commercial IREs are zinc selenide or diamond, materials with higher refractive indices such as germanium and silicon can yield infrared IREs with much smaller active areas. The refractive indices of germanium and silicon are 4 and 3.4, respectively. The effective focus is determined by the geometry of the IRE and the refractive index of the IRE material. If the refractive index is high enough, the focused beam diameter can be quite small, that is, as small as 250 μm in diameter. The active site of the element can vary in size depending on window material and accessory design.

Composition of the IRE is important in any ATR experiment. The depth of penetration of the radiation into the sample is inversely proportional to the refractive index of the IRE and materials with a low refractive index allow a greater depth of penetration. In the mid IR region, 4000 cm^{-1} to 450 cm^{-1}, the depth of penetration for a typical organic sample with a refractive index of 1.5 varies from 0.13 μm to 1.2 μm for a silicon IRE with a 45° angle of incidence. Zinc selenide, however, has a refractive index of 2.4 and the depth of penetration for the same sample varies between 0.22 μm and 1.94 μm in the same spectral region. Therefore, lower refractive index IREs require a larger sample volume to cover the depth of penetration fully and obtain a high quality spectrum. The depth of penetration, d_p, is:

$$d_p = \frac{\lambda}{2\pi\eta_1(\sin^2\theta - \eta_{21}^2)^{1/2}} \qquad (5.1)$$

where λ is the wavelength of the input radiation, η_{21} is the refractive index of the sample (η_2) divided by that of the IRE (η_1), and θ is the angle of incidence. The electric field strength decreases exponentially as a function of distance from the IRE surface. Thin samples do not absorb sufficient radiation to produce a quality spectrum while much thicker samples are limited by the wavelength dependence described above. Intermediate samples, however, produce ATR spectra that are similar to transmission spectra and the dependence on wavelength is reduced. If only *qualitative* analysis is carried out and the sample is homogenous, the depth of penetration can exceed the sample thickness, as long as the sample is thick enough to produce an acceptable signal-to-noise ratio in the spectrum. The depth of penetration and the sample thickness do become important when *quantitative* analysis is desired. The sample must exceed the depth of penetration of the radiation at all wavelengths in the spectrum to record a spectrum with photometric veracity. Nonetheless, the total sample cannot be measured; hence quantitative analysis is restricted to relative concentrations of components within the sample. One goal of the depositor system described herein is to standardize sample thickness and therefore improve spectral quality and throughput.

Deposition methods have been used for a number of years as a way to measure sample solutions that are not easily analyzed with traditional FT-IR spectrometric methods. There is a number of different methods used to make deposits onto infrared transparent windows. These include manual deposition, semi-automated deposition, and interface deposition. Manual deposition is often used in our laboratory to produce very small deposits for analysis with an FT-IR microspectrometer as well as for FT-IR/ATR spectrometry. When liquid deposits are made, several facts must be considered. For any

drop of liquid, solvent evaporates fastest at the perimeter where the drop is thinnest and surface tension is lowest. This property causes the remaining solvent and solute to migrate toward the droplet edges.[17] The resulting solute deposit has very thick edges and a thin central area that is usually unsuitable for spectrometric analysis. If a thin deposit is analyzed with ATR where its thickness does not reach d_p, a low signal-to-noise ratio spectrum may result. If sample thickness exceeds d_p for an ATR measurement, analyses are expected to be very reproducible. It is possible to make a deposit of excessive volume onto the active site in order to cover d_p and perform successful ATR analyses, but this process is wasteful in sample volume and time. In addition, multiple deposits can result in a larger deposit size or reduced analyte concentration over a given area, and can wash previously deposited sample away from the active area. Perhaps the most detrimental of these disadvantages is the waste of sample as some samples may be difficult to obtain or may only exist in limited quantities. This phenomenon is also a problem in transmission FT-IR microspectrometric analyses because uneven deposit thickness leads to variations in pathlength. When samples with variable thickness are analyzed with a microscope, the non-uniform thickness requires the user to canvas the deposit for a region of suitable thickness, which increases the time required for analysis. Transmission quantitative analysis, which requires standardized deposit thicknesses, is nearly impossible with manual deposition methods. Altering the evaporation pattern and forcing solvent migration toward the center of the droplet allows minor control of both thickness and deposit size, which yields deposits suitable for both transmission and internal reflection analyses. The success of manual methods, however, is variable and cannot be depended upon for quality spectrometric analyses.

To overcome the drawbacks of manual deposition, a novel semi-automated depositor has been developed for use with either a single reflection internal reflection element or an IR microscope for the analysis of a number of different samples. The deposits are analyzed spectrometrically and compared with spectra of manual deposits. The deposits made with the depositor are suitable for both ATR and microspectrometric analyses and can be made under ambient pressure and temperature. The system is relatively simple and removes many variables and obstacles encountered with other deposition methods.

The work described here uses a hemispherical single reflection IRE with an active area of 250 μm and an FT-IR microscope for transmission analyses. The IRE accessory is mounted inside the sample compartment of the FT-IR spectrometer and can be used to analyze both liquid samples and bulk solid samples although the work described here involves neat solids after solvent evaporation. Because of the nature of liquid deposits, contact is inherently maintained. Although neat liquids can be examined, a method is presented herein where a solution is deposited as a droplet directly onto the IRE or transmission analysis window and the solvent is allowed to evaporate. The remaining solid is then in direct contact with the IRE or transmission window surface and is confined to the area covered by the droplet. An ideal deposit leaves a solid with several ideal characteristics, that is, it has uniform thickness, it is circular, and its area just covers the active site of the IRE or the sampling area of the transmission window. For analysis with this technique, the deposit must be made at ambient temperature and pressure, and the solvent should evaporate rapidly. The apparatus is placed close to the IRE or microscopy window for precise deposition but can be removed when the surface is

cleaned. Suitable solutes for deposition with this system are readily soluble in a high to moderately volatile solvent, and should not adhere to glass or silica in order to deposit the total sample. Samples with adhesive properties not only decrease the possible concentration of the sample deposit due to material left behind in the syringe or depositor, but also introduce a high degree of cross contamination between samples. Finally, the solute must be relatively inert and nonvolatile to ensure that it remains on the IRE or transmission window.

Experimental

Chemical Reagents. Caffeine, sodium benzoate, ammonium formate, and salicylic acid were purchased from Sigma-Aldrich Chemical Company (St. Louis, MO, USA). All these samples were made to 1.0 x 10^{-2} M with 18 MΩ deionized water, which was obtained in-house with a Barnstead Nano ultrapure water purifier. Ammonium formate was made to 5-10 x 10^{-2} M with water from the same purifier. Methanol and methylene chloride were obtained from Fisher Scientific (Atlanta, GA, USA) and were used as obtained. Other reagents used included 5 and 10 mM caffeine, 10 and 20 mM sodium benzoate, and dilute and concentrated Erythrosin B (Sigma-Aldrich, St. Louis, MO).

Manual Deposits. The manual method of direct deposition was performed with 1-μL capillary tubes and Pasteur pipettes (Fisher Scientific, Atlanta, GA, USA). The sample deposit is placed directly onto a Harrick SplitPea™ silicon IRE (Ossining, NY, USA), a calcium fluoride (CaF_2) window, or a zinc selenide (ZnSe) window (Spectral Systems, Hopewell Junction, NY, USA).

Semi-Automated Depositor. The sample depositor was fashioned from fittings purchased from Upchurch Scientific (Oak Harbor, WA, USA) and Swagelok (Solon, OH, USA). The main body of the depositor was designed by the authors to have a 4 mm extended tip of 226 μm i.d. and was manufactured by J. E. Meinhard Associates (Santa Ana, CA, USA). Single deposits were made onto a Harrick SplitPea™ silicon IRE (Harrick Scientific, Ossining, NY, USA), a CaF_2 window, or ZnSe window and allowed to dry. Samples were loaded with a 10 μL Hamilton syringe (Hamilton Co., Reno, NV) using 182 mm of fused silica (184 μm o.d., 50 μm i.d.) as the injection needle (Polymicro Technologies, Phoenix, AZ, USA). Helium (National Welders Supply Co., Charlotte, NC, USA) was used to expel the sample plug.

Deposit Measurements. Size determination of the manual and semi-automated deposits were carried out with a Perkin-Elmer Spectrum 2000 FT-IR spectrometer (PerkinElmer Instruments, Shelton, CT, USA). The spectrometer was coupled with a PerkinElmer i-series FT-IR microscope. The microscope is equipped with a remote aperture that can be used in conjunction with the spectrometer software to obtain the size of the deposits. Images were obtained with an ausJENA stereomicroscope (Jenavert, Germany) with a Hitachi digital camera (Hitachi America, Ltd., New York, NY, USA). Surface projections were constructed from spectra collected on the PerkinElmer microscope with Image software.

ATR/FT-IR Spectrometry. Infrared spectra of manual and semi-automated deposits were collected with a Bio-Rad FTS-4000 spectrometer with a DTGS detector (Digilab LLC, Randolph, MA) and a Harrick SplitPea™ microATR accessory (Harrick

Scientific, Ossining, NY, USA). A total of 100 co-added scans was collected at a resolution of 4 cm^{-1} for each spectrum.

Results and Discussion

One way to manipulate minute sample quantities for spectral analyses is to dissolve the sample in a suitable solvent, place a droplet onto the desired analysis apparatus, and eliminate the solvent through heating or evaporation. In this manner, the sample is easily confined to a small area and is neat, which eliminates any solvent interference. Although not recommended for all samples due to possible morphological changes, modified evaporation was chosen as the solvent elimination scheme. While there are several methods to accomplish this task, solvent elimination creates several problems through the evaporation process discussed above. Therefore, modified evaporation systems were developed and used to collect sample deposits.

Initial deposition attempts were completed using the manual deposition system shown in Figure 5.1a. The analyte solution was loaded into a microcapillary and deposited directly onto the IRE or transmission window. During deposition, a vacuum is situated above the deposit area to force solvent evaporation from the center of the deposit. The apparatus consists of a glass pipette attached to a vacuum line and is placed about 3 mm above the center of the deposition area. Evaporation from the center of the droplet creates a migration of solvent and solute from the edges of the droplet toward the center. A 200 W heat lamp is placed directly above the droplet to provide radiant heat and increase the rate of evaporation. The vacuum and heat act quickly to contain the deposit to a central area and eliminate solvent flow outside the droplet area. When a

comparison of deposits is made with and without the evaporation modification apparatus, the deposit with modified evaporation has a higher concentration in the center, which is ideal for site coverage and for concentrating dilute samples. One of the disadvantages of manual deposition is that, during the deposition process, the microcapillary causes a great deal of splatter. The division of the sample droplet into several smaller droplets reduces the analyte concentration in each droplet and can render the deposit(s) useless for analysis.

In an effort to develop a more consistent sample deposition system, a semi-automatic sample depositor was designed. As shown in Figure 5.1b, the apparatus was fashioned from an elongated microconcentric glass nebulizer with an extended capillary tip. Two valves allow for sample loading, helium introduction, and washing the nebulizer. A vacuum pump was attached to a lower sidearm that extends to the outer shell of the nebulizer. The entire sample deposition process is rapid and requires little skill. Sample was injected into the tip of the depositor body with a micro-syringe and fused silica needle, and the syringe was withdrawn. The gas valves and vacuum were closed off during injection, and the sample remained lodged in the depositor tip. After closing the loading valve, the samples were expelled from the depositor tip with helium while vacuum was applied to the outer cavity of the depositor to increase the rate of evaporation and solvent elimination. Gas flow rates were varied to achieve the desired deposit size.

In order to determine the performance of the semi-automated sample deposition system, a series of studies was conducted. A number of aqueous and volatile deposits was obtained by both semi-automatic and manual deposition. Aqueous deposits were

Figure 5.1: **A.** Schematic of manual deposit method onto either an ATR accessory or an infrared window for transmission analyses. **B.** Semi-automatic depositor design.

A.

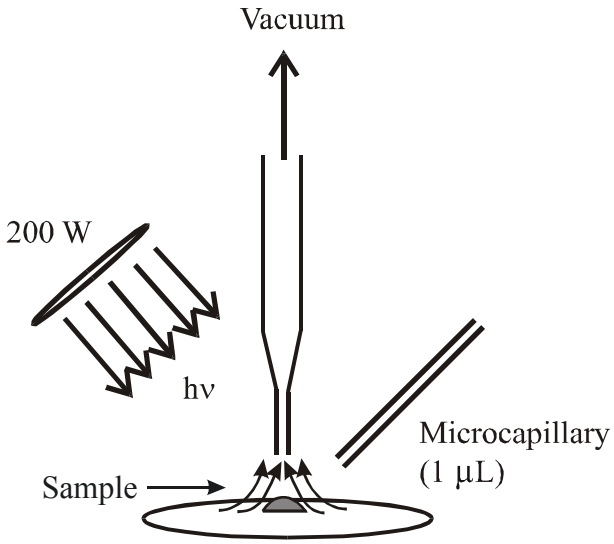
Vacuum
200 W
hν
Microcapillary
(1 μL)
Sample

B.

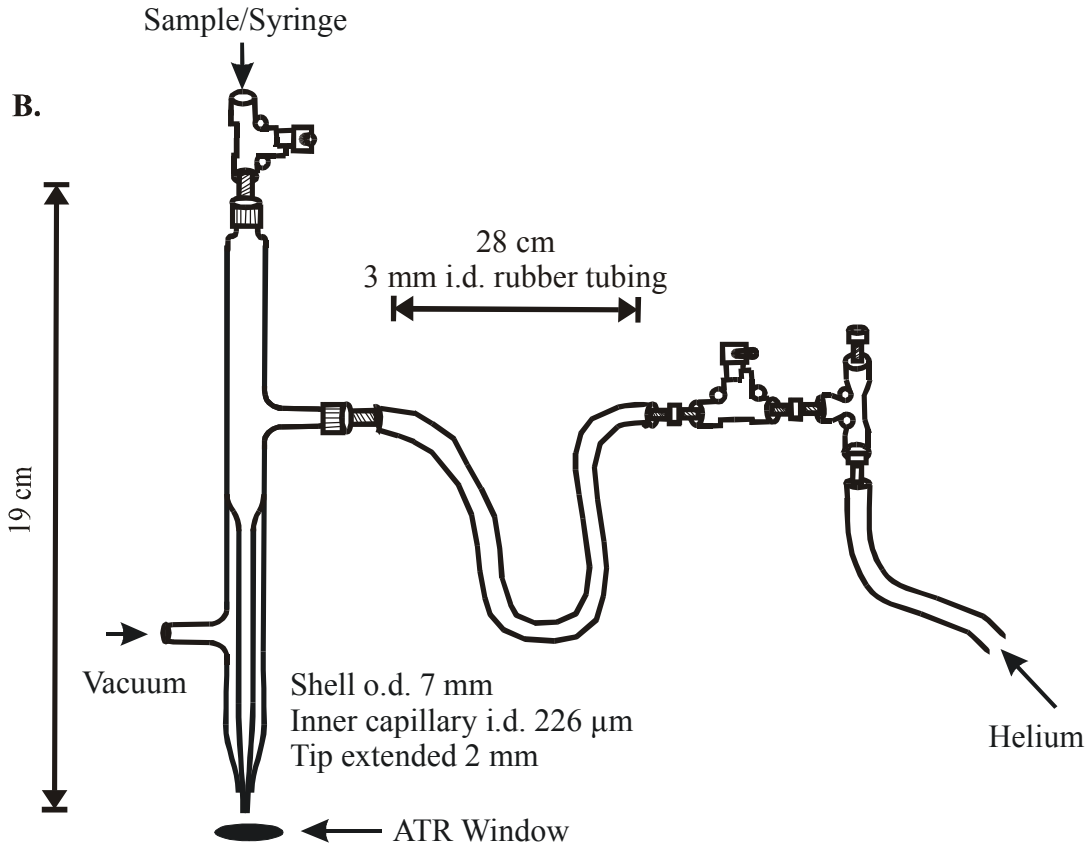
Sample/Syringe
28 cm
3 mm i.d. rubber tubing
19 cm
Vacuum
Shell o.d. 7 mm
Inner capillary i.d. 226 μm
Tip extended 2 mm
Helium
ATR Window

collected from 5-10 mM of caffeine or salicylic acid in deionized water. Evaporation of the water from semi-automated deposits required approximately 3 minutes, which is comparable to evaporation required for manual deposits. More volatile deposits were made both manually and semi-automatically with 5-10 mM solutions of the same analytes in methylene chloride, methanol, or ammonium formate. While solvent evaporation was significantly faster for highly volatile solvents, it was more difficult to confine the sample to a specific location, and the average deposit size increased, probably due to reduced surface tension. Therefore, solvents that are moderately volatile such as water, aqueous ammonium formate, or methanol are better suited for use with the depositor. In contrast, methylene chloride did not prove advantageous when used as the solvent. A certain amount of solvent surface tension is essential in order to maintain control over droplet placement and size, and low volatility liquids typically have a higher surface tension. Therefore, it was determined that highly volatile liquids are therefore unsuitable for semi-automatic sample deposition.

Manual and semi-automatic deposits were compared visually and spectroscopically to determine the advantages of the deposition system over manual deposition. Visual analysis revealed that even with assisted evaporation shown in Figure 5.1a, manual deposits exhibited non-uniform evaporation patterns and thickness variations throughout the entire series of deposits. Evidence of this is found in Figure 5.2, which shows the thickened edge of a representative deposit of an aqueous caffeine solution. The edge is highly defined by the arc of thick analyte crystallization. Deposits of this type are highly concentrated around the outer edge with smaller areas of analyte crystallization in the center of the deposit, which are also visible here.

Figure 5.2. Manual deposit of an aqueous 5 mM caffeine solution that shows the thickened edge and uneven analyte concentration caused by solvent evaporation from the outer edges of the deposit.

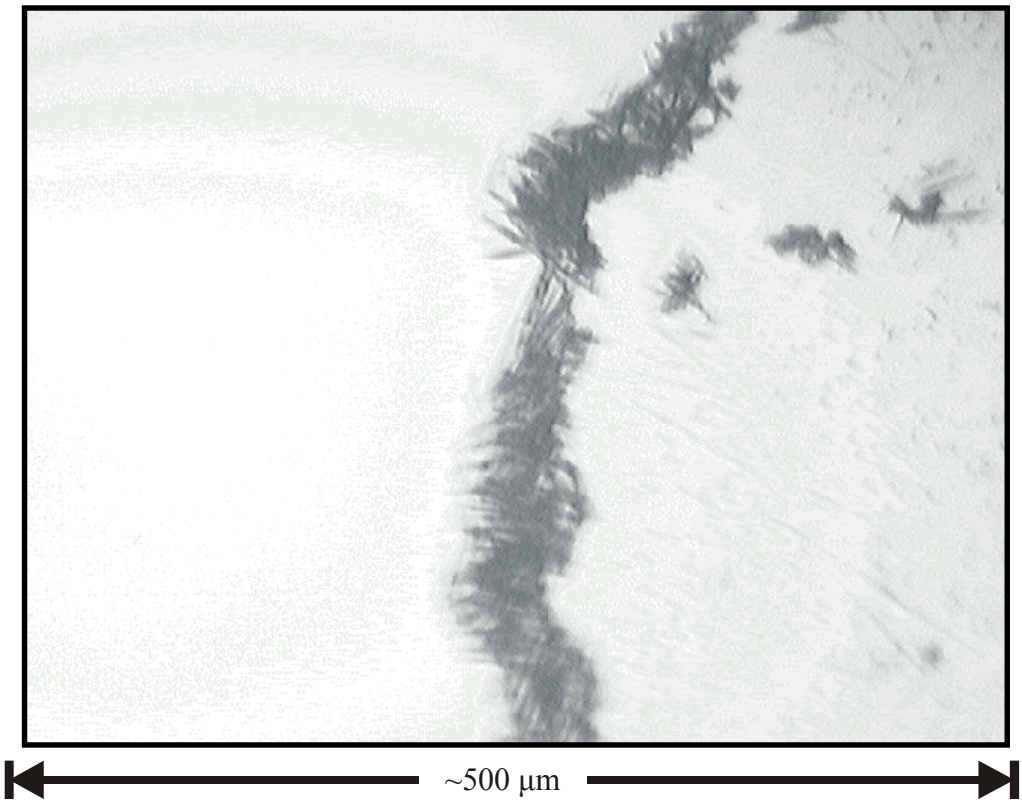
~500 μm

Transmission and reflection analyses on this type of deposit are not possible due to the absence of sample in the central area combined with a ring that is too thick to allow radiation penetration. Typically, manual deposits had dimensions on the order of ~1000 μm and were oblong in shape, as shown in Figure 5.3a. In contrast, the semi-automatic deposits measured between 300 and 600 μm in diameter and were consistently circular. Additionally, while manual deposits exhibited highly uneven evaporation patterns and thickness variations, semi-automatic deposits did not. Figure 5.3b shows a dry semi-automatically deposited sample of caffeine. There is no evidence of a thick outer ring of analyte deposits, and the deposit appears to be smooth and of uniform thickness throughout the center as well. A deposit with these features is ideal for both ATR and transmission analyses. Further demonstration of the evaporation patterns in manual and semi-automatic deposits is shown in Figure 5.4, which is produced from infrared microspectrometric maps. These are surface projections of maximum IR absorbances over the entire deposit area and extending out onto the surrounding window. The semi-automatic deposit, Figure 5.4a, clearly shows a more even evaporation pattern than the manual deposit, despite the use of vacuum and a heat lamp (Figure 5.4b). Splatter patterns are evident in the manual deposit as shown by the small hump on the left side of the deposit. Additionally, the expected ring of heavy analyte concentration is evident and there is an obvious absence of analyte in the center of the deposit. Figure 5.5 shows a comparison of ATR spectra between manual and semi-automated deposits of caffeine, Erythrosin B, and sodium benzoate. Comparison of the spectra reveals slight differences in the intensities of the absorption bands, but the relative intensities are identical. These differences are likely attributed to concentration variations in the

Figure 5.3. A. A typical manual deposit of an aqueous solution of caffeine. Dimensions exceed those suited for high quality ATR analysis and there are obvious regions of uneven deposit thickness. **B.** A typical aqueous caffeine deposit, after solvent evaporation, from the semi-automatic depositor. The deposit is round in shape, shows no evidence of uneven thickness, and has been digitally enhanced in order to see the outer edge.

A.

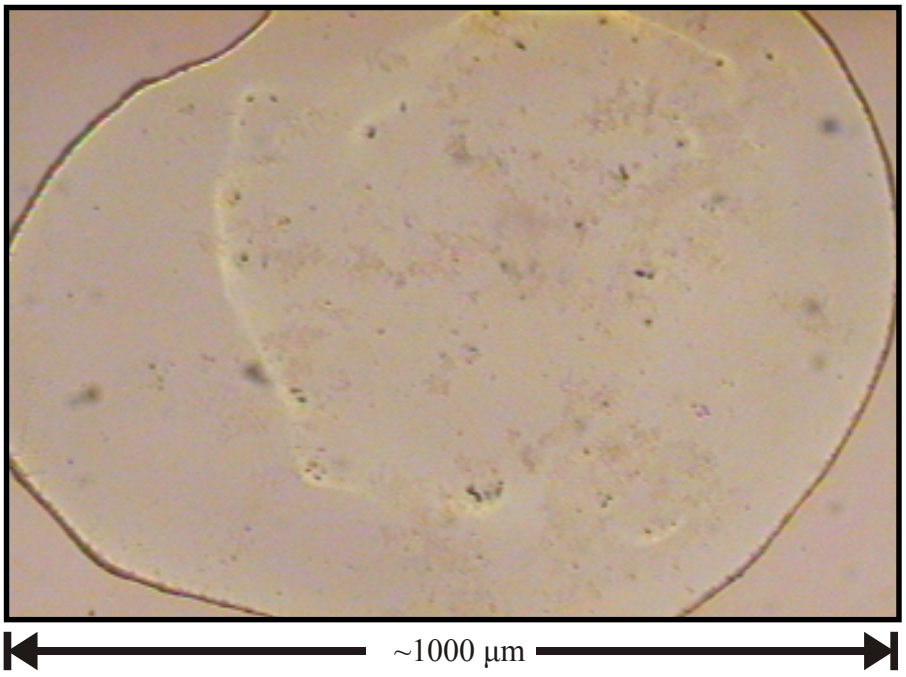

B.

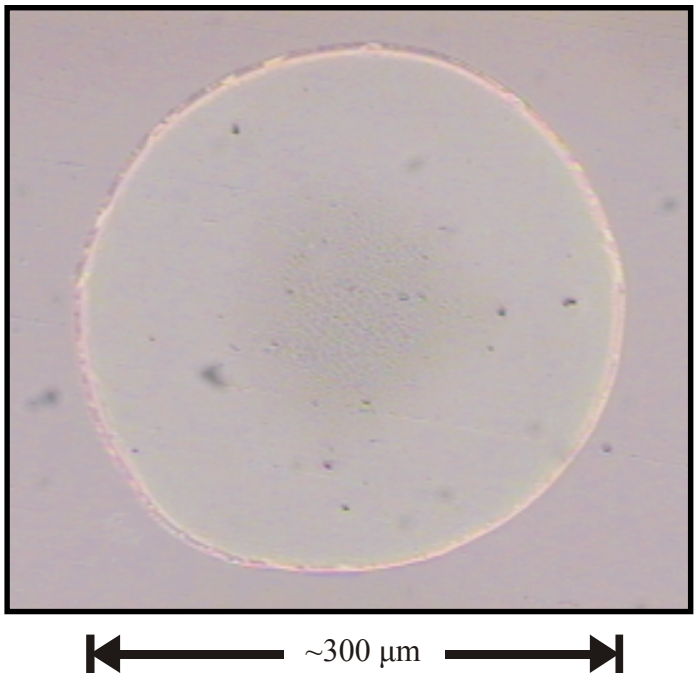

Figure 5.4. **A.** Surface projection of a typical semi-automatic deposit of 20 mM aqueous sodium benzoate. Slight increased absorbance along the back edge is attributed to positioning of the heat lamp. All other regions of the deposit exhibit even absorbance, and thus even thickness. **B.** Surface projection of a typical manual deposit of 20 mM aqueous sodium benzoate. Thickened edges are evident as is a small droplet on the left due to the splatter patterns seen in manual deposits. These deposits are unsuitable for transmission and ATR analyses due to extremely low analyte concentrations in the center, and crystals around the edge that block and scatter radiation.

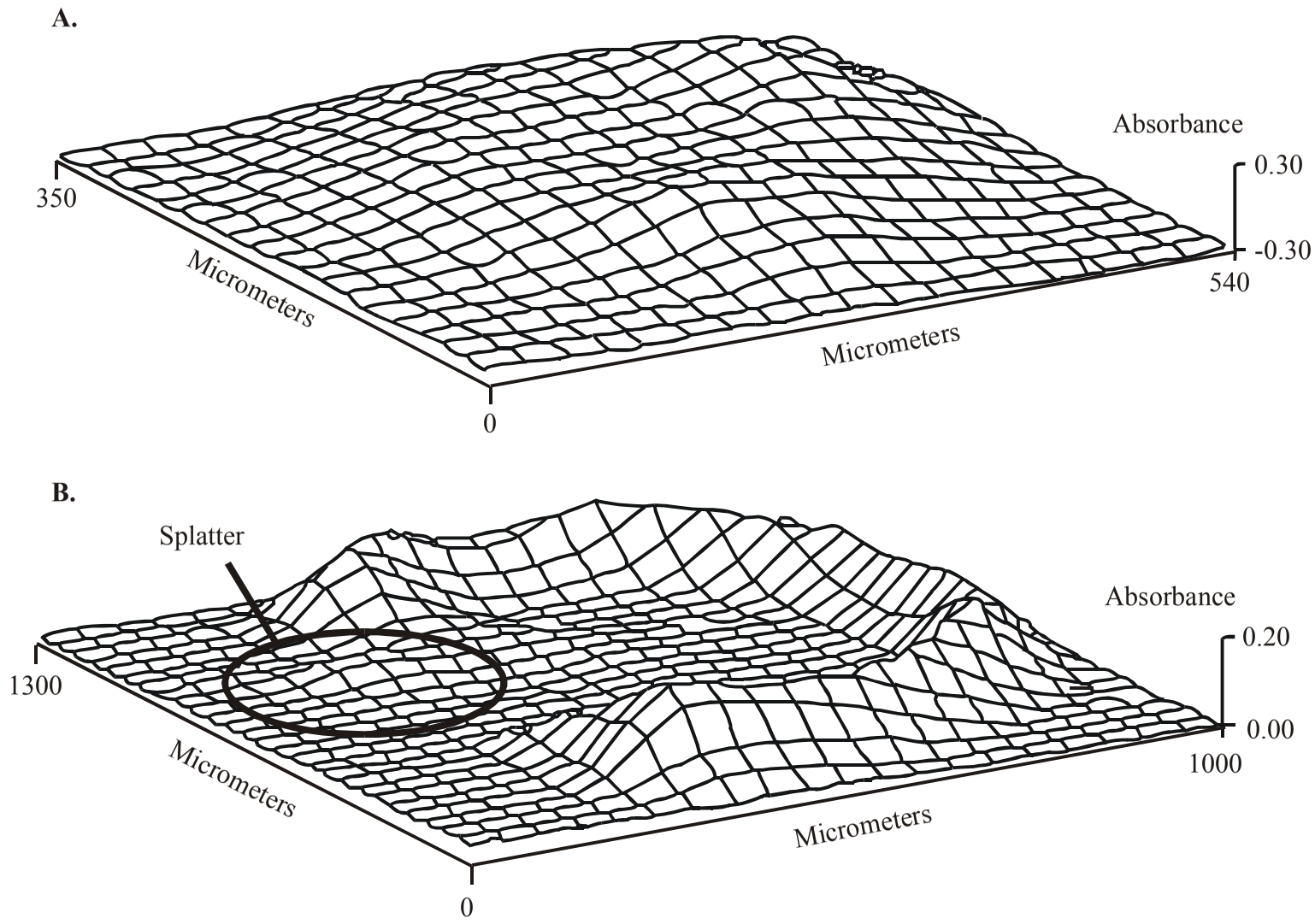
A.
Absorbance
0.30
-0.30
350
Micrometers
540
Micrometers
0
B.
Splatter
Absorbance
0.20
0.00
1300
Micrometers
1000
Micrometers
0

Figure 5.5. Comparison FT-IR/ATR spectra of manual and semi-automatic deposits of caffeine, Erythrosin B, and sodium benzoate. While there are very slight differences in absolute intensities of characteristic bands, relative intensities are identical. Therefore, deposits from the semi-automated depositor are quite suitable for ATR spectrometric analyses.

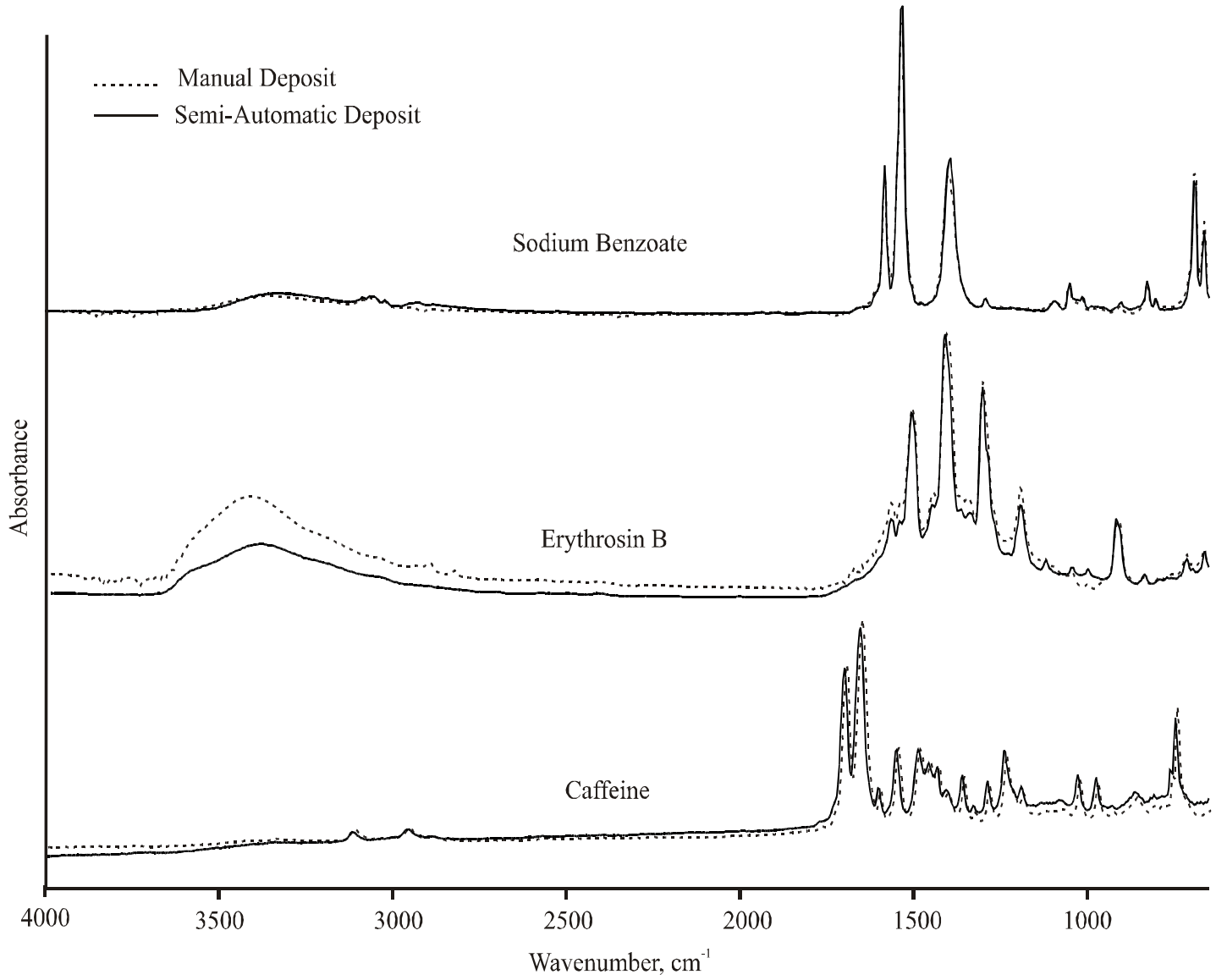
Manual Deposit
Semi-Automatic Deposit
Sodium Benzoate
Erythrosin B
Caffeine
Absorbance
4000
3500
3000
2500
2000
1500
1000
Wavenumber, cm-1

deposits due to variable deposit diameters. It is also possible that the IRE active site was not completely covered with the manual deposits.

To determine the reproducibility of deposit size, a series of deposits onto CaF_2 was visually characterized and measured. Aqueous samples were measured to determine average deposit diameter and standard deviation. As mentioned above, one of the problems with manual deposition is consistent deposit size; therefore, one of the main goals of the new deposition method was to maintain control of this characteristic. Significant improvements in average deposit size variations were observed with the elongation and stabilization of the glass depositor. The average deposit dimensions were measured as 517 x 415 μm with a standard deviation of ±89 and ±102 μm, respectively. It should be noted that the size of the deposit is greatly dependent on the amount of solution that is loaded into the semi-automated depositor. The sizes of deposits recorded are about twice the size needed to cover the active site of the IRE. Deposits closer in size to the 250-μm active site are preferred since these deposits are more concentrated over that active site. Larger loaded sample volumes yield larger deposits, thus it is very important to control the amount of sample loaded. From the height of the sample plug in the tip of the depositor, the amount of sample being deposited can be calculated. If a 5 mM sample solution is loaded into the depositor to a height of 1 mm, roughly 39 ng of sample is deposited onto the surface for analysis. This amount, however, is in excess of the minimal requirements. For an active area of 250 μm, a neat caffeine deposit thick enough to cover d_p requires only 480 pg of sample material.

Another major concern when using the sample deposition method is the reproducibility of the deposit placement. Transmission methods such as deposition onto

CaF_2 windows for FT-IR spectrometric microscope analysis require areas of uniform thickness for deposit comparisons. At times, this can be a significant obstacle and several individual deposits must be made to obtain one with sufficient thickness characteristics. Usually, however, extremely thin deposits are more easily used in transmission analyses than in ATR analyses due to the fact that deposits can be surveyed for appropriate sampling areas and because the radiation aperture is operator defined. That is, the user determines the active site instead of the instrument. In contrast, deposit placement is crucial when the ATR/FT-IR spectrometric system is used due to the small active area. When analyte molecules are concentrated on that active site, maximum spectral sensitivity is achieved, but reproducible deposition onto this very small area with the use of manual methods is difficult at best. To aid in the ease of deposition, the helium flow was regulated in a more precise manner to allow for optimization of deposit size and thickness and the depositor was mounted over a metal variable-height platform with guides attached to it such that the window used for analysis is placed in an exact location.

Three studies were completed to determine the deposit precision of the semi-automatic sample depositor. Data from each of these studies are presented graphically in Figure 5.6. The center of each deposit is shown with a symbol and a region of 150 μm in diameter is circled in the center. This region represents the area within which a 400-μm deposit's center must fall in order to fully cover the 250-μm diameter IRE. Each study is presented as deviations from the average value, which is an accurate depiction of deposit placement when measured from a randomly placed reference point and leads to conclusions about the precision of the system. Outlying points were eliminated based on

Q test calculations regarding distance from the reference point. Accuracy of deposition was not addressed in these studies.

In Study I, forty deposits were made and analyzed. Twenty of the deposits were made with the vacuum assistance and twenty were made without the use of the vacuum. Each deposit was then visually measured to determine the distance from the target to the center of the deposit. The target remained in the same location for every deposit made. It was expected that because the slide onto which the deposits were made was precisely positioned, the deposits would be in exactly the same place. Examination of the data, however, provided significant insight as to the functionality of the deposition system. Deposits made without the vacuum deviated far more from the average than those made with the vacuum. For deposits made with the vacuum, the standard deviation from the average position was ±150 μm. Without the vacuum, the standard deviation increased to ±190 μm. Unfortunately, only two of these deposits fell within the appropriate region, but the results from this study reiterate the importance of the vacuum in the design of the semi-automatic depositor.

Study II involved regulation of the helium used to expel droplets from the depositor tip. In an effort to eliminate as much operator variation as possible, the helium flow was set using a test droplet. Upon release of the helium plug during subsequent deposition attempts, it was observed that the bursts of air seemed larger and caused a great deal of deviation from the reference position as droplets skated across the surface. The standard deviation from average distances was calculated to be ±181 μm, and it is apparent from Figure 5.6 that the grouping of deposits was significantly improved over Study I, despite the single deposit falling within the designated central region. The

deposit movement resulted from the buildup of helium within the gas lines during finishing steps from the previous deposit. During the course of this study, it was determined that regulation of the plug size should be done in a way such that pressure does not build up inside the gas tubing.

It was then determined in Study III that manipulations of the depositor valves and window support stage caused a large degree of variability in apparatus placement because the depositor moved slightly upon valve opening or closing, and the stage did not always return to the same position after being raised or lowered. For this reason, rubber tubing was placed between the main body of the depositor and the knobs and valves for manipulating airflow. With these changes, the valves can be turned on and off with minimal effect on the depositor position. In fact, precision improved such that the standard deviation of distances was calculated to be only ±93 μm and grouping significantly improved. While precision has clearly improved, the low number of deposits within the central area indicates that there is significant room for apparatus optimization. It should be noted, however, that while deposits should be within the central region for successful quantitative analysis, high quality qualitative analysis could be performed as long as the deposit is partially within that region. Further examination of Figure 5.6 then reveals that many additional deposits are suitable for qualitative analysis. Finally, these limitations only apply to ATR analyses. Transmission analyses do not require central region limitation, such that each of the 100 deposits examined in these studies is suitable for spectral interrogation.

After the three precision studies, the d_p coverage for the IRE was determined with a series of single and multiple-layer deposits. Spectra of 10 mM caffeine were collected

Figure 5.6. Graphical representation of Studies I (▲), II (■), and III (●) for the determination of semi-automatic depositor precision. The central region indicates the area within which a 400-μm deposit center must fall in order to completely cover the IRE surface. Improvement in grouping and standard deviation is apparent, although apparatus design is still undergoing optimization.

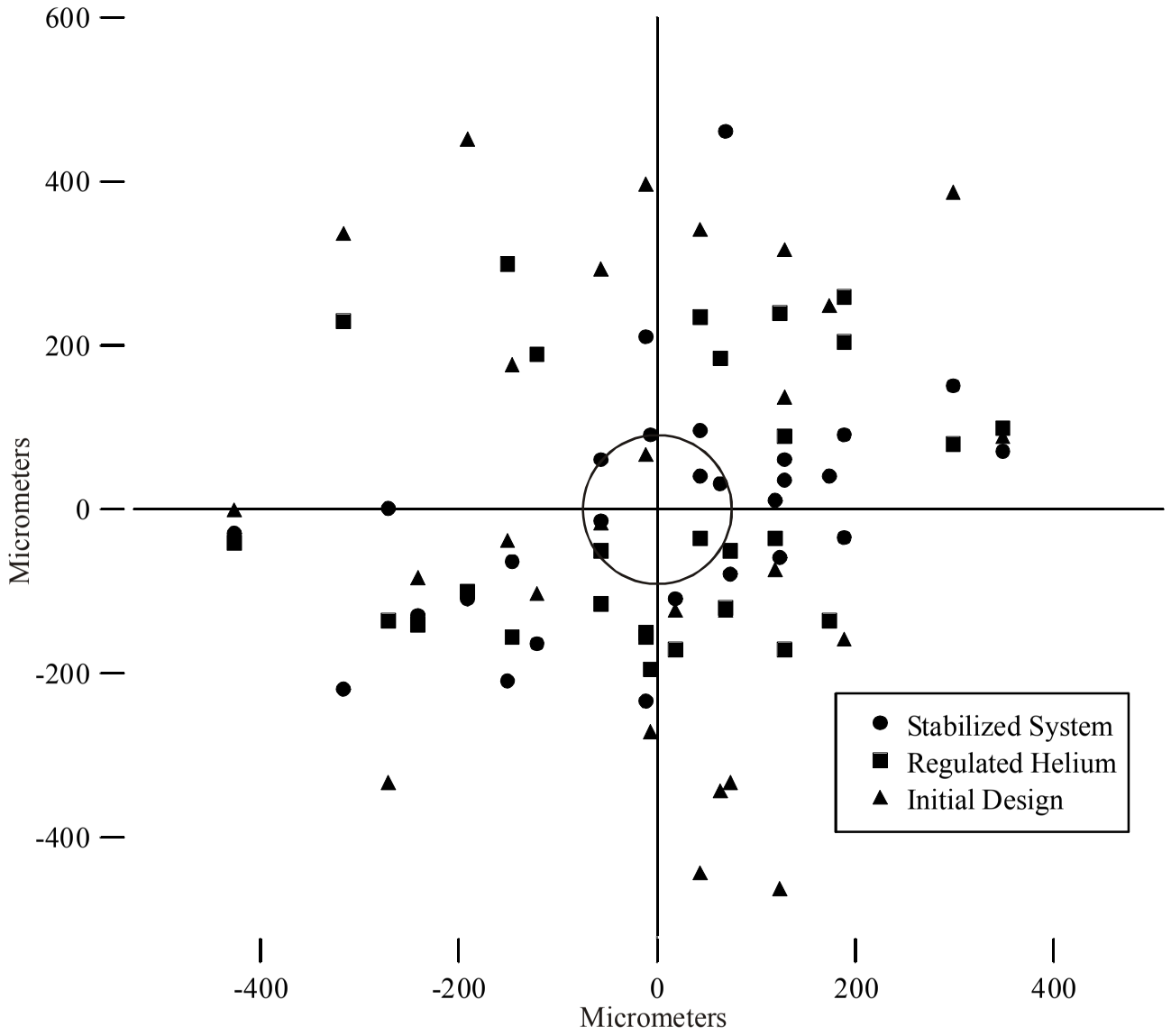
600
400
200
0
-200
-400
Micrometers
-400
-200
0
200
400
Micrometers
Stabilized System
Regulated Helium
Initial Design

first from single deposits on the IRE, and then again after an additional deposit was placed directly on top of the first deposit. The procedure for single deposition was identical to that which was used in the precision studies. Approximately twenty deposits of each type were analyzed, and the resulting spectra were averaged. Overlaid average spectra are shown in Figure 5.7a.

Comparison of the results of the single and double drop spectra indicate that d_p was not covered as fully in the single drop as it was in the double drop. This might suggest that double deposits are necessary in order to achieve maximum absorbance. It can be noted, however, that the maximum absorbance values for the duplicate deposit samples was not greatly improved and that the single deposit spectra are high quality spectra suitable for infrared analyses. During the process of making the deposits, however, some observations were made that affect how these results can be interpreted. Deposits closer in size to the active site yielded much higher absorbance values. It is somewhat difficult to control the size of analyte injected by the syringe, therefore it is difficult to determine the exact maximum absorbance possible for single and double deposits with good precision.

In addition, maximum absorbance is achieved when the deposit thickness reaches or exceeds d_p. If the maximum absorbance was not reached with the initial deposit, the absorbance was expected to increase upon application of the second deposit. In the event that the maximum absorbance was reached with the initial deposit, the absorbance was not expected to change. In contrast to these expectations, however, a less intuitive trend was observed. As shown in Figure 5.7b, it is possible to observe a decrease in maximum absorbance after the application of the second deposit. This has been attributed to the

Figure 5.7. A. Overlaid average spectra of 20 single and dual-droplet semi-automatic deposits of aqueous 10 mM caffeine. Maximum absorbance increases only slightly. Again, relative intensities are identical while there is minimal variation in maximum absorbance values. Results indicate that single droplet deposits are acceptable for ATR spectrometric analyses although care should be taken for quantitative analyses.
B. Overlaid spectra from a single droplet and a dual-droplet semi-automated deposit showing a common outcome of dual-deposit analyses. While it is reasonable to expect absorbance to increase with the addition of the second droplet, analyte is often washed away from the sampling area with the application of additional solvent and maximum absorbance decreases.

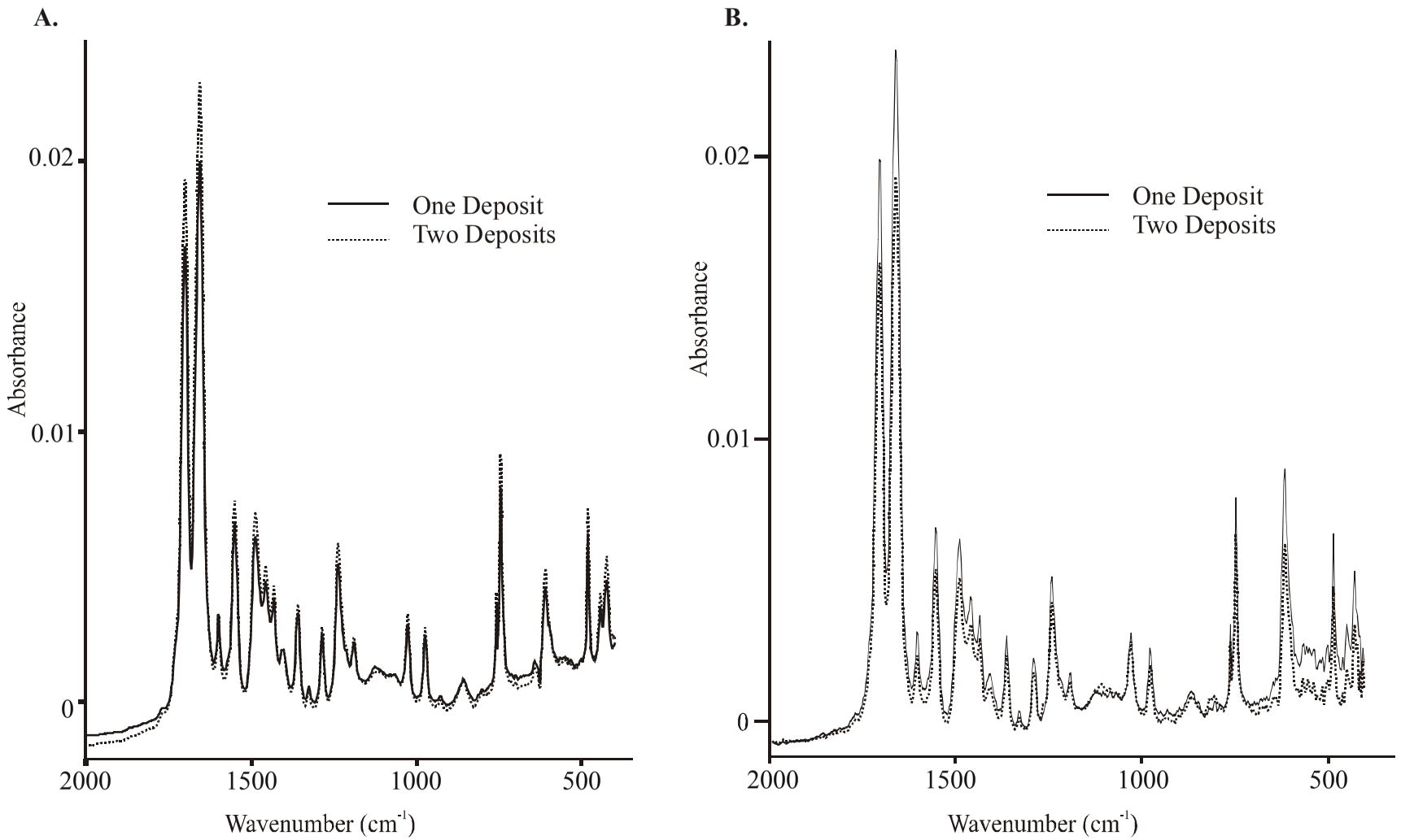
A.
0.02
0.01
0
Absorbance
One Deposit
Two Deposits
2000
1500
1000
500
Wavenumber (cm-1)
B.
0.02
0.01
0
Absorbance
One Deposit
Two Deposits
2000
1500
1000
500
Wavenumber (cm-1)

second deposit washing away or diluting the first deposit and may be related to the shape of the IRE, which has gently sloping sides. Upon collection of the spectra of both the initial and doubly deposited samples, this event was often observed and indicates that the application of a second droplet may actually be detrimental to analytical measurements.

Conclusions

Perhaps the most significant conclusion gleaned from the data presented here is that minute sample volumes are now easily manipulated using a simple apparatus that minimizes operator error and difficulty. The sample placement, size, and geometry are more reproducible and therefore better suited for microspectrometric and single-reflection ATR analyses. The sample deposition system described is a significant improvement over manual deposition systems. The active area of the IRE is uniformly covered by the deposited sample, which reduces noise and other interference from the resulting signal. Spectral analyses of manual and semi-automated deposits are nearly identical. Moreover, the time required for semi-automatic deposition is less than or equivalent to time required for manual deposition, and supply costs are minimal. Because the semi-automated depositor requires only a small sample volume, the depositor is ideal for rare or difficult to obtain samples and is a highly effective microsampling technique. Analyses can be carried out with a single sample plug instead of requiring multi-layered deposits as in many manual deposition techniques. Furthermore, because deposit size is directly dependent on the amount of sample loaded into the depositor, the load amount can be regulated for highly reproducible results. In order to achieve this, the syringe used is tightly fitted with the fused silica needle and is

not changed between samples unless absolutely necessary. Once assembled, the depositor is a single piece of simple laboratory equipment that can help to eliminate a number of tedious steps between sample runs. Technical expertise, therefore, is not essential for quality analyses. In order to build a more robust system, kinematic mounting over the spectrometer and further stability improvements are already underway. These and future developments of the deposition system will only increase its usability, cost-effectiveness, and high throughput characteristics.

Acknowledgements

The authors wish to thank the National Institutes of Health (grant number 2P41-RR-05351) for financial support in the form of a National Center for Research Resources. We thank Lindell C. Ward, Billy Flowers, and Dr. John L. Stickney of the University of Georgia Department of Chemistry for the use of their stereomicroscope and digital camera. We also thank Lasse Kalervo, Helinski, Finland, who described to one of us (JAdeH) the manual deposition system, which led us to the development of the semi-automated sample depositor.

References

1. N. J. Harrick, Phys. Rev. Lett. **4,** 226 (1960).
2. N. J. Harrick, Phys. Rev. **125,** 1165 (1962).
3. N. J. Harrick, Ann. NY Acad. Sci. **101,** 928 (1963).
4. R. S. Levitt and N. J. Harrick, J. Opt. Soc. Am. **56,** 557 (1966).
5. N. Winograd and N. J. Harrick, Appl. Spectrosc. **25,** 143 (1971).
6. B. I. Molochnikov, I. S. Vasileva, and N. N. Gubel, Sov. J. Opt. Tech. **46,** 661 (1979).
7. F. J. Deblase, N. J. Harrick, and M. Milosevic, J. Appl. Polym. Sci. **34,** 2047 (1987).
8. L. W. Liebmann, J. A. Robinson, and K. G. Mann, Rev. Sci. Instrum. **62,** 2083 (1991).
9. J. S. Jeon, R. P. Sperline, and S. Raghavan, Appl. Spectrosc. **46,** 1644 (1992).
10. B. W. Johnson and K. Doblhofer, Electrochim. Acta **38,** 695 (1993).
11. M. K. Gunde, Informacije Midem-J. Microelec. Elec. Comp. Mat. **27,** 120 (1997).
12. S. Widayati, S. M. Stephens, and R. A. Dluhy, Mikrochim. Acta 679 (1997).
13. P. E. Poston, D. Rivera, R. Uibel, and J. M. Harris, Appl. Spectrosc. **52,** 1391 (1998).
14. W. Z. Lu, S. A. Shamsi, T. D. McCarley, and I. M. Warner, Electrophoresis **19,** 2199 (1998).
15. K. A. Oberg and A. L. Fink, Anal. Biochem. **256,** 92 (1998).
16. H. Y. Cheung, J. X. Cui, and S. Q. Sun, Microbiology UK **145,** 1043 (1999).

17. R. D. Deegan, O. Bakajin, T. F. Dupont, G. Huber, S. R. Nagel, and T. A. Witten, Lett. Nature **389,** 827 (1997).

18. N. J. Harrick *Internal Reflection Spectroscopy* (Harrick Scientific Corp., Ossining, New York, 1987).

19. L. Pleserova, G. Budinova, K. Havirova, P. Matejka, F. Skacel, and K. Volka, J. Mol. Struc. **565-566,** 311 (2001).

20. N. J. Harrick, M. Milosevic, and S. L. Betets, Appl. Spectrosc. **45,** 944 (1991).

21. N. J. Harrick, M. Milosevic, and S. L. Berets, Am. Lab. **24,** 50 (1992).

22. N. J. Harrick, M. Milosevic, and S. L. Berets, Am. Lab. **24,** 29 (1992).

23. J. Fritsche, H. Steinhart, M. M. Mossoba, M. P. Yurawecz, N. Sehat, and Y. Ku, J. Chromatogr. B, **705,** 177 (1998).

CHAPTER 6

CONCLUSIONS AND FUTURE STUDIES

While the projects presented in this dissertation may have slightly different areas of emphasis, each is concerned with developing a high quality method for the purposes of chemical analyses. Compound characterization is addressed with various forms of capillary electrophoresis (CE), Fourier transform infrared (FT-IR) transmission microspectrometry, or single reflection Fourier transform infrared attenuated total reflection (FT-IR/ATR) spectrometry.

The determination and characterization of enantioselective pesticides revealed previously unknown properties of two classes of pesticides. This characterization will lead easily to determinations of active components in soils and persistence of potentially toxic compounds. These studies need to be repeated in each soil of interest and the enantiomer of interest must be identified and characterized as much as possible in order to increase understanding of enantioselective microbial degradation processes. Interests may include toxicity, solubility, pesticide activity, and elution order. Other degradation pathways to be investigated include hydrolytic and photolytic processes, both of which are vital for complete compound characterization. Once a complete set of information is developed, chiral pesticide activity will be much more reliable and understood.

Continued work on the interface of CE and FT-IR spectrometry can only lead to a more reliable, robust system. First and foremost, detection limits should be determined in order to characterize the feasibility of the interface. These limits include not only CE limits with the existing UV detection, but also FT-IR spectrometric limits for both ATR and transmission analyses. It is apparent that many deposits may be unsuitable for transmission analyses due to extremely short pathlengths, but when these deposits are recovered, they yield high quality single-bounce ATR spectra. The logical next step is

the development of a system for time-resolved spectral collection, which will also help facilitate automation. Although buffer and electrical conditions still need to be optimized for each method or group of analytes, a more automated system will yield faster analyses with significantly less operator involvement. Interfaced systems to be automated could include a traveling microspectrometric transmission window or a traveling ATR element, either of which can be interfaced to a third instrument such as a mass spectrometer. In short, the CE/FT-IR technique is still in its infancy and the potential applications are innumerable.

Finally, manipulation of minute quantities of either liquid or solvated samples continues to be in demand, and developments are currently underway to continue apparatus optimization. Kinematic mounting of the depositor over a support stage or ATR accessory will greatly enhance transmission or ATR analyses by improving depositor stability and deposition precision. In addition, the apparatus needs to be characterized for actual deposition limits to determine realistic sample quantities required to give high quality transmission or ATR spectra. Special consideration should be given to those samples that require quantitative analysis to ensure full coverage of the depth of penetration for the ATR element. Finally, a variety of solvents should be thoroughly investigated to determine deposit limitations due to surface tension and volatility. Because of the properties of the solvents, glass, and interactions between the depositor and the sample material, it is possible that the apparatus may need to be optimized for different systems.

Each of the projects described in this dissertation indicate additional projects that would greatly increase the available information for CE and FT-IR spectrometric

analyses. Increased knowledge of chiral pesticide degradation patterns can help reduce environmental contamination, cost of application, and potential for accidental misuse. Utilization of a CE/FT-IR interface allows more information to be collected from a smaller amount of sample material and can dramatically improve existing separation and identification procedures. Finally, minute sample manipulation is frequently encountered in multiple areas of scientific interest, and an apparatus to improve sample conservation and ease of manipulation and analysis is quite valuable.

"What we call results are beginnings."

-Ralph Waldo Emerson